Contents of this document

List of summarized manuscript changes

We have summarized the manuscript changes in the list below. Subsequently, a list of changes to figures is provided.

- Model setup
  - The lower boundary of our heat transfer model (1DHT) was defined by a constant geothermal gradient at 300 m below ground level. As pointed out by referee#1, this definition allowed for considerable temperature changes at the model base, which implies that the geothermal heat flux was not constant. In the revised manuscript, we have extended the lower boundary to a depth of 1 km so that the temperature change here is close to constant (throughout the simulations). The new setup resulted in different simulated permafrost aggradation rates, which in turn caused changes to input for the groundwater model.
  - In the old version of the manuscript, the modelling approach did not consider dynamic storage effects. Due to the steady-state setup of the groundwater model, such are not possible to incorporate directly in the modelling of groundwater flow. In the revised manuscript, we have compensated for dynamic storage by applying a time-moving average to the estimated permafrost aggradation rates before calculating the present pressure contribution on the groundwater model. This new step in the modelling scheme is explained in a new paragraph added to the end of Sect. 4.3.4.
- As suggested by referee#2, the flow chart describing the model approach has been updated and moved from the Supplement to the main article as a new Fig. 4.
- Material properties
  - Hydraulic conductivities – The likely ranges of hydraulic conductivity for all pre-Cenozoic units have been tightened as suggested by referee#1:
    - Festningen Sandstone, Janusfjellet Subgroup and the detachment zone - The former lower end of the ranges is considered unlikely and the range now span across half an order of magnitude.
    - Carolinefjellet and u. Helvetiafjellet formations narrowed by applying a probability density function to the values measured by the Longyearbyen CO2 Laboratory Project. See details in the new version of the Supplement (S2).
  - Porosity of Janusfjellet Subgroup – In the first submission, we based the likely porosity range of Janusfjellet Subgroup on a single reference (Manger, 1963). As pointed out by referee#1, this parameter deserved more attention, because of its crucial importance when calculating the equivalent recharge from the simulated permafrost aggradation rates. In the revised manuscript, we improve the derivation of the likely porosity range by considering the estimated burial depth of Janusfjellet Subgroup and empirical works on the relationship between compressibility of clays and mudstones and effective stress. See further explanation and six new references in Sect. 4.3.2.
- More clearly defined manuscript structure
  - Section titles more clearly indicating intro, results, methods, etc.

    - Paragraphs moved to different sections
- Description of the groundwater model simulations is added to the methods section
- Tables
    - Captions added to tables
    - References to values in tables are indicated more clearly
- Corrections
    - A handful of errors pointed out by the reviewers have now been corrected.
- Improved readability
    - Many terms and concepts are now better explained to expand readership.
    - Sentences and phrasing that appeared unclear have now been rephrased.
    - To avoid confusion and improve readability, the usage of words like ‘this’ have been constrained where possible.
    - All abbreviations not used in common language are now explained.
    - Using the same word to describe different things or using different words to describe the same thing is now avoided.
    - Figures are made easier to read by explaining their content more thoroughly in the captions and by improving symbology and adding new components (see details in ‘List of changes to figures’ below).

List of changes to figures

- Figure 4 (old figure S1)
  - Moved to main article as a new figure 4
  - Modelling scheme clarified by using different box types and colour codes
  - New caption:
    - **"Figure 4** Schematic overview of the inner workings of the decoupled heat and groundwater model. Model setup, calculations and algorithms are indicated with sharp corners and bold text. Validation and comparison of simulations and observations are indicated with round corners and italics. Input and output data are indicated with rounded corners, grey background and normal text."
- Figure 1
  - Panel labels and descriptive texts concatenated and moved to upper left corners.
  - Shading added to indicate frozen ground
- Figure 2
  - 2a
    - The location of Longyearbyen is shown
    - Compass added
    - Tidal flat drawn
  - 2b
    - Simple geological time scale added to legend
  - New caption:
    - "**Figure 2 (a)** Map of Lower Adventdalen with the location of data resources, pingos and the Holocene marine limit. LP=Lagoon Pingo, LYRP=Longyear Pingo, FHP=Førstehytte Pingo, IHP=Innerhytte Pingo, RP=River Pingo. Core logs from boreholes S1–3 and D1–D7 (respectively, Gilbert et al., 2018, and Olaussen et al., 2020, and references therein), seismic lines (Bælum et al., 2012, and unpublished commercial lines from Norsk Hydro) and a geological map (Norwegian Polar Institute, 2019) were used to build the geological model (Fig. 5a) (see details in Hornum, 2018). Permafrost depth measurements at the Sarkofagen, DH4 and Breinosa sites are from Liestøl (1977), Braathen et al. (2012), and Christiansen et al. (2005), respectively. The freezing front depth at LP is from Yoshikawa and Harada (1995). Data used to develop the map including topography, glacial extent, and fluvial network by courtesy of Norwegian Polar Institute (2019). **(b)** Geological cross sections constructed based on the resources mentioned above. The Quaternary unit overly well-consolidated sedimentary strata of pre-Cenozoic age (i.e. Cretaceous or older). See Sect. 3.1 for a (hydro)geological description of the layers shown in the cross sections A, B and C."
- Figure 3
  - Curves drawn in different colours – not dash styles
  - Shaded area (minimal arrival of driftwood) made more visible
  - New caption:

- "**Figure 3** Holocene temperature reconstructions in and around Svalbard. Dashed grey area indicate time of minimal driftwood arrival (Farnsworth et al., 2020). The unit of the time axis is ka = 10^3 years before present. **(a)** MSST curves (= MSAT, see text). Red line from Mangerud and Svendsen (2017). Orange line from Hald et al. (2007). Blue line from van der Bilt et al. (2018). **(b)** MAAT used in this work. Based on Mangerud and Svendsen (2017) and Førland et al. (1997) (see Sect. 4.3.3)."

- Figure 5 (old version Fig. 4)
  - We have clarified the meaning of the inset by making the labelling of the zones (now only called 'zones') more visible.
  - 1D simplifications are now only called so.
  - The labelling of the zones is now explained in the caption. Isochrones added to the figures.
  - Legend added to make the figure easier to read.
  - A zone map is now provided in a new panel b.
  - New caption:
    - "**Figure 5 (a)** 3D geological model of the subsurface below the valley floor in Adventdalen and vertical 1D simplifications (inset in upper right corner) below zones of the model area. The former determines the hydrogeological properties in the groundwater model (Table 3), whereas the latter determines the geothermal properties in the 1DHT model (Table 2). The domain of the 1DHT model extends to 1000 m b.g.l. (not shown). Deeper than 300 m b.g.l., geothermal properties were defined as for Janusfjellet Subgroup. The sea retreat reconstruction was inferred from absolute datings (Table 1) and is illustrated by valley floor exposure isochrones (red dashed lines). Pingos are indicated with blue arrows. **(b)** Vertical view of the model area showing the zonation. The aforementioned isochrones defined the zone names so that the valley floor exposure age of a zone is apparent from its name (i.e. zone 0-1 became sub-aerially exposed between 1 and 0 ka, zone 1-2 between 2 and 1 ka, etc.). "
- Figure 6 (old version Figure 5)
  - No changes
- Figure 7 (old version Figure 6)
  - Changed due to new model setup.
  - New caption:
    - "**Figure 7** (previous page) Present-day permafrost conditions as simulated by the 1DHT model. **(a)** Freezing front and permafrost depths. The upper and lower edge of the shaded area corresponds to the maximum and minimum limits of the porosity range, while the curve and the points corresponds to the intermediate (Table 2). **(b)** Rate of permafrost aggradation. The point symbols represent the present permafrost aggradation, while the shaded area is drawn by applying a time-moving average as described in Sect. 4.3.4. and represents the values used to calculate the equivalent recharge rates. *It is the -0.7 °C isotherm, which has been used to calculate this as the greatest phase change rate takes place at that temperature. **(c)** Equivalent recharge rate (net rate of loss in pore space). The

points on the curve and the outer edges of the shaded area represent the recharge rates, which were assigned to the corresponding zones in the groundwater model."

- Figure 8 (old version figure 7)
  - Changed due to new model setup
  - Legend for the colour fill indicating heads in m a.g.l. is made identical for all scenarios and moved to bottom of the figure.
  - New caption:
    - **"Figure 8** (next page) Groundwater model simulations from all 9 scenarios. The individual diagrams are sorted so that the hydraulic conductivity increase along the right-hand axis **(**scenarios **Sc1**–**3*x*)** and the equivalent recharge produced by permafrost aggradation increase along the left-hand axis **(**scenarios **Sc*X*a**–**c)**. On each diagram, the following simulation results are illustrated: Heads from the uppermost grid layer are shown in m a.s.l. by isopotential contours (note that the colour scales are different) and in m a.g.l. by the colour fill (see scale at the bottom of the figure). The latter indicates if artesian conditions are simulated (reddish) or not (blueish). The outflow distribution and discharge rates are illustrated by pie charts with the location of the discharge points (pingos and fjord) indicated on **(1c)**. *For minimun Q_{REq} scenarios (**1a**, **2a** and **3a**) part of the outflow is caused by basal permafrost thaw (Figs. 7b–c). Flow patterns are illustrated by thin blue lines, which each depict pathways of particles released in the uppermost grid layer. The mean pore water velocities, shown in the upper left-hand corners, were calculated from the aforementioned particles and using the same porosities for all scenarios (Table 3). The areas outlined with thick dashed lines show where each outlet point were simulated to receive water from during 3 kyr. In the lower right-hand corner, the simulated head in well DH4 is illustrated on a range plot with the range defined as deduced by Braathen et al. (2012). The colour of the bar indicates if the simulated head falls within (green) or outside the deduced range with less (yellow) or more (red) than 10 % of the total range. The location of DH4 and the pingo springs is marked on **(1c)**."
- Figure 9 (old version figure 8)
  - Changed due to new model setup
- Figure 10 (old version Figure 9)
  - Changed due to new model setup
- Figure 11 (old version figure 10)
- Figure 12 (old version figure 11)

Point-to-point reply to reviews

On the following pages, we give a point-to-point reply to the reviews. Please note that the original referee comments are written in **bold red text**, answers to comments are written in *italics*, and changes to the manuscript are written in *blue italics.*

Reply to comments by referee 1# (Melissa Bunn)

Summary:

In this paper, the authors investigate permafrost aggradation and the associated increase in subpermafrost groundwater pressures over millennial scales as the potential cause of pingo springs in a high Arctic valley (Aventdalen, Svalbard). Continuous permafrost, high desert conditions, and a lack of wet-based glaciers in the adjacent highlands preclude recent groundwater recharge as a source of the spring water. Using a 1D heat flow model the authors quantify potential rates of permafrost aggradation. This aggradation is then related to a water flux which is applied as recharge in a 3D groundwater flow model. These processes are fully decoupled. The groundwater flow model represents the steady state flow of groundwater to the pingos (and the adjacent Fjord) that results from the additional subpermafrost water flux. Although validating field data is limited to sporadic spring flow measurements and hydraulic head measurements at a single borehole, what is available is compared to this data to support the development of the model and the proposed conceptualization of the pingo spring flow.

The mechanism proposed by the authors is new, and their use of numerical models to illustrate and quantify this mechanism is of value. The discharge of subpermafrost groundwater to the surface has the potential to introduce methane to the environment and other solutes to freshwater systems. Understanding of the mechanism that generates the driving hydraulic heads in a variety of geological settings improves our ability to forecast future conditions under a changing climate. Overall the conceptual model and the numerical approach is well presented. However, the paper gives the sense that the modelling work proves the conceptual model to be correct. In general, assumptions are made in numerical modelling to align the numerics with the conceptualization. The modelling presented in this paper is no different, and as such, the model output does not prove the conceptual model to be correct. Some factors that warrant further investigation to support the numerical modelling assumptions are detailed below. Value could be added to the paper by using the model to further explore the physical factors required to form pingo springs under this conceptual model.

Melissa Bunn's review of our manuscript clearly shows that she has studied our work carefully and evaluated it very professionally. We are pleased to read that the reviewer acknowledges the novelty of the pingo-forming mechanism we propose and that she overall find that our research is well presented.

The reviewer is of the impression that the paper "gives the sense that the modelling work proves the conceptual model to be correct". We did not intend to make such claim, but we acknowledge the reviewer's impression and hope that this revision improves that. It appears to us that a number of the reviewer's quite specific comments regarding the numerical modeling work arise from the above impression. Although this was not intended, these comments are still of great value for improving our paper.

Freezing pressure from permafrost aggradation is well known from closed-system pingos, but has not previously been considered for open-system pingos as this research does. This is, as also noted by the reviewer, a novelty. Based on our investigation, we argue that permafrost aggradation deserves

attention as a driver for deep permafrost springs and open-system pingos. We do so because the modelling results suggest that the conceptual model represents a feasible mechanism for how open-system pingos can form. However, we do not think that it is the only option for the pingos in Adventdalen and we have tried to clarify this view in the revised manuscript. All of the following changes and corrections were done with this in mind and the ones directly below are examples of this.

Old version, Abstract, Lines 19:

"Our results show that the pingos in lower Adventdalen easily conform to this conceptual model."

New version:

"Our results suggest that the conceptual model represents a feasible mechanism for the formation of open-system pingos in lower Adventdalen and elsewhere."

Old version, Sect. 6.3, Line 530:

"The amount of hydrogeological data from Adventdalen was insufficient for automatic calibration of model parameters."

New version:

"The amount of hydrogeological data from Adventdalen was insufficient for automatic calibration of model parameters and the model simulations should therefore at best taken as possible scenarios for the conditions in Adventdalen."

The boundaries of the numerical groundwater flow model create a closed "bathtub" like system. Although the amount of recharge added is quite low (<1 mm/year), the presence of permafrost throughout the top of the model domain, a lower boundary that is within 100 m of the base of the permafrost, and no flow across lateral boundaries, leaves only the Fjord and the pingo springs as discharge points. Additional details, or discussion would be useful in supporting the boundary selection for the groundwater flow model as follows:

- **The paper investigates the effect of the lower boundary position by lowering the model depth by 100 m. A more illustrative demonstration of the effect of the lower boundary may be to lower the boundary to the detachment zone that separates the upper overpressured and lower underpressured groundwater flow systems (i.e., to a depth where there is field evidence of a no-flow boundary);**

While we agree with the reviewer's comment that a lower boundary defined by field evidence would be preferred to the somewhat arbitrary approach, we have used, we do not find such in the investigated system. The reviewer suggests that the detachment zone could define the lower model boundary, but this is found at such shallow depths in the Eastern part of the model area (~ 50 m b.g.l., Fig. 2b) that this would not be part of the groundwater model domain (after the permafrost layer has been removed). Seismic investigations at IHP suggest that pingo spring water rise vertically from rocks deeper than 50 m (Rossi et al., 2018) and thus likely from below the detachment zone. At the same time, hydrogeochemical

similarities and consistent trends (water type and concentrations of Cl- and stable water isotopes) from all pingo springs suggest that they formed in the same hydrogeological system (Hodson et al., In review). Complete hydrological separation between the lower (NW) and upper (SE) part of the system therefore appears unlikely.

Although no field evidence exists for a uniform model domain depth, it may be justified if we assume that groundwater flow at least partly is controlled by secondary permeability induced by glacial loading and unloading (Leith et al., 2014). *We have added this consideration in the discussion of the model extent (see changes in the revised manuscript below the answer to the next comment).*

- **There is no evidence provided for the presence of hydraulic divides at the flanks of the valley that would support the use of lateral no flow boundaries in the groundwater flow model as specified. This boundary prevents any regional flow in to or out of the valley. Were groundwater flow to follow the modest slope of the formations, flux through the Festningen Member may be sufficient to dissipate the recharge flux specified in the model. If field data is not available, the sensitivity of model results to deeper regional flow across the valley should be explored;**

There is indeed no field evidence for the presence of hydraulic divides at the flanks of valley and we hence write that the lateral model extent is "somewhat arbitrary" (Old version, Section Line 519).

The reviewer suggests that we investigate how regional flow through Festningen member or other presumably permeable hydrogeological units (i.e. fractured bedrock) may affect dissipation of the recharge flux. However, do to its stratigraphical orientation, the Festningen member does not cross the model domain and as such, it cannot facilitate regional flow across the system (Figs. 2b and 4): Eastwards, it is not present, and in the Northeastern part of the domain, it is cut by the surface/Quaternary strata.

Although no field evidence exists for a "bathtub" system, there is likewise no evidence for the contrary. As should be clear from our manuscript, we focus our study on effects of freezing expansion. Our model design attempts to isolate this mechanism (taking variable Holocene temperatures and sensitivity analyses into account) and we attempt to emphasize this in the revised manuscript:

Old version, Section 6.2.2., Lines 518-529:

"Given the lack of known geological boundaries or groundwater divides, the lateral extent of the model domain was defined using a simplified outline of the HML, but this may be somewhat arbitrary. Due to Early Holocene warming (Fig. 3), the 1DHT simulation results showed that continuous frozen ground in Adventdalen is likely younger than 6.5 ka even where the valley floor is older (Fig. 5). This is supported by geomorphological and geochronological evidence (Humlum, 2005). As such, there seems to be no reason why permafrost dynamics outside the HML should be markedly different from that in the up-valley part of the model area. Based on the above, it is possible that basal permafrost aggradation goes on beyond the model area (HML) and model simulations may have underestimated the freezing-induced pressures affecting spring discharge.

The dominantly low-permeable groundwater system challenged a physically determined lower boundary for the model domain. From the significant low-pressures observed in deeper stratigraphic layers (~ 800 m b.g.l., Braathen et al., 2012), we inferred isolation of the investigated groundwater system from that below and simply assigned the base to a depth of 300 m b.g.l. By simulating scenarios with a lower base of 250 and 400 m b.g.l., we found that simulation results did not change significantly (< 1 % deviation of simulated heads and discharge rates)."

New version:

"The boundary conditions of the groundwater model define a bathtub-like system with the pingo springs and the fjord as the only discharge points, and with the expansion of water upon freezing within the model regime as the only source of hydraulic pressure. In reality, the hydrological system in Adventdalen may not entirely conform to this description as groundwater flow across the model boundaries cannot be rejected. Additional recharge could, for example, occur through microcracks below the valley floor induced during glaciation (Leith et al., 2014). Likewise, hydraulic pressures may, to a greater extent than simulated, dissipate directly to the fjord through unknown pathways. In this respect, our model serves to isolate the pressure effect of freezing expansion in Adventdalen and systems like it. This should be taken into account before drawing site-specific conclusions from the modelling results.

Due to Early Holocene warming (Fig. 3), the 1DHT simulation results showed that continuous frozen ground in Adventdalen is likely younger than 6.5 ka even where the valley floor is older (Fig. 6). This is supported by geomorphological and geochronological evidence (Humlum, 2005). As such, there seems to be no reason why permafrost dynamics in the valley bottom outside the HML should be markedly different from that in the up-valley part of the model area. Based on the above, it is possible that basal permafrost aggradation goes on beyond the model area (HML) and model simulations may have underestimated the freezing-induced pressures affecting spring discharge.

The dominantly low-permeability groundwater system challenged a physically determined lower boundary for the model domain. From the significant low-pressures observed in deeper stratigraphic layers (~ 800 m b.g.l. at DH4, Braathen et al., 2012), we inferred isolation of the investigated groundwater system from that below and simply assigned the base to a depth of 300 m b.g.l. By simulating scenarios with a lower base of 250 and 400 m b.g.l., we found that simulation results did not change significantly (< 1 % deviation of simulated heads and discharge rates)."

- **As stated by the authors, the drain boundaries used to represent the pingo springs are placed within the upper most active cells closest to the spring, but within the Festningen Sandstone. Additional details and discussion of this placement would be of use. Figure 2(a) and Figure 4 indicate that the sandstone is not present at the Innerhytte Pingo. Figure 7 shows that the drain associated with the Førstehytte Pingo is opposite the valley axis from the surface expression. It is understood that the fractured nature of this sandstone could permit the required subhorizontal flow to the pingo; however the paper would benefit from additional discussion of this conceptualization (what is the inferred orientation of the fracturing that allows formation of the pingos). The sensitivity of the model results to the geological unit that the drain boundary is placed in should be discussed;**

The reviewer here point to an error in the first version of our manuscript. The drains representing the pingo springs were placed within the uppermost active cells closest to the spring, but within Festningen Sandstone if present in the underlying stratigraphy. As the reviewer rightfully notes, Festningen Sandstone is not present at Innerhytte and River Pingos, and the drains were here placed in the uppermost active cells. The reasoning behind placing the drains within Festningen Sandstone is that the permeability of this unit presumably makes it a pathway for groundwater flow. Assessing the fracture orientation within this unit is beyond the scope of this paper, and its hydraulic conductivity was thus assumed uniform.

Old version, Section 4.3.4., Lines 325-326:

" […] the drains were assigned to the uppermost active cells located closest to springs, but within the conductive Festningen Sandstone."

New version:

" […] the drains were assigned to the uppermost active cells located closest to springs, but within the conductive Festningen Sandstone if present in the underlying stratigraphy (i.e. Lagoon and Førstehytte Pingos, Fig. 5a)."

- **The boundary representing the Fjord is described as being applied to the relevant cells. Please describe this assignment in more detail (are the boundaries assigned to the upper most active layer only, or are they assigned to several layers to the approximate seafloor depth in the Fjord). As the boundary at the Fjord represents the highest flux from the model (approximately 40% to 90% of the total flux) model results can be expected to be very sensitive to the vertical location of this boundary, and should be investigated further; and,**

The reviewer is not sure whether the fjord BC is assigned only to the uppermost active cells only or extended to the approximate depth of the seafloor. Both are true because the fjord depth is less than 5 m. It is not stated in the first submission, but the model extent towards the fjord aligns with the approximate terminus of the tidal flat. We have now drawn the tidal flat on Fig. 2a and made the following correction:

Old version, Section 4.3.1., Lines 276-277:

"The horizontal model boundary was a simplified outline of the valley bottom and the lower boundary was at 300 m b.g.l. (Fig. 4)."

New version

"Towards northwest, the model covers the tidal flat (Fig. 2a), but no other sea-covered areas were included. Elsewhere, the horizontal model boundary was a simplified outline of the HML. The lower boundary is at 300 m b.g.l. (Fig. 5a)."

- **The potential for subpermafrost discharge to the Adventdalen River has not been considered in the conceptual model development. Rossi et al. (2017) suggest that this discharge may occur**

near the Innerhytte Pingo. Although the rate of subpermafrost discharge to this River may be low, the potential for it to occur should be considered in the overall balance of flows.

We are aware of (Rossi et al., 2018) and have now included this reference. The reviewer writes that the potential for subpermafrost discharge to the Adventdalen River has not been considered. Based on seismic surveys (Rossi et al., 2018) suggest the discharge area at Innerhytte Pingo (IHP) may extent some meters below Adventdalen River. In the summer when Adventelva is active, a minor amount of spring discharge directly to the river could very well be overseen, but during winter when the river is dry, all perennial discharge points are easily recognized by continuously growing icings. At IHP, there is only one icing observed (covering the pingo apex and extending down to the river). If the reviewer would like it, we will be happy to include a speculative uncertainty bar on Fig. 8, which could account for the potential minor discharge to the river. However, based on our observations of outflow from the winter icing, this would be less than Liestøl's (1977) estimate of 1 L/s, which is already considered in the balance of flows.

Elsewhere than at IHP, perennial discharge to the river would results in winter season icings. As these have not been observed, we do not regard discharge of subpermafrost groundwater to the river to be plausible.

No changes to the manuscript were made based on this comment.

In general, further investigation of the effect of these various boundary conditions on the groundwater model results are required before it could be concluded that the model results show that the basal permafrost aggradation produces the hydraulic pressures to sustain the pingo spring water outflows as the authors have stated at the start of Section 7.

The reviewer here refers to the first paragraph of Sect. 7. This paragraph was intended to refer to open-system pingo formation in general, and not specifically to the pingos in Adventdalen. As such, we did not mean to give the impression that the basal permafrost aggradation, per se, produces hydraulic pressures that sustain the outflow in Adventdalen. Instead, we argue that the model experiments show that permafrost aggradation alone may drive open-system pingo and subpermafrost spring systems, if conditions like for the modeling experiments exists.

Old version, Sect. 7, Lines 622-623:

"Results from the decoupled heat and groundwater model show that millennial-scale basal permafrost aggradation may alone produce hydraulic pressures sufficient for the formation of pingos and their spring water outflows."

New version

"Results from the decoupled heat and groundwater model show that millennial-scale basal permafrost aggradation may alone produce hydraulic pressures sufficient for the formation of pingos and their spring water outflows when the right conditions are met."

The observed hydraulic head at DH4 is stated to range from 9 m to 60 m above hydrostatic. It is unclear if this range is due to temporal variability, or the range in the correction for the effect of dissolved gasses. With limited field data for model validation, this warrants further discussion. As shown on Figure 7 (2a, 3b, 3a) simulations in which the hydraulic head at DH4 is on the lower end of this range (and with the lower to middle recharge flux) do not produce sufficient flow at the pingo springs.

The range of the "observed" head at DH4 is uncertainty. The head range is calculated from a single hydraulic pressure (range) estimate by (Braathen et al., 2012) excluding the potential pressure effect of dissolved gasses. This was already stated in the first submission in Sect. 3.1 lines 145-148. (Braathen et al., 2012) deduce the plausible hydraulic pressures based on outflow from the well during drilling. We have now expressed this explicitly:

Old version, Line 144:

"Nearby, […]"

New version:

"Based on artesian outflow during a drilling experiment nearby, …"

The equivalent recharge applied to the model ranges from 25.4 m^3/day to 56.7 m^3/day. This range is related to the porosity of the formation through which permafrost aggradation is occurring. Based on the 1D columns shown on Figure 4, and the model results shown on Figure 5, much of this aggradation would occur within the shale units. The porosity of the Janusfjellet subgroup has been derived from Manger (1963). How was the range from 0.1 to 0.3 selected from the values provided in Manger (1963). The higher porosity units in this reference are related to high clay content shales or claystones. Is this valid for the Janusfjellet formation? Given that the higher porosity ranges were required to produce a water flux that could sustain the pingo flows, further details should be provided on the derivation of these values.

Indeed, by being the dominant geological unit Janusfjellet Subgroup is where most permafrost aggradation takes place. The porosity values (0.1-0.3) were chosen because Agardhfjellet Formation (Janusfjellet subgroup) is the Svalbard analogue to the Kimmeridge Clay Fm, which in (Manger, 1963) is reported to have porosities between 0.19-0.307 (only two samples from one outcrop location). We realize that basing the most crucial parameter for permafrost aggradation (and thus equivalent recharge) on so little empirical data is insufficient. We have now regarded the estimated burial depths of the Janusfjellet Subgroup (Grundvåg et al., 2019; Marshall et al., 2015) and inferred a porosity range based on empirical works on compressibility of clays and mudstone as function of effective vertical stress (Burland, 1990; Okiongbo, 2011; Yang and Aplin, 2004). Using these new references, we find a possible porosity range of 0.08 to 0.3. See changes to the manuscript below the answer to the comment regarding the hydraulic conductivity range of Carolinefjellet and Helvetiafjellet formations.

How is the lower boundary of the 1D heat transfer model specified? If the geothermal gradient from surface is maintained, does that imply that temperature of the lower boundary changes with time?

How would the rate of permafrost aggradation be changed if the depth of the 1D model was extended such that the heat flux at the bottom boundary could be kept constant through time? How would a cessation of permafrost aggradation up valley effect results?

The lower boundary (z=300 m) has a BC defined by a geothermal gradient of 0.025 C/m. Because the geothermal properties in the lowermost cell are constant throughout all simulations (i.e. the pore water does not freeze), this BC is equivalent to a constant heat flux. The reviewer is right that the temperature of the lower boundary changes with time, and we agree that this is problematic. Keeping the remainder of the model setup as before, we have now lowered the lower boundary to a depth of 1 km, so that the temperature change here is close constant (ΔT less than 0.22, 0.42, and 0.65°C for max, mid, and min porosity scenarios, respectively). The new setup simulates results in different simulated permafrost aggradation rates and we thank the reviewer for improving the estimate of these. Correction made and included in the modeling experiments of the revised manuscript.

Old version, Sect. 4.3.3, Lines 311-317:

"The model domain contained 12 one-dimensional grids, each 300 m long and consisting of 150 cells with a height of 2 m. Each individual grid was associated to the model area zones (Fig. 4) and the geothermal properties were defined accordingly. The names of the zones refer to the age of subaerial exposure (Table 1), which defined the simulation run time (e.g. for zone 0-1 the simulation period was 0.5 to 0 ka, for zone 1-2 it was 1.5 to 0 ka, etc. For zone 10, the simulation period was 10 to 0 ka). The initial ground temperature distribution followed the geothermal gradient reported by Liestøl (1977) (0.025 °C m^{-1}) from a surface temperature of 0 °C. At any subsequent time, the lower boundary condition was defined from the same geothermal gradient."

New version:

"The model domain contained 12 columns, each 1000 m long and consisting of 500 cells with a height of 2 m. One column was associated to each of the model area zones and the geothermal properties were defined according to the associated geological 1D simplifications (see insert on Fig. 5b). Deeper than 300 m b.g.l., the properties were that of Janusfjellet Subgroup. The simulation run time was defined by the valley floor age inferred for that zone (Fig. 5), so that, for zone 0-1 the simulation period was 0.5 to 0 ka, for zone 1-2 it was 1.5 to 0 ka, etc. For zone 10, the simulation period was 10 to 0 ka. The initial ground temperature distribution followed the geothermal gradient reported by Liestøl (1977) (0.025 °C m^{-1}) from a surface temperature of 0 °C. At any subsequent time, the lower boundary condition was defined from the same geothermal gradient resulting in a basal temperature change of less than 0.65°C."

In Table 3, the rock unit hydraulic conductivities derived from literature (the Festingen sandstone, the Janusfjellet subgroup, and the detachment zone) range within one order of magnitude across the three scenarios. While this could be considered a large range in this type of study, comparison to the observed hydraulic head at DH4 indicates that Scenario 1 (low hydraulic conductivity) values are unlikely, leaving a more reasonable half order of magnitude range.

We agree with this consideration and narrow the conductivity range of these units in the modeling experiments of the revised manuscript.

Old version, in Table 3:

Festingen Sandstone	*Fractured sandstone*	10^{-2}	$5{\cdot}10^{-2}$	0.1	0.1
Janusfjellet Subgroub	*Shale*	10^{-4}	$5{\cdot}10^{-4}$	10^{-3}	0.1
Detachment zone	*Fractured shale*	10^{-3}	$5{\cdot}10^{-3}$	10^{-2}	0.1

New version, in Table 3:

Festingen Sandstone	*Fractured sandstone*	$5{\cdot}10^{-2}$	$7.5{\cdot}10^{-2}$	0.1	0.1
Janusfjellet Subgroub	*Shale*	$5{\cdot}10^{-4}$	$7.5{\cdot}10^{-4}$	10^{-3}	0.1
Detachment zone	*Fractured shale*	$5{\cdot}10^{-3}$	$7.5{\cdot}10^{-3}$	10^{-2}	0.1

For the rock units with field data (the Carolinefjellet and Hevetiafjellet formations), the hydraulic conductivities applied range over two orders of magnitude. Does this range represent the maximum and minimum of tested values? It would be of value to plot the probability density function for the hydraulic conductivity values for each formation, selecting the geometric mean as scenario 2, and a more realistic percentile as scenarios 1 and 3 to tighten the potential range for these formations. As stated on line 406, the hydraulic conductivity is the most important parameter in determining the distribution of outflows between the pingos and the Fjord. Assignment of this parameter should be constrained where possible.

We agree with the author that the hydraulic conductivity ranges should be tightened where possible. The proposed approach is included in the revised manuscript and the ranges tightened accordingly.

Old version, Section 4.3.2., Lines 290-301

"Due to the sparse data available from the field area, geothermal and hydrogeological properties of the lithologies in the model domain (Tables 2 and 3) were largely based on typical values found in the literature. An exception was the measurements of porosity and vertical permeability, , in the sandstone units carried out by the Longyearbyen CO2 Laboratory Project (Olaussen et al., 2020, and references therein). Porosity was found to be the most important parameter for permafrost growth, and realistic minimum, mean, and maximum values were therefore defined for the 1DHT model (Table 2). The small-scale horizontal permeability, κ_h, for sandstones is typically a factor two higher than κ_v (Domenico and Schwartz, 1998). The horizontal hydraulic conductivity, K_h, was therefore calculated using the measurements of κ_v by Braathen et al. (2012) as

$$K_h = C_{Kh/Kv} \cdot \frac{\kappa_v \cdot \rho_w \cdot g}{\mu} \quad (7)$$

where $C_{Kh/Kv}$ is the conversion factor (i.e. 2 for this work), κ_v is permeability [m^2], ρ_w is the density of water [kg m^{-3}], g is the gravitational acceleration [m s^{-2}], and μ is the dynamic viscosity of water [kg (m s) $^{-1}$]. Ranges of hydraulic conductivity for the fluvio-deltaic succession were based on literature values from (Fitts, 2002). For the bedrock units we also regarded the influence of fractures (Singhal and Gupta, 2010)."

New version

"Due to the sparse data available from the field area, geothermal and hydrogeological properties of the lithologies in the model domain (Tables 2 and 3) were largely based on the available literature. The considerable contrast between the thermal properties of water and ice implied that porosity was the most important parameter for permafrost growth, and realistic minimum, intermediate, and maximum values were therefore defined for the 1DHT model (Table 2). The permafrost base is presently located within the upper two thirds of the Janusfjellet Subgroup (Figs. 2b and 5a). Estimated burial depths and thicknesses of overlying units (Grundvåg et al., 2019; Marshall et al., 2015) indicate that this strata has been buried to maximum depths between 2150 to 2600 m b.g.l. corresponding to effective vertical stresses between 34 to 41 MPa (assuming a rock density of 2.6 kg m^{-3} and hydrostatic equilibrium). Different studies on the compressibility of lithological and age equivalent rocks in the North Sea thus suggest porosities between 0.08 to 0.3 (Burland, 1990; Okiongbo, 2011; Skempton, 1969; Yang and Aplin, 2004) and we therefore used this range in our modelling experiments. An exception to the purely literature-based values is the sandstone units of which the matrix porosity and vertical permeability, κ_v, were measured as part of the Longyearbyen CO_2 Laboratory Project (Olaussen et al., 2020, and references therein). The small-scale horizontal permeability, κ_h, for sandstones is typically a factor two higher than κ_v (Domenico and Schwartz, 1998). The horizontal hydraulic conductivity, K_h, was therefore calculated using the measurements of κ_v by Braathen et al. (2012) as

$$K_h = C_{Kh/Kv} \cdot \frac{\kappa_v \cdot \rho_w \cdot g}{\mu} \quad (7)$$

where $C_{Kh/Kv}$ is the conversion factor (i.e. 2 for this work), κ_v is permeability [m^2], ρ_w is the density of water [kg m^{-3}], g is the gravitational acceleration [m s^{-2}], and μ is the dynamic viscosity of water [kg (m s) $^{-1}$]. The range of the hydraulic conductivity values of the Carolinefjellet and Helvetiafjellet formations (Festningen Sandstone not included) was defined by the 25 %, 50 % and 75 % percentiles of a Weibull probability fit of the measured values (Supplement). Ranges of hydraulic conductivity for the fluvio-deltaic succession were based on literature values from (Fitts, 2002). For the remaining bedrock units we also regarded the influence of fractures (Singhal and Gupta, 2010)."

Old version, Sect. 4.3.2, in Table 2:

Shale	*$4.73 \cdot 10^{7}$*	*800*	*2600*	*0.1[III]*	*0.2[III]*	*0.3[III]*

New version

Shale	*$4.73 \cdot 10^{7}$*	*800*	*2600*	*0.08[III]*	*0.19[III]*	*0.3[III]*

Old version, Section 4.3.2., in Table 3:

[I]Carolinefjellet Fm	*Sandstone*	*10^{-4}*	*10^{-3}*	*10^{-2}*	*0.1*
[I]u. Helvetiafjellet Fm	*Sandstone*	*10^{-4}*	*10^{-3}*	*10^{-2}*	*0.1*

New version

[I]Carolinefjellet Fm	*Sandstone*	*$2 \cdot 10^{-4}$*	*$5 \cdot 10^{-4}$*	*10^{-3}*	*0.1*
[I]u. Helvetiafjellet Fm	*Sandstone*	*$2 \cdot 10^{-4}$*	*$5 \cdot 10^{-4}$*	*10^{-3}*	*0.1*

In new version of Supplement

"S3 Hydraulic conductivity of Carolinefjellet and Helvetiafjellet Formations

The vertical permeability, κ_v, of the sandstone-dominated Carolinefjellet and Helvetiafjellet formations were measured as part of the Longyearbyen CO_2 Laboratory Project (Olaussen et al., 2020, and references therein). The small-scale horizontal permeability, κ_h, for sandstones is typically a factor two higher than κ_v (Domenico and Schwartz, 1998) and we converted the horizontal hydraulic conductivity, K_h, accordingly (Eq. 7). The ranges of hydraulic conductivity of these units were defined by the 25 %, 50 % and 75 % percentiles of a Weibull probability fit to the measured values (Fig. S5).

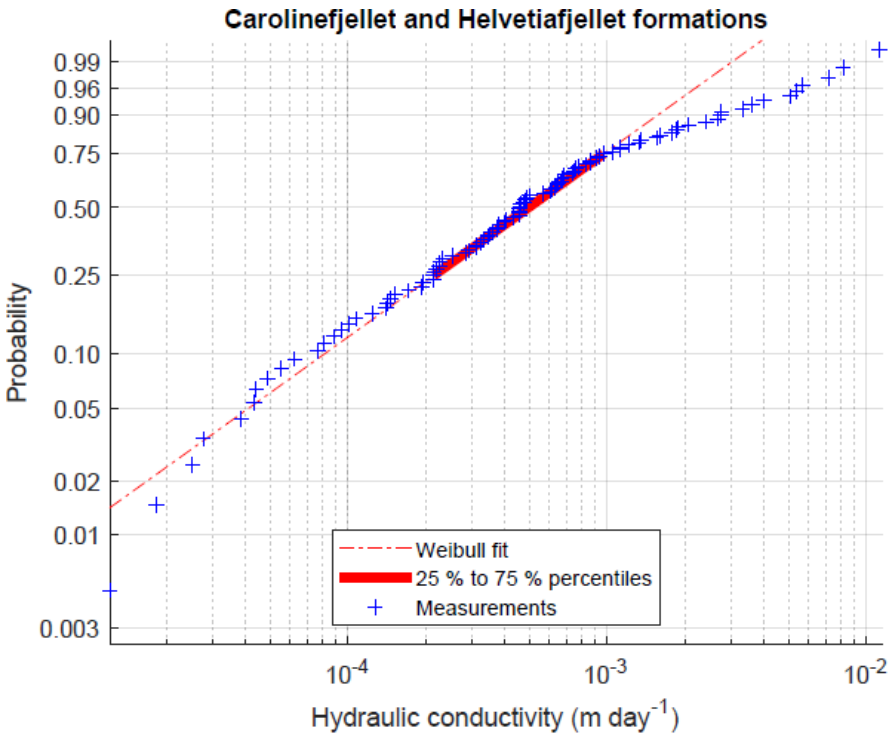

Figure S5 *Weibull fit to measured hydraulic conductivities of Carolinefjellet and Helvetiafjellet formations. Original data from the Longyearbyen CO_2 Laboratory Project (Olaussen et al., 2020, and references therein).”*

On line 515 it is stated that the steady-state assumption for the groundwater flow model results in an underestimate of the present-day pressures. This statement may oversimplify the transient groundwater dynamics that could occur as permafrost aggrades and the sea level retreats. Permafrost aggradation is highest in proximity to the Fjord, which is also where the greatest potential for discharge to the Fjord occurs. It is possible that any excess pressure would be dissipated as the sea level retreats, and that a transient simulation may not show higher pressures.

As stated in Section 3.2 (lines 182-183), sea-level reached close to present levels ~ 5 ka. As such, the sea retreat since then is explained to progradation of the fluvio-deltaic system. Pressure dissipation due to land emergence is therefore not plausible. The statement referred to by the reviewer (Old version, Line 515-516) considers that the omission of dynamic storage effects implies that the predominantly greater permafrost aggradation rates simulated in the past are not taken into account in our model. Effectively, this implies an underestimate of the equivalent recharge. In the revised manuscript, we account for this by applying a moving average to the simulated permafrost aggradation, where the time window is determined by the range of possible adjustment times.

New version, paragraph added to Sect. 4.3.4.:

“The only source of water in the groundwater model was defined from the basal permafrost aggradation rate simulated by the 1DHT model and assigned as recharge to the uppermost active cells in the model domain. To compensate for the lack of dynamic storage effects in the steady-state model, we applied a moving time-average to the simulated basal permafrost growth (or decay) before calculating the

recharge equivalent (Eq. 6). The time window of the moving average was based on the possible range of the adjustment time, t_a, which is the time needed for fluids to redistribute to a pressure perturbation (e.g. Neuzil, 2012; Šuklje, 1969):

$$t_a = l^2 \, S_s \, K^{-1} \qquad (8)$$

where l is half of the shortest dimension of the system (the characteristic length), S_s is the specific storage, and K is the hydraulic conductivity. We found t_a to be shortest in the vertical dimension, but assumed that hydraulic pressures could only dissipate in the horizontal dimension after the formation of continuous permafrost no earlier than 6 ka (Humlum, 2005; this research). Specifically, we estimated the horizontal t_a to be between 20 and 19000 yrs. To quantify this, we used a characteristic length of 1 km. For S_s, we used a matrix compressibility of $7{\cdot}10^{-10}$ to $7{\cdot}10^{-8}$ Pa^{-1} (based on common estimates for fractured rocks, e.g. Domenico and Mifflin, 1965; Domenico and Schwartz, 1998; Fitts, 2002) yielding a S_s of $7{\cdot}10^{-6}$ to $7{\cdot}10^{-4}$ m^{-1} (in line with literature values, c.f. Singhal and Gupta, 2010). For K, we used the values estimated for the dominating geological unit (Janusfjellet Subgroup, Table 3). The time window used to compensate for dynamic storage effects were defined from the above, but no longer than the age of permafrost (i.e. 6000 yrs or less)."

On line 635 it was stated that simulated flows to the pingo springs are likely underestimated as basal permafrost aggradation outside of the model domain is not included. Were this aggradation to contribute to the pingo spring flows, it would imply that the lateral boundaries of the model domain are not hydraulic divides (i.e., no flow boundaries). This statement should be reconciled with the boundary selection.

We have not changed the boundary conditions of the groundwater model. See comments above.

Technical Corrections:

Line 13: ...wet-based glaciers are not present in the adjacent highlands

done

Line 18: ..and groundwater (3D -Steady-state)

done

Line 229 Equation 1: The _z in the denominator should be _z2

done

Line 235: ...heat conduction will flow heat will be conducted through a matrix of solids (i.e sediment or rock) and liquid water, ice or a mixture

done

Line 288: ..The fraction of liquid water

Done (we assume this correction concerns line 238)

Line 247: ...When temperature change occurs

done

References

Rossi, G., Accaino, F., Boaga, J., Petronio, L., Romeo, R., Wheeler, W., 2018. Seismic survey on an open pingo system in Adventdalen Valley, Spitsbergen, Svalbard. Near Surface Geophysics 16, 89–103. https://doi.org/10.3997/1873-0604.2017037

Author response to Referee #2

In this paper, the authors investigate the question: "Why are there pingos in Adventdalen when there seem to be no groundwater recharge? They do this with a conceptual model, and find that the observed pingos are sustained by groundwater supply with residence times exceeding the duration of Holocene. In addition to the modeling, the work relies on a wide range of field observations.

The work presented in this paper is impressive. A new model is developed and data from many different sources are used in the study. However, the manuscript would benefit from revisions to improve readability and clarity. Currently, the manuscript contains many terms and context that need to be explained to expand readership beyond immediate experts and to the diverse backgrounds of the readers of The Cryosphere. The minor comments below provide many examples.

We are very pleased to read that Referee#2 acknowledge our work as impressive and its use of many different data sources. Further, the Referee#2's view is that the manuscript has room for improvement when it comes to clarity and readability, and a number of specific changes to the manuscript are suggested. We agree with the majority of these and abide to them in the revised manuscript.

1. **Many terms and concepts are provided without much context. I give several examples in the minor comments.**

We have strived to use a more concise language in the revised manuscript. The reviews of our manuscript have been very helpful with this.

2. **Organize the manuscript into sections according to the traditional structure of a scientific paper (Abstract, intro, study site, methods and data, results, discussion, conclusions). In the current paper, there is no clearly defined method section and sections 2 to 4 gradually move from introduction to results. a. For example, the section 3.2 title suggests this section contains background information about the study site. However, besides that background information it also explains how climate history was reconstructed. Separate these two so that the background info on lines 150-154 goes in a study site description section, and the rest in a methods subsection about reconstructed temperatures b. Another benefit of a dedicated method section is that you can provide an overview of the methods at the beginning providing the reader with a sort of road map.**

The major headings now read:

- *Abstract*
- *Introduction*
- *Conceptual model of permafrost aggradation driven pingo formation*
- *Study site*
- *Method – Numerical modelling*
- *Results*
- *Discussion*

- *Conclusions*

We have moved the information of how the Holocene temperature was constructed to the method subsection 4.3.3. and rephrased both sections:

Old version, Sect. 3.2., L156-165:

"The mean summer air temperature (MSAT) has consistently been 10 °C warmer than the MAAT (on the 30-yr scale, Førland et al., 1997).

Holocene temperatures on and around Svalbard are relatively well constrained by fossil-based temperature reconstructions. Mangerud and Svendsen (2017) infer a mean summer sea temperature (MSST) curve from the distribution and ^{14}C–dating of thermophilous bivalves and point out that the MSST is essentially identical to the MSAT. As illustrated on Fig. 3a, their MSST curve is largely in agreement with MSST temperature reconstructions from west and southwest of Svalbard (van der Bilt et al., 2018; Hald et al., 2007). Assuming that the present difference between MAAT and MSAT was alike for the entire Holocene, we use a MAAT reconstruction inferred by subtracting 10 °C from the MSST curve by Mangerud and Svendsen (2017) for the modelling of ground temperatures in this work (Fig. 3b). We choose to rely on Mangerud and Svendsen (2017) because; a) their curve is more local to our field area than the alternatives and; b) the suggested timing of the Holocene thermal minimum at ~ 3 to 2 ka is in agreement with the maximum of perennial or semi-permanent land fast sea ice at ~ 2.5 to 2 ka inferred from the minimal occurrence of dated driftwood (Dyke et al., 1997; Farnsworth, 2019; Funder et al., 2011). Furthermore, their curve is better supported by geomorphological evidence of glacier dynamics (Farnsworth, 2019)."

New version:

"For the entire temperature record, the mean summer air temperature (MSAT) has consistently been 10 °C warmer than the MAAT (on the 30-yr scale, Førland et al., 1997). Further back in time, Holocene mean summer sea temperatures (MSST) in and around Svalbard are relatively well constrained by fossil-based temperature reconstructions (Fig. 3a, van der Bilt et al., 2018; Hald et al., 2007; Mangerud and Svendsen, 2017). Mangerud and Svendsen (2017) point out that the MSST is essentially identical to the MSAT."

Old version, Sect. 4.3.3, L317:

"The Holocene temperature curve (Fig. 3) defined the upper boundary condition."

New version:

"The upper boundary condition was defined by the Holocene MAAT curve presented in Fig. 3b. Assuming that the present 10 °C difference between MAAT and MSAT (Førland et al., 1997) was alike for the entire Holocene, we constructed this curve (Fig. 3b) by subtracting 10 °C from the MSST curve by Mangerud and Svendsen (2017) (Fig. 3a). As illustrated on Fig. 3a, their MSST curve is largely in agreement with MSST temperature reconstructions from west and southwest of Svalbard (van der Bilt et al., 2018; Hald et al., 2007). We chose to rely on Mangerud and Svendsen (2017) because; a) their curve is more local to our

field area than the alternatives and; b) the suggested timing of the Holocene thermal minimum at ~ 3 to 2 ka is in agreement with the maximum of perennial or semi-permanent land fast sea ice at ~ 2.5 to 2 ka inferred from the minimal occurrence of dated driftwood (Dyke et al., 1997; Farnsworth et al., 2020; Funder et al., 2011). Furthermore, their curve is better supported by geomorphological evidence of glacier dynamics (Farnsworth et al., 2020)."

3. **None of the tables has captions. It should be possible for a reader to understand tables and figures based on the caption.**

All tables now have captions. See changes in our reply to the comment on tables.

4. **Adding a description of the model simulations (number of simulations, parameterizations etc). in the methods would be helpful for the reader to anticipate the results.**

New paragraph added at the end of section 4.3.4:

New version:

"To represent the uncertainty of how permafrost aggradation affects sub-permafrost groundwater flow, we simulated nine different scenarios that were defined by having three sets of values for the two fundamental parameters in any combination; hydraulic conductivity (Scenarios Sc1–3x, Table 3) and equivalent recharge (Scenarios ScXa–b, values calculated as described above and by Eq. 6). The nine scenarios are all labelled ScXx where X and x indicates the minimum, intermediate or maximum value sets of hydraulic conductivity and equivalent recharge, respectively. We further simulated a tenth scenario that takes additional pressure sources into account."

5. **The simulations with the groundwater model need to be better explained. Clarify what scenarios were run and why. What is the significance of the 3 kyr catchment. How were they drawn in the first place? Figure 7 is very complicated and should be simplified and ideally split up into several figures. In the text, it is stated that each of the 12 zones were run with a different REq. However, the y-axis suggests that only three values were used. Explain why head is visualized with two different types of units?**

Referee#2 is not sure which equivalent recharge rates (REq) were used for which scenario of the groundwater model. We read this confusion as due to a misunderstanding that the subzones of the groundwater model were run individually ("it is stated that each of the 12 zones were run with a different REq"). This was not the case (without specific reference to the text, we can also not find this statement in our manuscript). Instead, the entire surface of the model domain was assigned with the maximum, intermediate or minimum estimates of the REq rate as calculated from heat transfer model results (Fig. 6c). As illustrated on Fig. 6c, the maximum, intermediate or minimum REq value was not uniform, but decreased in the inland direction, and each subzone was thus assigned with the relevant REq rate. As indicated by the y-axis on Fig. 7 and as stated in the text (Old version, L381-382) this resulted in three different total inflow rates of water to the groundwater model.

We have clarified and corrected the manuscript according to the suggestions in this comment (see changes in replies to minor comments) except for splitting up figure 7. Figure 7 was simplified as a consequence of changes arriving from comments by referee#1.

Minor comments:

L13: "methane emissions/release"

Is the suggestion here that " methane" is followed by "emissions" or "release"? This would not be grammatically correct, but we could rephrase. No changes made to the revised manuscript.

L40: Clarify what "they" refers to, e.g. springs

"they" refer to springs. Replaced.

"they" replaced with "springs".

L47-L50. Clarify where the liquid water is coming from if not from the surface (e.g. relic groundwater?)

Old version, L50:

"This would remove the need to invoke groundwater recharge from the surface."

New version:

"This would remove the need to invoke groundwater recharge from the surface as spring outflow derives from relict groundwater."

L70: Here and other places. Be careful with using words like "this" without being more specific about what "this" refers too (here pressure). It is easy for the reader to get lost.

"this" replaced with "pressures"

L72: Define "talik"

Definition added after first use of talik:

Old version, L72

"[…] closed talik (Mackay, 1998)"

New version:

"[…] closed talik (i.e. a perennially unfrozen part of the permafrost) (Mackay, 1998)"

L73: "suggest that and open: : :"

done

L65-72: Somewhere here it would be good to explain the difference between open and closed pingo systems.

Sentence added at the beginning of the section previously starting "Liestøl (1977) suggests…" (Old version, L73):

New version:

"In contrast to closed-system pingos, an open-system pingo is sourced from a body of groundwater that is not enclosed by frozen ground."

L75: be more specific about what "the system" refers to.

Old version, L75:

"[…] the system […]"

New version:

"[…] spring outflow […]"

L82: Avoid abbreviations as much as possible. If you need the, make sure to write them out the first time they are mentioned.

In the old version, the abbreviation was written out, but not at the first occurrence.

Old version, L82:

"MAAT"

New version:

"mean annual air temperature (MAAT)".

Old version L152:

"mean annual air temperatures (MAAT)"

New version:

"MAATs".

L89: Explain what a "through-talik" is and how is it different than a "talik".

Change added to previous sentence. See below.

Old version L82-86:

"Close to the sea, groundwater flows towards the shoreface, but at some distance inland, higher advective heat transfer, associated with higher groundwater velocities, prevents frozen ground formation and groundwater flows through an intrapermafrost talik (through-talik) towards the surface along the most hydraulically conductive path, and a spring (or pingo) forms (as modelled by Scheidegger et al., 2012)."

Replaced with:

"Close to the sea, groundwater flows towards the shoreface, but at some distance inland, higher advective heat transfer, associated with higher groundwater velocities, prevents frozen ground formation. As a consequence, groundwater may flow through a talik that perforates the permafrost (i.e. a through-talik) towards the surface along the most hydraulically conductive path, resulting in a spring (or pingo) (as modelled by Scheidegger et al., 2012)."

L112: Reformulate. It is not clear from Fig 2b that the sediments are fine-grained or pre-Cenozoic.

Simple geological timescale added to the legend on Fig. 2b.

Old version L113:

"As illustrated on Fig. 2b, fine-grained Quaternary sediments (< 70 m thick Gilbert et al., 2018) overly pre-Cenozoic, well-consolidated sedimentary strata in Adventdalen, […]"

New version:

"In Adventdalen, fine-grained Quaternary sediments (< 70 m thick Gilbert et al., 2018) overly pre-Cenozoic, well-consolidated sedimentary strata (Fig. 2b), […]"

L116: What does "these" refer to. All layers or just the surface layers < 70 m? Needs clarification.

"these" refers to all of the aforementioned stratigraphy. Clarified:

Old version, L116-117:

"Together, these form a low-permeability groundwater system. "

New version:

"Together, all these units form a low-permeability groundwater system. "

L131: Explain the term "OSL"

First occurrence of OSL is written out:

Old version, L131:

"OSL"

New version

"optically-stimulated luminescence (OSL)"

L154: Specify period

Old version L153:

"The mean summer air temperature (MSAT) has consistently been […]"

New version:

"For the entire temperature record, the mean summer air temperature (MSAT) has consistently been […]"

L191: Clarify the source of these depth observations and the permafrost depths inferred from those observations.

We now mention the observations sites in the text and the associated references. However, we do not think that writing out the depths helps the reader without having the map (Fig. 2a) to reference the locations. As such, the depths still only appear from Fig. 2a.

Old version, L190-191:

"Specific depth observations support this regional characterisation (Fig. 2a)."

New version:

"One observation of the freezing front depth at Lagoon Pingo (Harada and Yoshikawa, 1996) and permafrost depth observations at well DH4 (Braathen et al., 2012), Endalen, Sarkofagen (both Liestøl, 1977), and Breinosa (Christiansen et al., 2005) support this regional characterisation (Fig. 2a)."

L220: Expand abbrevations, i.e. explain what GMS 10.4 is

In the first submission, we erroneously had the explanation for GMS (as below) at the second occurrence in the text. We do not expand the abbreviation (Groundwater Modelling System) as we think that "groundwater modelling software" is more eloquent.

Old version, L220:

"GMS"

New version:

"the groundwater modelling software GMS"

Old version, L280:

"the groundwater modelling software GMS"

New version:

"GMS"

L252: Rephrase "validate the model we" (you are validating the model, not the code itself)

Old version, L252:

"To validate the model code we […]"

New version:

"To validate the model we […]"

L253: Briefly explain the limitations of the analytical solutions (i.e. answering the question why can't you use these model for your study). Also summarize the findings about the model performance. Make sure to provide quantitative estimates of model performance (e.g. RMSE as in Supp. L79). Statements such as "relatively good performance" (Supp. L58) are not sufficient.

The problems dealt with by the analytical solutions are described in detail in the supplement and the reason why they cannot be used in our study is apparent there. We think it would be too lengthy to put it in the main article as the reasoning demands a description of the analytical solutions.

We now summarize the model performance by having added a sentence:

Sentence added after L254 (Old version):

"The model code was able to reproduce the analytical results with root-mean-square errors of respectively $1.1 \cdot 10^{-2}$ and $1.3 \cdot 10^{-5}$ and these numbers were regarded to represent reasonable accuracy."

L271: Explain the term "A" in equation 6.

Old version, L271:

"where Q_{REq} is equivalent to the source term Q_N in Eq. (5)."

New version:

"where Q_{REq} is equivalent to the source term Q_N in Eq. (5), and A is an area [m^2]."

L281: Better define subzones. The text says that 12 subzones are defined. However, figure 12 does not show these clearly. Table 1 says nothing about subzones.

(There is no Fig. 12 in our manuscript, but we assume that it is Fig. 5 (Fig. 4 in first submission), which is referred to here.)

In the old version of our manuscript, we used both of the terms "subzone" and "zone" to describe the same thing. All occurrences of "subzone" are now replaced with "zone". The definition of the zones is now

expressed more explicitly in the text as well as in the caption of Fig. 5. Figure 5 has also been subject to changes. See these in the list of changes to figures.

Old version, L281-282:

"For the 1DHT model, the geology was simplified into one-dimensional columns for a total of 12 subzones defined based age of the valley floor (Table 1).

New version:

"For the 1DHT model, the geology was simplified into one-dimensional columns for a total of 12 zones of the model area. The zones were defined as follows: The age of the valley floor (Table 1) was used to infer isochrones of valley floor exposure with intervals of 1000 yrs (Fig. 5a). The isochrones defined boundaries between zones and their names (i.e. the zone located between the 5 ka and 6 ka isochrones was named zone 5-6, Fig. 5b). The area between isochrones 9 ka and 10 ka was divided into two zones to incorporate geological variation. "

L293: Explain how you found out that porosity was the most important parameter

Old version, L293-294:

"Porosity was found to be the most important parameter for permafrost growth, and realistic minimum, mean, and maximum values were therefore defined for the 1DHT model (Table 2)."

New version:

"The considerable contrast between the thermal properties of water and ice implied that porosity was the most important parameter for permafrost growth, and realistic minimum, intermediate, and maximum values were therefore defined for the 1DHT model (Table 2)."

L311: Can a grid be one dimensional? Isn't it by definition 2D? I suggest rephrasing.

In our understanding, a grid can be 1D, 2D or 3D. By 1D grid we mean a 3D grid with only one grid line in two out of three dimensions, and where both these grid lines equal unity. However, we agree that rephrasing will add clarity. By rephrasing, we avoid confusion between the domains of the heat transfer model and groundwater model (columns and grid, respectively) We have employed rephrasing as suggested and replaced '1d grid' with 'column':

Old version, L311:

"The model domain contained 12 one-dimensional grids […]"

New version:

"The model domain contained 12 columns […]"

L312: It is not clear from Figure 4 where these 12 grids/columns are located. I suggest adding a point or arrow to identify the locations of the 12 grid/columns

See changes to Fig. 5 in the list of changes to figures.

Old version, L312:

"Each individual grid was associated to the model area zones (Fig. 4) and the geothermal properties were defined accordingly."

New version:

"One column was associated to each of the model area zones and the geothermal properties were defined according to the associated geological 1D simplifications (see insert on Fig. 5b)."

L313. Table 1 shows site locations, not geological units. Do you mean table 3? Either way, explain how the names of the zones refer to the age. It is unclear. Provide a better connection to Figure 4. I suggest making a table with parameters for each of the 12 zones.

Please, also see the changes arising from the comment to L281 (old version).

Old version, L313:

"The names of the zones refer to the age of subaerial exposure (Table 1), which defined the simulation run time (e.g. for zone 0-1 the simulation period was 0.5 to 0 ka, for zone 1-2 it was 1.5 to 0 ka, etc. For zone 10, the simulation period was 10 to 0 ka)."

New version:

"The simulation run time was defined by the valley floor age inferred for that zone (Fig. 5), so that, for zone 0-1 the simulation period was 0.5 to 0 ka, for zone 1-2 it was 1.5 to 0 ka, etc. For zone 10, the simulation period was 10 to 0 ka."

L319: Clarify that this grid is different from the one in the previous section.

This should be obvious now, as we no longer call the 1DHT model domain 'grid'. Clarified further by the following rephrasing:

Old verison, L319-320:

"Each grid cell measured 100 by 100 by 5 m (x y z) and their hydrogeological properties were defined from the geology (Fig. 4, Table 3)."

New version:

"For the groundwater model, each grid cell measured 100 by 100 by 5 m (x y z) and their hydrogeological properties were defined from the geology (Fig. 5a, Table 3)."

L331: Clarify how you dealt with the active layer at the surface (i.e. unfrozen too, but also inactivated?)

Annual temperature variations was not included in the model setup and the seasonal thaw of the active layer was therefore not considered. No changes made to the manuscript based on this comment.

L331: Clarify the meaning of "raw" and how it differs from non-raw simulations

Rephrased to clarify:

Old version, L331-332:

"The raw simulation results from the 1DHT model were […]"

New version:

"The direct output from running the 1DHT model code was […]"

L333: The interpolation is unclear. What was interpolated, time or space? Explain.

Old version, L332-333:

"The evolution of the permafrost and freezing front depths were evaluated by interpolating the associated temperatures for each time step."

New version:

"For each time step, the permafrost and freezing front depths were calculated by interpolating the depth at which the associated temperatures occurred."

L335: Be more specific and clarify. Isn't it the permafrost aggradation in m/s that is inferred from the freezing front?

Strictly speaking, permafrost aggradation is defined by the progression of the 0°C isotherm. What we attempt to express here is that the progression of the -0.7C isotherm is more relevant for the contribution of hydraulic pressures on the GW system, because this is the temperature where the phase change rate if fastest (in our model, that is). We have rephrased and added a sentence to clarify:

Old version, L333-335:

"The greatest phase change rate in the 1DHT model occurs at a temperature of -0.7 °C (following from Eq. 3) and the (always) downwards progression rate of this isotherm was therefore used for the calculation of the equivalent recharge (by net pore space loss, Eq. 6)."

New version:

"The greatest phase change rate in the 1DHT model occurs at a temperature of -0.7 °C (following from Eq. 3) and it was therefore the progression rate of this isotherm that was used for the calculation of the

equivalent recharge (by net pore space loss, Eq. 6). Hereafter, 'permafrost aggradation' therefore means the downwards progression rate of this isotherm (-0.7 °C), although this is not entirely congruent with the thermal definition of permafrost (ground perennially below 0 °C, French, 2017)."

L340: Table 2 does not mentioned "intermediate" values, only, min/mean/max for three materials. Clarify what porosity values was used, and why those were used over other values.

Old version, L294: "mean" replaced with "intermediate"

Table 2: "Mean" replaced with "Intermediate"

L371: Cross reference with tables so that the reader can check this statement. Also provide the name of the layer.

Column added to Table 2 with values of thermal diffusivity.

Old version, L370-374:

"This was due to the different properties of the sediments and bedrock undergoing freezing (Fig. 4). In zone 0-1, closest to the shore, phase change took place at < 60 m b.g.l. corresponding to the most porous and least thermally diffusive unit (the fluvio-deltaic succession). Thus, a relatively high amount of latent heat had to be released for the freezing front to aggrade. By contrast, the opposite was the case in zone 1-2, where the freezing front just entered the sandstone unit that possessed the lowest porosity."

New version

"This was due to the different properties of the sediments and bedrock undergoing freezing. In zone 0-1, closest to the shore, phase change took place at < 60 m b.g.l. corresponding to the most porous and least thermally diffusive unit (Qt1, insert on Fig. 5 and Table 2). Thus, a relatively high amount of latent heat had to be released for the freezing front to aggrade. By contrast, the opposite was the case in zone 1-2, where the freezing front just entered the sandstone unit that possessed the lowest porosity (Carolinefjellet Fm, insert on Fig. 5 and Table 2)."

L374: What about the thermal properties. Also cross-reference with table.

See change in answer to comment above.

L389: Explain how you know this was artesian.

Reference to Fig. 7. Added:

Old version, L389:

"Entirely or almost entirely […]"

New version:

"As illustrated by the colour fill on Fig. 7, entirely or almost entirely […]"

L390: Explain how you know that hydraulic pressures were below hydrostatic as well as the significance of this.

Wrong usage of hydrostatic.

Old version, L390:

"[…] where the up-valley part of the system has hydraulic pressures below hydrostatic."

New version:

[…] where the up-valley part of the system has hydraulic pressures below ground level.

L392: Explain the 3 kyr catchments. Why 3 and not 4 kyr? What is the significance of these "catchments"

The 3 kyr catctments were drawn to visualize a slow moving groundwater system. On Fig. 7, the mean pore water velocities are also provided and indicate the same, but not in a visual manner. The catchment size (time) could also have been 4 kyr, but not 50 yr or 15 kyr. 3 kyr years was chosen as this is the time order on which the modelled conditions have existed.

Old version, L392-393:

"This enabled us to draw 3 kyr catchment zones for each outlet point (the term 'catchment' is somewhat misleading in this context as no actual recharge takes place)."

New version:

"In order to visualise groundwater movement towards the outlet points, we used the particle tracking to draw 3 kyr catchment zones (the term 'catchment' is somewhat misleading in this context as no actual recharge takes place). The 3 kyr duration was chosen because it is on that order of time that the modelled permafrost and groundwater conditions likely existed."

L401: Rephrase and clarify. It reads as if both artesian and non-artesian determine spring sites and has small QREq and high K. Earlier it is written that most of the area was artesian.

Old version, L401-402:

"The artesian/non-artesian conditions clearly determine whether outflow takes place at all pingo spring sites, as was indeed the case for all but three simulations (small Q_{REq} and high K, Figs. 7-2a and 7-3a–b)."

New version:

"The colour fill and the pie charts on Fig. 8 together show that outflow at a pingo site only takes place if the hydraulic pressure is artesian. Outflow from all pingo sites were simulated for four scenarios including all three with maximum Q_{REq} and the one with intermediate Q_{REq} and minimum K (Figs. 8-1b–c, 8-2c and 8-3c)."

L445: Clarify if the characteristic length is equal to l, and why 200 m was selected.

In the revised manuscript, the concept of adjustment time is introduced earlier in a new paragraph added to section 4.3.4 and we here clarify that l denotes the characteristic length (see the paragraph in our reply to referee#1's comment to line 515, old version). As a consequence, section 6.1.1 is now completely rewritten:

New version, Sect. 6.1.1:

"A possible interpretation of anomalous overpressure is that a previous perturbation was long-lived enough to redistribute groundwater (and other fluids) and recent enough for groundwater not to have adjusted to the present conditions (Bahr et al., 1994). The notion of adjustment time (Sect. 4.3.4, Eq. 8) becomes convenient when assessing whether an ice-load removed > 10^4 yr ago could be responsible for present anomalous pressures. For shallow, low-permeable and well-consolidated bedrock systems like the one investigated in this work, we found the vertical t_a to be between 80 and 7500. To calculate this, we used the lowest K-estimate of the dominant hydrogeological unit (Janusfjellet Subgroup, Table 3) and a characteristic length of 200 (approximating half of the thickness of the aforementioned unit). The specific storage was defined like when calculating the horizontal adjustment time (Sect. 4.3.4). Conclusively, we argue that overpressures in systems like the investigated case cannot be explained by equilibration from past glacial loading."

L453: Clarify. Pertubations of what

Old version, L453:

"Past geological or climatic events may be indirectly responsible for ongoing perturbations"

New version:

"Past geological or climatic events may be indirectly responsible for ongoing pressure perturbations"

L536: Be specific about which scenarios you are referring to here.

Rephrased and specific references to scenarios added.

Old version, L534-536:

"Further, discharge from all of the observed pingo springs was not simulated for scenarios with high K's and low equivalent recharge. This could indicate that the real K-values are in effect lower than those employed for these scenarios."

New version:

"Further, discharge from the up-valley pingo springs was not simulated for scenarios with minimum Q_{REq} and maximum K (ScXa and Sc3b, Figs. 8-1a, 8-2a, 8-3a–b)."

L547: Explain why max K values where used. In the previous text you argued for intermediate K values to be the most reasonable.

The high K values were used in order to allow the highest amount of recharge to enter the system. We add this statement in the revised manuscript.

The argument for intermediate K values was an error in the first version of the manuscript and it has been removed from the revised manuscript.

Old version, L549:

"[…] alone (Fig. 7). Figure 9 […]"

New verison:

"[…] alone (Fig. 8). We used the maximum K-values to allow for the highest amount of recharge to enter the system. Figure 10 […]"

Comments on figures and tables ==========

Tables: Add captions

Changes to the tables are explained below

Table 1:

First row removed from table (i.e. number and title)

Added caption:

*"**Table 1** Absolute ages from Adventdalen constraining delta propagation. Depending on the dated material and the host sediment, the dating indicates minimum, approximate or maximum valley floor ages. See Fig. 2 for site locations. HML = Holocene marine limit. Compiled from [I]Åhman (1973), [II]Svensson (1970), [III]Gilbert et al. (2018), [IV]Yoshikawa and Nakamura (1996) and [V]Lønne and Nemec (2004)."*

Sentence removed in revised manuscript:

Old version, L185-186:

"Depending on the dated material and the host sediment, the dating indicates minimum, approximate or maximum ages of subaerial exposure (i.e. exposure to MAATs)."

Table 2

First row removed from table (i.e. number and title)

Column added showing thermal diffusivities

Reference indicated for all values

Caption added:

*"**Table 2** Geothermal material properties used in the heat transfer model. Density and thermal properties compiled from [I]Williams and Smith (1989), [II]Robertson (1988), and [III]Manger (1963). Porosities from [IV]Fitts (2002), [V]Braathen et al. (2012), and based on works by [VI]Burland (1990), Grundvåg et al. (2019), Marshall et al. (2015), Okiongbo (2011), and Yang and Aplin (2004) (see text)."*

Table 3:

"Table 3" removed from table

References for values indicated for all hydrogeological units

Caption added:

*"**Table 3** Properties of the hydrogeological units used in the groundwater model. Values based on [I]Fitts (2002) and [II]Singhal and Gupta (2010) or evaluated from [III]Braathen et al. (2012) (see Supplement)."*

Table 2: Be more specific about what source you sued for what properties by using. The way it is done for porosity is great, do this for all parameters and other tables as well.

See changes in reply to the previous comment.

Figure S1 should be in the main article. However, I suggest creating different types of boxes in the flow chart to distinguish between data outputs and inputs, calculations/algorithms, and decisions. Make sure the groundwater model MODFLOW in the diagram

The figure is now removed from the supplement and placed in the main article as a Fig. 4. Figure changed according to suggestions.

Old version, Supplement, caption to Figure S1:

"Figure S1 Schematic overview of the inner workings of the decoupled heat and groundwater model."

New version, Caption fig. 4:

*"**Figure 4** Schematic overview of the inner workings of the decoupled heat and groundwater model. Model setup, calculations and algorithms are indicated with sharp corners and bold text. Validation and comparison of simulations and observations are indicated with round corners and italics. Input and output data are indicated with rounded corners, grey background and normal text."*

Figure 1: This is a great figure to illustrate the conceptual model. To improve., consider using another shading to identify permafrost

Shading added to indicate frozen ground.

Figure 2 caption. Several words, terms, sites mentioned within parenthesis are unclear without context. Clarify the meaning/context of these, including: "temperature loggings", "Sarkofagen",

"Breinosa", "geophysics". Be specific about what "Map data" you refer to, e.g. topographic data in panel a. Add at the end "description of the layers shown in cross sections A, B, and C". Add compass to the map since directions are discussed in the text later. Also point out the direction towards Longyearbyen

- *Compass added. The location of Longyearbyen is now indicated. Site name "Longyeardalen" removed to make room for this. The location of Longyearbyen airport is now shown.*
- *"(temperature logging)" and "(geophysics)" was written to indicate the methods that were used to measure the depths. Now removed to avoid confusion. Site names in parenthesis (i.e. Sarkofagen, DH4 and Breinosa) all appear from the figure. Sentence rephrased to clarify that these are site names.*
- *"Map data" specified.*
- *Sentence added at the end of the caption as suggested.*

Old version, caption to Figure 2, L104-111:

*"**Figure 2 (a)** Map of Lower Adventdalen with the location of data resources, pingos and the Holocene marine limit. LP=Lagoon Pingo, LYRP=Longyear Pingo, FHP=Førstehytte Pingo, IHP=Innerhytte Pingo, RP=River Pingo. Core logs from boreholes S1–3 and D1–D7 (respectively, Gilbert et al., 2018, and Olaussen et al., 2020, and references therein), seismic lines (Bælum et al., 2012, and unpublished commercial lines from Norsk Hydro) and a geological map (Norwegian Polar Institute, 2019) were used to build the geological model (Fig. 4) (see details in Hornum, 2018). Permafrost depths (temperature logging) are from Liestøl (1977) (Sarkofagen), Braathen et al. (2012) (DH4), and (Christiansen et al., 2005) (Breinosa). The freezing front depth (geophysics) is from Yoshikawa and Harada (1995). Map data by courtesy of Norwegian Polar Institute (2019). **(b)** Geological cross sections constructed based on the resources mentioned above. See Sect. 3.1 for a (hydro)geological description."*

New version:

*"**Figure 2 (a)** Map of Lower Adventdalen with the location of data resources, pingos and the Holocene marine limit. LP=Lagoon Pingo, LYRP=Longyear Pingo, FHP=Førstehytte Pingo, IHP=Innerhytte Pingo, RP=River Pingo. Core logs from boreholes S1–3 and D1–D7 (respectively, Gilbert et al., 2018, and Olaussen et al., 2020, and references therein), seismic lines (Bælum et al., 2012, and unpublished commercial lines from Norsk Hydro) and a geological map (Norwegian Polar Institute, 2019) were used to build the geological model (Fig. 5a) (see details in Hornum, 2018). Permafrost depth measurements at the Sarkofagen, DH4 and Breinosa sites are from Liestøl (1977), Braathen et al. (2012), and Christiansen et al. (2005), respectively. The freezing front depth at LP is from Yoshikawa and Harada (1995). Data used to develop the map including topography, glacial extent, and fluvial network by courtesy of Norwegian Polar Institute (2019). **(b)** Geological cross sections constructed based on the resources mentioned above. The Quaternary unit overly well-consolidated sedimentary strata of pre-Cenozoic age (i.e. Cretaceous or older). See Sect. 3.1 for a (hydro)geological description of the layers shown in the cross sections A, B and C."*

Figure 3. Explain the time axis. Time in relation to what (i.e. what is time 0 = present day). Use colors instead of dashed lines. The grey shaded are of driftwood arrival is almost impossible to see, use colors for this too.

- *The time axis is in 'ka' and with this unit we means 1000 years before present. This was already stated in the first version of the manuscript (at the first occurrence, L129). To further clarify, we now also explain the unit in the caption.*
- *We now use colors instead of the dashed lines.*
- *We have kept the grey dashed area, but darkened it to make it more visible.*

Old version, caption for Figure 3, L170-172:

*"F**igure 3** Holocene temperature reconstructions. Dashed light grey area indicate time of minimal driftwood arrival 170 (Farnsworth, 2019). **(a)** MSST curves (= MSAT, see text). Solid line from Mangerud and Svendsen (2017). Dotted line from Hald et al. (2007). Dashed line from van der Bilt et al. (2018). **(b)** MAAT used in this work. Based on Mangerud and Svendsen (2017) and Førland et al. (1997)."*

New version:

*"**Figure 3** Holocene temperature reconstructions in and around Svalbard. Dashed grey area indicate time of minimal driftwood arrival (Farnsworth et al., 2020). The unit of the time axis is ka = 10^3 years before present. **(a)** MSST curves (= MSAT, see text). Red line from Mangerud and Svendsen (2017). Orange line from Hald et al. (2007). Blue line from van der Bilt et al. (2018). **(b)** MAAT used in this work. Based on Mangerud and Svendsen (2017) and Førland et al. (1997) (see Sect. 4.3.3)."*

Figure 4: Clarify that the inset maps shows the 1D simplifications of the model area. Choose one word to describe the 1D simplification (simplifications or interpretation). Explain the numbering of the subzones. Why does it start with zero and why is there a 10b. Why not go from 1 to 12? Explain everything shown in the figure, e.g. the red arrows pointing out pingo locations.

- *Figure 4 is now fig 5*
- *We have clarified the meaning of the inset by making the labelling of the zones (now only called 'zones') more visible.*
- *1D simplifications are now only called so.*
- *The labelling of the zones is now explained in the caption. Isochrones added to the figures.*
- *Legend added to make the figure easier to read.*
- *A zone map is now provided in a new panel b.*

Old caption:

*"**Figure 4** 3D geological model of subsurface below the valley floor in Adventdalen and vertical 1D simplifications below subzones of the model area. The former determines the hydrogeological properties in the groundwater model (Table 3), whereas the latter determines the geothermal properties in the 1DHT model (Table 2). The subzones were defined based on the reconstruction of fjord retreat and their names indicate the exposure ages (i.e. zone 0-1 became sub-aerially exposed between 1 and 0 ka, zone 1-2 between 2 and 1 ka, etc.)."*

New caption:

*"**Figure 5 (a)** 3D geological model of the subsurface below the valley floor in Adventdalen and vertical 1D simplifications (inset in upper right corner) below zones of the model area. The former determines the hydrogeological properties in the groundwater model (Table 3), whereas the latter determines the geothermal properties in the 1DHT model (Table 2). The domain of the 1DHT model extends to 1000 m b.g.l. (not shown). Deeper than 300 m b.g.l., geothermal properties were defined as for Janusfjellet Subgroup. The sea retreat reconstruction was inferred from absolute datings (Table 1) and is illustrated by valley floor exposure isochrones (red dashed lines). Pingos are indicated with blue arrows. **(b)** Vertical view of the model area showing the zonation. The aforementioned isochrones defined the zone names so that the valley floor exposure age of a zone is apparent from its name (i.e. zone 0-1 became sub-aerially exposed between 1 and 0 ka, zone 1-2 between 2 and 1 ka, etc.). "*

Figure 5: This figures shows better what the zones are. Something like this is needed in figure 4 but indicating all zones. Why not just label the zones 1, 2, 3 and so on. But you also need to explain in the caption what all elements in the figure are (including the zone map)

Old caption:

*"**Figure 5** Development of simulated freezing front and permafrost front depths from zones 2-3, 7-8 and 9-10b (Fig. 4). These simulation results derive when using the intermediate porosity values (Table 2). Note that completely frozen ground does not establish permanently until ~ 6.5 ka."*

New caption:

*"**Figure 5** Development of simulated freezing front and permafrost front depths from zones 2-3, 7-8 and 9-10b of the model area (see Fig. 4). These simulation results derive when using the intermediate porosity values (Table 2). Note that completely frozen ground does not establish permanently until ~ 6.5 ka."*

Figure 6: Clarify that the uncertainty fields are uncertainty due to porosity. Why are symbols include in the middle chart, but not in the top and bottom chart? Make the chart constant.

Now figure 7.

Figure changed due to new model setup.

Figure 7: The nine scenarios need to be explained in the method section. Explain how were they selected and parameterized. The figure is difficult to understand. Simplify and split up into multiple figures and tables. What does the colors mean for the DH4 borehole?

Now figure 8.

Scenarios explained in the methods sections.

The figure was simplified as a result of changes suggested by Referee #1. In order to ease comparison and keep an overview of the modelling results from all scenarios, we have not split up the figure. However, if the reviewer still thinks that this would add clarity, we will be happy to do so.

References in replies to comments

Åhman, R.: Studier av pingoer i Adventdalen och Reindalen på Spetsbergen, Lunds Univ. Naturgeografiska Institution. Rapp. och Not., 15, 27–44, 1973.

Bælum, K., Johansen, T. A., Johnsen, H., Rød, K., Ruud, B. O. and Braathen, A.: Subsurface structures of the longyearbyen CO2 lab study area in central spitsbergen (arctic Norway), as mapped by reflection seismic data, Nor. Geol. Tidsskr., 92(4), 377–389, 2012.

Bahr, J. M., Moline, G. R. and Nadon, G. C.: Anomalous Pressures in the Deep Michigan Basin, in AAPG Memoir 61: Basin Compartmensts and Seals, pp. 153–165., 1994.

van der Bilt, W. G. M., D'Andrea, W. J., Bakke, J., Balascio, N. L., Werner, J. P., Gjerde, M. and Bradley, R. S.: Alkenone-based reconstructions reveal four-phase Holocene temperature evolution for High Arctic Svalbard, Quat. Sci. Rev., 183, 204–213, doi:10.1016/j.quascirev.2016.10.006, 2018.

Braathen, A., Bælum, K., Christiansen, H. H., Dahl, T., Eiken, O., Elvebakk, H., Hansen, F., Hanssen, T. H., Jochmann, M., Johansen, T. A., Johnsen, H., Larsen, L., Lie, T., Mertes, J., Mørk, A., Mørk, M. B., Nemec, W., Olaussen, S., Oye, V., Rød, K., Titlestad, G. O., Tveranger, J. and Vagle, K.: The Longyearbyen CO2 Lab of Svalbard, Norway - Initial Assessment of the Geological Conditions for CO2 Sequestration, Nor. Geol. Tidsskr., 92(4), 353–376, 2012.

Burland, J. B.: On the compressibility and shear strength of natural clays., 1990.

Christiansen, H. H., French, H. M. and Humlum, O.: Permafrost in the Gruve-7 mine, Adventdalen, Svalbard, Nor. Geogr. Tidsskr., 59(2), 109–115, doi:10.1080/00291950510020592, 2005.

Domenico, P. A. and Mifflin, M. D.: Water from low-permeability sediments and land subsidence, Water Resour. Res., 1(4), 563–576, doi:10.1029/WR001i004p00563, 1965.

Domenico, P. A. and Schwartz, F. W.: Physical and chemical hydrogeology, Wiley & Sons., 1998.

Dyke, A. S., England, J., Reimnitz, E. and Jette, H.: Changes in driftwood delivery to the Canadian Arctic Archipelago, Arctic, 50(1), 1–16, 1997.

Farnsworth, W. R., Ingólfsson, Ó., Alexanderson, H., Allaart, L., Forwick, M., Noormets, R., Retelle, M. and Schomacker, A.: Holocene glacial history of Svalbard: Status, perspectives and challenges, Earth-Science Rev., doi:10.1016/j.earscirev.2020.103249, 2020.

Fitts, C. R.: Groundwater Science, 1st ed., Academic Press., 2002.

Førland, E. J., Hanssen-Bauer, I. and Nordli, Ø.: Climate statistics and longterm series of temperature and precipitation at Svalbard and Jan Mayen, Norwegian Meteorological Institute, DNMI Nor. Meteorol. Inst. Rep., 21, 1997.

French, H. M.: The Periglacial Environment, 4th ed., John Wiley & Sons Ltd., 2017.

Funder, S., Goosse, H., Jepsen, H., Kaas, E., Kjær, K. H., Korsgaard, N. J., Larsen, N. K., Linderson, H., Lysså, A., Möller, P., Olsen, J. and Willerslev, E.: A 10,000-year record of Arctic Ocean Sea-ice variability - View from the beach, Science (80-.)., 333(6043), 747–750, doi:10.1126/science.1202760, 2011.

Gilbert, G. L., O'Neill, H. B., Nemec, W., Thiel, C., Christiansen, H. H. and Buylaert, J. P.: Late Quaternary

sedimentation and permafrost development in a Svalbard fjord-valley, Norwegian high Arctic, Sedimentology, 65(7), 2531–2558, doi:10.1111/sed.12476, 2018.

Grundvåg, S.-A., Jelby, M. E., Sliwinska, K. K., Nøhr-Hansen, H., Aadland, T., Sandvik, S. E., Tennvassås, I., Engen, T. and Olaussen, S.: Sedimentology and palynology of the Lower Cretaceous succession of central Spitsbergen: integration of subsurface and outcrop data, Nor. J. Geol., 99(2), doi:10.17850/njg006, 2019.

Hald, M., Andersson, C., Ebbesen, H., Jansen, E., Klitgaard-Kristensen, D., Risebrobakken, B., Salomonsen, G. R., Sarnthein, M., Sejrup, H. P. and Telford, R. J.: Variations in temperature and extent of Atlantic Water in the northern North Atlantic during the Holocene, Quat. Sci. Rev., 26, 3423–3440, doi:10.1016/j.quascirev.2007.10.005, 2007.

Harada, K. and Yoshikawa, K.: Permafrost age and thickness near Adventfjorden, Spitsbergen, Polar Geogr., 20(4), 267–281, doi:10.1080/10889379609377607, 1996.

Hodson, A., Nowak, A., Senger, K., Redeker, K. R., Christiansen, H. H., Jessen, S., Hornum, M. T., Betlem, P., Thornton, S., Turchyn, A. V., Olaussen, S. and Marca, A.: Open system pingos as hotspots for sub-permafrost methane emission in Svalbard, in review, Cryosph. Discuss., doi:10.5194/tc-2020-11, 2020.

Hornum, M. T.: Postglacial Rebound, Permafrost Growth, and its Impact on Groundwater Flow and Pingo Formation, University of Copenhagen. [online] Available from: https://www.researchgate.net/profile/Mikkel_Hornum2, 2018.

Humlum, O.: Holocene permafrost aggradation in Svalbard, Geol. Soc. Spec. Publ., 242, 119–130, doi:10.1144/GSL.SP.2005.242.01.11, 2005.

Leith, K., Moore, J. R., Amann, F. and Loew, S.: Subglacial extensional fracture development and implications for Alpine Valley evolution, J. Geophys. Res. Earth Surf., 119(1), 62–81, doi:10.1002/2012JF002691, 2014.

Liestøl, O.: Pingos, springs, and permafrost in Spitsbergen, Nor. Polarinstitutt Årb. 1975, 7–29, 1977.

Lønne, I. and Nemec, W.: High-arctic fan delta recording deglaciation and environment disequilibrium, Sedimentology, 51(3), 553–589, doi:10.1111/j.1365-3091.2004.00636.x, 2004.

Manger, G. E.: Porosity and Bulk Density of Sedimentary Rocks, Geol. Surv. Bull., 1144-E, doi:10.1111/nan.12452, 1963.

Mangerud, J. and Svendsen, J. I.: The Holocene Thermal Maximum around Svalbard, Arctic North Atlantic; molluscs show early and exceptional warmth, The Holocene, 28(1), 65–83, doi:10.1177/0959683617715701, 2017.

Marshall, C., Uguna, J., Large, D. J., Meredith, W., Jochmann, M., Friis, B., Vane, C., Spiro, B. F., Snape, C. E. and Orheim, A.: Geochemistry and petrology of palaeocene coals from Spitzbergen - Part 2: Maturity variations and implications for local and regional burial models, Int. J. Coal Geol., 143, 1–10, doi:10.1016/j.coal.2015.03.013, 2015.

Neuzil, C. E.: Hydromechanical effects of continental glaciation on groundwater systems, Geofluids, 12(1), 22–37, doi:10.1111/j.1468-8123.2011.00347.x, 2012.

Norwegian Polar Institute: Map data, [online] Available from: https://geodata.npolar.no/ (Accessed 13 May 2020), 2019.

Okiongbo, K. S.: Effective Stress-Porosity Relationship above and Within the Oil Window in the North Sea Basin, Res. J. Appl. Sci. Eng. Technol., 3(1), 32–38, 2011.

Olaussen, S., Senger, K., Braathen, A., Grundvåg, S.-A. and Mørk, A.: You learn as long as you drill; research synthesis from the Longyearbyen CO2 Laboratory, Svalbard, Norway, Nor. J. Geol., 99(2), 157–187, doi:10.17850/njg008, 2020.

Robertson, E. C.: Thermal properties of rocks. Report 88-441, US Dep. Inter. Geol. Surv., 106, 1988.

Rossi, G., Accaino, F., Boaga, J., Petronio, L., Romeo, R. and Wheeler, W.: Seismic survey on an open pingo system in Adventdalen Valley, Spitsbergen, Svalbard, Near Surf. Geophys., 16(1), 89–103, doi:10.3997/1873-0604.2017037, 2018.

Scheidegger, J. M., Bense, V. F. and Grasby, S. E.: Transient nature of Arctic spring systems driven by subglacial meltwater, Geophys. Res. Lett., 39(12), 1–6, doi:10.1029/2012GL051445, 2012.

Singhal, B. B. S. and Gupta, R. P.: Applied Hydrogeology of Fractured Rocks, 2nd ed., Springer Netherlands., 2010.

Skempton, A. W.: The consolidation of clays by gravitational compaction, Q. J. Geol. Soc. London, 125(1–4), 373–408, doi:10.1144/gsjgs.125.1.0373, 1969.

Šuklje, L.: Rheologic Aspects of Soil Mechanics, 1st ed., Wiley-Interscience., 1969.

Svensson, H.: Pingos i yttre delen av Adventdalen, Nor. Polarinstitutt Årb. 1969, 168–174, 1970.

Williams, P. J. and Smith, M. W.: The ground thermal regime, in The Frozen Earth, pp. 83–121, Cambridge University Press., 1989.

Yang, Y. and Aplin, A. C.: Definition and practical application of mudstone porosity-effective stress relationships, Pet. Geosci., 10(2), 153–162, doi:https://doi.org/10.1144/1354-079302-567, 2004.

Yoshikawa, K. and Harada, K.: Observations on nearshore pingo growth, Adventdalen, Spitsbergen, Permafr. Periglac. Process., 6(4), 361–372, doi:10.1002/ppp.3430060407, 1995.

Yoshikawa, K. and Nakamura, T.: Pingo growth ages in the delta area, Adventdalen, Spitsbergen, Polar Rec. (Gr. Brit)., doi:10.1017/S0032247400067565, 1996.

Numerical modelling of permafrost spring discharge and open-system pingo formation induced by basal permafrost aggradation

Mikkel T. Hornum[1,2], Andrew J. Hodson[1,3], Søren Jessen[2], Victor Bense[4], Kim Senger[1]

[1]Department of Arctic Geology, The University Centre in Svalbard (UNIS), N-9171 Longyearbyen, Norway.
[2]Department of Geosciences and Natural Resource Management, University of Copenhagen, 1350 Copenhagen K, Denmark.
[3]Department of Environmental Science, Western Norway University of Applied Sciences, ~~Røyrgata 6,~~ N-6856 Sogndal, Norway
[4]Department of Environmental Sciences, Wageningen University, 6708PB Wageningen, Netherlands.

Correspondence to: Mikkel T. Hornum (~~toftmikkel@gmail.com~~mth@ign.ku.dk)

Abstract

In the high Arctic valley of Adventdalen, Svalbard, sub-permafrost groundwater feeds several pingo springs distributed along the valley axis. The driving mechanism for groundwater discharge and associated pingo formation is enigmatic because wet-based glaciers are not present in the adjacent highlands and the presence of continuous permafrost seem to preclude recharge of the sub-permafrost groundwater system by either a sub-glacial source or a precipitation surplus. Since the pingo springs enable methane that has accumulated underneath the permafrost to escape directly to the atmosphere, our limited understanding of the groundwater system brings significant uncertainty to ~~the understanding~~predictions of how methane emissions will respond to changing climate. We address this problem with a new conceptual model for open-system pingo formation wherein pingo growth is sustained by sub-permafrost pressure effects, as related to the expansion of water upon freezing, during millennial scale basal permafrost aggradation. We test the viability of this mechanism for generating groundwater flow with decoupled heat (1D-transient) and groundwater (~~2D~~3D-steady-state) transport modelling experiments. Our results ~~show~~suggest that the conceptual model represents a feasible mechanism for the formation of open-system pingos in lower Adventdalen ~~easily conform to this conceptual model.~~and elsewhere. Simulations also suggest that the generally low-permeability hydrogeological units cause groundwater residence times ~~that~~to exceed the duration of the Holocene. The likelihood of such pre-Holocene groundwater ages is also supported by the ~~hydrogeochemistry~~geochemistry of the pingo springs, which ~~demonstrate a~~ demonstrates an unexpected sea-~~wards~~ward freshening of groundwater, potentially ~~supplied~~caused by a paleo-subglacial ~~melting during~~melt water "wedge" from the Weichselian. ~~Such waters form a~~This sub-permafrost ~~fresh water~~ wedge ~~that~~ progressively thins inland, ~~where the duration of~~as permafrost ~~aggradation is longest. The mixing ratio of the underlying marine waters therefore~~thickness (and age) increases ~~in this direction because~~and so, less unfrozen freshwater is available for mixing. Although this unusual hydraulic system is most likely governed by permafrost aggradation, the potential for additional ~~pressurization~~pressurisation is also explored. We ~~conclude~~find that methane production and methane clathrate formation ~~may also affect~~ /dissolution deserve particular attention on account of their likely effects upon the hydraulic ~~the~~ pressure ~~in sub-permafrost aquifers, but additional research is needed to fully establish their influence~~at the study site

and others like it.

1. Introduction

Sub-permafrost groundwater systems are highly inaccessible and so their investigation usually relies on sparse data (van der Ploeg et al., 2012). However, cold regions increasingly become hydrogeologically active after surface warming and associated permafrost degradation. This implies, for example, an increased outflow of deeper groundwater to rivers and lakes (Bense et al., 2012), increased rates of biogeochemical processes (Grosse et al., 2016), and potentially increased fluxes of methane or other compounds into the surface environment and atmosphere (Schuster et al., 2018). The surface discharge of sub-permafrost groundwater is currently exemplified by springs in the high Arctic ~~(Andersen et al., 2002; Grasby et al., 2012; Haldorsen et al., 1996; Williams, 1970)~~(Andersen et al., 2002; Grasby et al., 2012; Haldorsen et al., 1996; Williams, 1970). If conditions are ~~favorable~~favourable, spring outflow may instead freeze below the active layer and initiate the growth of an ice-cored hill or pingo. By definition, this would classify as an open-system pingo because of the open connection to the sub-permafrost groundwater (Liestøl, 1996). Considerable methane stocks may exist below continuous permafrost and where no such springs exist, the only rapid escape route goes to the ocean, where methane oxidation prevents much of it from reaching the atmosphere (Mau et al., 2017; Myhre et al., 2016). Where ~~they~~springs do exist, however, sub-permafrost methane may escape directly to the atmosphere, contributing significantly to the total landscape methane emissions (Betlem et al., 2019; Hodson et al., ~~In Review~~2019).

The hydrogeological mechanisms causing the sustained flow of sub-permafrost groundwater to surface springs remain elusive (Scheidegger et al., 2012). Earlier it was proposed that subglacial meltwater from underneath warm-based ice sheets or glaciers would sufficiently recharge a sub-permafrost aquifer (Demidov et al., 2019; Liestøl, 1977; Scheidegger et al., 2012; Scheidegger and Bense, 2014). However, in regions of continuous permafrost lacking warm-based glaciers or other groundwater recharge pathways, such models do not seem applicable (Ballantyne, 2018; Grasby et al., 2014; Woo, 2012). An alternative model to explain the existence of perennial springs in such environments is that hydraulic head gradients in the sub-permafrost hydrogeological system are maintained by artesian pressure generated by past or current aggradation of basal permafrost (Fig. 1). This would remove the need to invoke groundwater recharge from the surface~~.~~ as spring outflow derives from relict groundwater. Furthermore, it might explain the formation of emergence-related open system pingos in coastal lowlands (Burr et al., 2009; Yoshikawa and Harada, 1995).

In this paper, we use field data from Adventdalen, Svalbard, in combination with numerical modelling of heat and groundwater transport to evaluate the hypothesis that perennial spring flow through continuous permafrost can be driven by sub-permafrost artesian pressure produced by basal permafrost aggradation. Alternative causes of anomalous pressures are also discussed, including overpressure remaining from past perturbations (e.g. glacial loading) or contemporary processes such as equilibration of groundwater density contrasts and gas production. The investigation of the above hypothesis is based on decoupled heat and groundwater modelling, but in the discussion, this is combined with inverse analyses of spring geochemistry from a series of open-system pingos within the valley. A 1D heat transfer model forced by reconstructed paleo-temperatures serves to simulate Holocene ground temperatures and permafrost development in the valley floor of Adventdalen. By considering the expansion of water upon freezing, the simulated rates of present permafrost aggradation must cause a loss in aquifer volume equivalent to a recharge rate. This apparent recharge defines the only inflow term to a steady-state 3D groundwater model that simulates the present state of the sub-

Formatted: English (United Kingdom)
Formatted: English (United Kingdom)
Formatted: English (United Kingdom)
Field Code Changed
Formatted: English (United Kingdom)
Field Code Changed
Formatted: English (United Kingdom)
Formatted: English (United Kingdom)
Field Code Changed
Formatted: English (United Kingdom)
Formatted: English (United Kingdom)
Field Code Changed
Formatted: English (United Kingdom)
Formatted: English (United Kingdom)
Formatted: Danish
Formatted: English (United Kingdom)
Formatted: English (United Kingdom)
Formatted: English (United Kingdom)
Formatted: English (United Kingdom)
Formatted: English (United Kingdom)
Formatted: English (United Kingdom)
Formatted: English (United Kingdom)
Formatted: English (United Kingdom)
Field Code Changed
Formatted: English (United Kingdom)
Field Code Changed
Formatted: English (United Kingdom)
Formatted: English (United Kingdom)
Formatted: English (United Kingdom)
Formatted: Danish
Formatted: English (United Kingdom)
Field Code Changed
Formatted: English (United Kingdom)
Formatted: English (United Kingdom)
Formatted: English (United Kingdom)
Field Code Changed
Formatted: English (United Kingdom)
Formatted: English (United Kingdom)

permafrost groundwater system. The modelling results are then discussed in relation to the hydrochemical observations of the pingo spring waters.

2. Conceptual model of permafrost aggradation-driven pingo formation

When permafrost aggrades into the ground, water in the pore space freezes, and hence expands. At shallower depths this is evident from ice lenses and other types of visible ground ice, resulting in ground heave, but from a certain depth downwards (e.g. ~ 5 m in Adventdalen: Gilbert et al., 2018), these cryostructures are no longer observed (French, 2017). Instead, the lithostatic pressure prevents ground heave and the ice expansion induces an overpressure (with regard to the hydrostatic pressure) on the sub-permafrost groundwater, especially where ~~this~~pressures cannot dissipate in an efficient manner. The process is well known from closed-system pingos, where groundwater is enclosed by aggrading permafrost and expelled to the surface from a closed talik (i.e. a perennially unfrozen part of the permafrost) (Mackay, 1998).

In contrast to closed-system pingos, an open-system pingo is sourced from a body of groundwater that is not enclosed by frozen ground. Liestøl (1977) suggests that an open-system pingo-spring can be driven by recharge from subglacial melting of warm-based glaciers. Scheidegger et al. (2012) developed a coupled model of transient permafrost formation and showed how hydraulic heads can maintain ~~the system~~spring outflow for millennia even when permafrost is aggrading (disregarding ice expansion). In our study, we test the hypothesis that permafrost aggradation itself can generate such excess head.

Figure 1 illustrates our conceptual model for open-system pingo formation by basal permafrost aggradation and presents the additional conditions that also have to be met. The assumed starting point is a coastal landscape with no permafrost and a subsurface consisting of a hydrogeological unit in which hydraulic pressures dissipate poorly (Fig. 1a). Figures 1b and 1c illustrate that a negative shift in the surface energy balance results in permafrost aggradation. Freezing pressure is induced at the freezing front resulting in hydraulic head gradients. The shift in the surface energy balance may occur due to a drop in the mean annual air temperature (MAAT) (Figs. 1b–c), a regressing shoreline (Fig. 1c), rapid erosion (not illustrated), or a combination of any of these. Close to the sea, groundwater flows towards the shoreface, but at some distance inland, higher advective heat transfer, associated with higher groundwater velocities, prevents frozen ground formation ~~and~~. As a consequence, groundwater ~~flows~~may flow through ~~an intra-~~a talik that perforates the permafrost ~~talik (~~(i.e. a through-talik) towards the surface along the most hydraulically conductive path, ~~and~~resulting in a spring (or pingo) ~~forms~~ (as modelled by Scheidegger et al., 2012). Freeze-up of the through-talik is further restricted if permafrost aggradation lowers the melting point by increasing pressure and/or salinity. Figure 1d illustrates that when ground temperatures are eventually in equilibrium with the MAAT, permafrost aggradation has stagnated, and so groundwater flow to the pingos has ceased. Due to the lack of advective heat transfer, the through-talik might therefore close and, if so, irreversibly de-activate pingo spring discharge (although salinity may keep the through-talik open, in spite of no-flow).

Formatted: English (United Kingdom)
Formatted: English (United Kingdom)
Formatted: English (United Kingdom)
Field Code Changed
Field Code Changed
Formatted: English (United Kingdom)
Formatted: English (United Kingdom)
Formatted: English (United Kingdom)
Formatted: English (United Kingdom)
Field Code Changed
Formatted: English (United Kingdom)
Formatted: English (United Kingdom)
Formatted: Indent: First line: 0 cm
Field Code Changed
Formatted: English (United Kingdom)
Formatted: English (United Kingdom)
Formatted: English (United Kingdom)
Field Code Changed
Formatted: English (United Kingdom)
Formatted: English (United Kingdom)
Formatted: English (United Kingdom)
Formatted: Indent: First line: 1,27 cm
Formatted: English (United Kingdom)
Formatted: English (United Kingdom)
Formatted: English (United Kingdom)
Formatted: English (United Kingdom)
Formatted: English (United Kingdom)
Formatted: English (United Kingdom)
Formatted: English (United Kingdom)
Formatted: English (United Kingdom)
Formatted: English (United Kingdom)
Field Code Changed
Formatted: English (United Kingdom)
Formatted: English (United Kingdom)

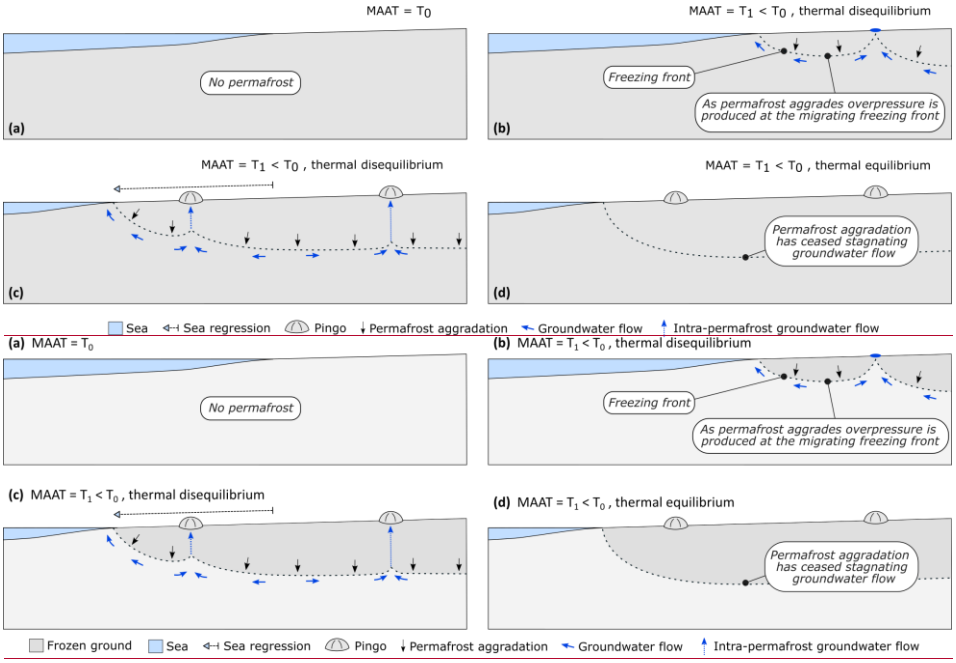

Figure 1 Conceptual model of pingo formation driven by permafrost aggradation in a low-permeable system. **(a)** No permafrost is present. **(b)** and **(c)** A negative shift in the surface energy balance results in permafrost aggradation. Freezing pressure is induced at the freezing front resulting in hydraulic head gradients. At some distance inland, higher advective heat transfer, associated with higher groundwater velocities, prevents the ground from freezing and groundwater flows to the surface and a spring (or pingo). **(d)** The ground is in thermal equilibrium with the MAAT, permafrost aggradation has stagnated, and groundwater flow to the pingos has ceased.

3 ~~Field~~Study site ~~and data~~

Adventdalen is a ~ 30 km long glacially cut valley in central Spitsbergen, Svalbard (Fig. 2a). Its high Arctic climate is ~~characterized~~characterised as polar tundra (Kottek et al., 2006) and the ground is dominated by continuous permafrost ~~(Humlum et al., 2003)~~(Humlum et al., 2003). Because of the dry climate with a mean annual precipitation of ~ 200 mm (Hanssen-Bauer et al., 2018) only a few, small glaciers exist today, the largest being Drønbreen, 9 km long and up to 200 m thick.

Formatted: English (United Kingdom)

Formatted: English (United Kingdom)

Formatted: English (United Kingdom)

Formatted: English (United Kingdom)

Field Code Changed

Formatted: English (United Kingdom)

Formatted: English (United Kingdom)

Formatted: English (United Kingdom)

Field Code Changed

Formatted: English (United Kingdom)

Formatted: English (United Kingdom)

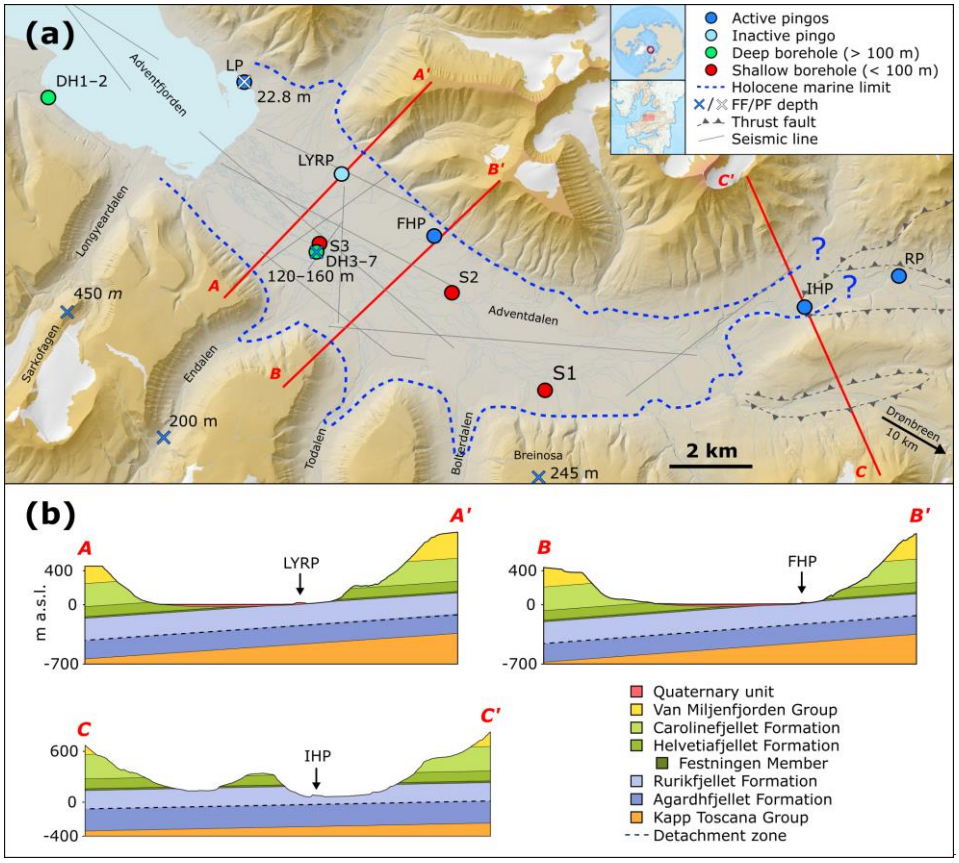
(a)
Active pingos
Inactive pingo
Deep borehole (> 100 m)
Shallow borehole (< 100 m)
Holocene marine limit
FF/PF depth
Thrust fault
Seismic line
DH1–2
Adventfjorden
LP
22.8 m
LYRP
FHP
S3
DH3–7
120–160 m
S2
S1
IHP
RP
450 m
200 m
Breinosa
245 m
Longyeardalen
Sarkofagen
Endalen
Todalen
Bolterdalen
Adventdalen
Dronbreen
10 km
2 km
A
A'
B
B'
C
C'
(b)
m a.s.l.
400
0
-700
600
-400
Quaternary unit
Van Miljenfjorden Group
Carolinefjellet Formation
Helvetiafjellet Formation
Festningen Member
Rurikfjellet Formation
Agardhfjellet Formation
Kapp Toscana Group
Detachment zone

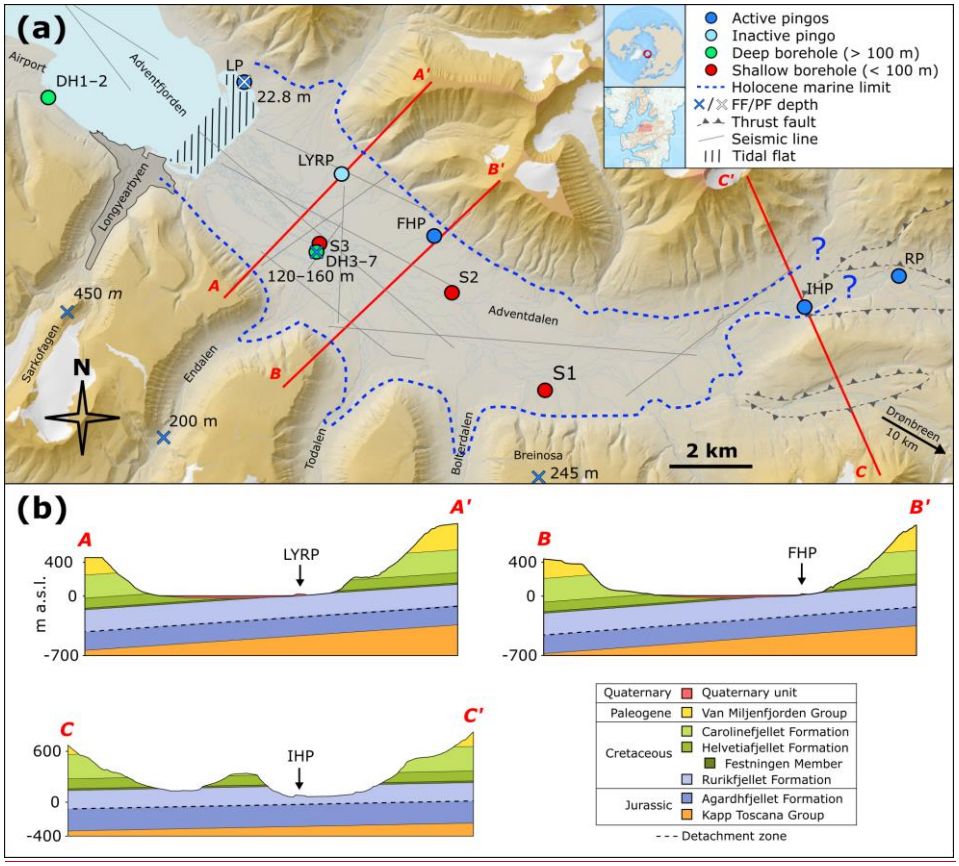

Figure 2 (a) Map of Lower Adventdalen with the location of data resources, pingos and the Holocene marine limit. LP=Lagoon Pingo, LYRP=Longyear Pingo, FHP=Førstehytte Pingo, IHP=Innerhytte Pingo, RP=River Pingo. Core logs from boreholes S1–3 and D1–D7 (respectively, Gilbert et al., 2018, and ~~Olaussen et al., in press~~Olaussen et al., 2020, and references therein), seismic lines (Bælum et al., 2012, and unpublished commercial lines from Norsk Hydro) and a geological map ~~(Norwegian Polar Institute, 2019)~~(Norwegian Polar Institute, 2019) were used to build the geological model (Fig. ~~4~~5a) (see details in Hornum, 2018). Permafrost ~~depths (temperature logging)~~depth measurements at the Sarkofagen, DH4 and Breinosa sites are from Liestøl (1977~~) (Sarkofagen~~), Braathen et al. (2012~~) (DH4~~), and ~~(Christiansen et al., 2005) (Breinosa). The freezing front depth (geophysics)~~Christiansen et al. (2005), respectively. The freezing front depth at LP is from Yoshikawa and Harada (1995). ~~Map data~~Data used to develop the map including topography, glacial extent, and fluvial network by courtesy of ~~Norwegian Polar Institute (2019). **(b)** Geological cross sections constructed based on the resources mentioned above. See Sect. 3.1 for a (hydro)geological description~~Norwegian Polar Institute (2019). **(b)** Geological cross sections constructed based on the resources mentioned above. The Quaternary unit overly well-consolidated sedimentary strata of pre-Cenozoic age (i.e. Cretaceous or older). See Sect. 3.1 for a (hydro)geological description of the layers shown in the cross sections A, B and C.

Formatted: English (United Kingdom)
Formatted: English (United Kingdom)
Formatted: English (United Kingdom)
Field Code Changed
Formatted: English (United Kingdom)
Formatted: English (United Kingdom)
Formatted: English (United Kingdom)
Field Code Changed
Formatted: English (United Kingdom)
Formatted: English (United Kingdom)
Formatted: English (United Kingdom)
Formatted: English (United Kingdom)
Formatted: English (United Kingdom)
Formatted: English (United Kingdom)
Formatted: English (United Kingdom)
Formatted: English (United Kingdom)
Field Code Changed
Formatted: English (United Kingdom)
Formatted: English (United Kingdom)

3.1 Geology and hydrogeology in Adventdalen

~~As illustrated on Fig. 2b~~In Adventdalen, fine-grained Quaternary sediments (< 70 m thick Gilbert et al., 2018) overly pre-Cenozoic, well-consolidated sedimentary strata ~~in Adventdalen,~~(Fig. 2b), which are likely the best described in Svalbard largely thanks to the Longyearbyen CO2 Laboratory Project ~~(Olaussen et al., in press, and references therein). Together, these~~(Olaussen et al., 2020, and references therein). Together, all these units form a low-permeability groundwater system.

The sedimentary strata gently dip in a west-south-westerly direction (Fig. 2b) and the youngest strata are thus found closest to Longyearbyen and the present-day coastline. The uppermost unit, the Early Cretaceous Carolinefjellet Fm (~ 300 m thick, Fig. 2b), consists of sandstone intercalated with shale beds and overlies the fluvial sandstones of the Helvetiafjellet Fm (59–72 m thick, Grundvåg et al., 2019). The Festningen Member of the Helvetiafjellet Fm (11–18 m thick), comprises fractured sandstones and is relatively hydraulically conductive, as proven by cross-well water injection tests (Bælum et al., 2012). Directly below is the ~ 450 m thick Janusfjellet Subgroup (Fig. 2b) that comprises two shale-dominated units, the Rurikfjellet (201–232 m thick, Grundvåg et al., 2019) Agardhfjellet Formations (253–264 m thick, Koevoets et al., 2018). A regional detachment zone with extensive fracturing and swelling clays propagates near the boundary of these two formations (Braathen et al., 2012) and is considered ~~the main seal for the potential of CO_2 storage (Olaussen et al., in press). The tectonic disturbances, as reflected in Festningen Sandstone and the detachment zone, makes~~a major barrier to fluid migration (Olaussen et al., 2020). The tectonic disturbances, as reflected in Festningen Sandstone and the detachment zone, make it possible that minor secondary permeability development is present elsewhere in the stratigraphy. This would have implications for groundwater movement in the system, which is otherwise predominantly through rocks with low hydraulic conductivity (Table 3).

The glacier advances during the last glacial maximum (LGM) on Svalbard (~ 20 ka (ka = 10^3 yr ~~BP~~before present)) are thought to have completely eroded any pre-existing glacial deposits in the inner fjords of Svalbard ~~(Elverhøi et al., 1995)~~(Elverhøi et al., 1995) and the Quaternary succession in Adventdalen thus postdates this event. ~~OSL~~Optically stimulated luminescence (OSL) datings in three cores from Adventdalen (S1, S2, and S3, Fig. 2a) support this (Gilbert et al., 2018). The Quaternary succession overlies fractures in the underlying sedimentary strata, possibly explained by glacier load/unload and freeze-thaw processes (Benn and Evans, 2010; Gilbert et al., 2018), as well as the significant tectonic uplift in the area. The presumed high hydraulic conductivity of this fracture zone is in contrast to the generally low-~~permeable sediments~~permeability of the Quaternary succession:. The lowermost Quaternary unit is a < 5 m thick, subglacial lodgement till deposited during the last Weichselian glacial advance. Overlying the till, a shallowing-upwards trend is observed in the gradually changing succession of marine muds (< 20 m), pro-deltaic to deltaic muds and very fine-grained sands (< 35 m), tidally influenced (saline) fluvial fine-grained sands (< 35 m), and aeolian loess deposits (< 5 m). This reflects Holocene progradation of the present delta-system ~~(Cable et al., 2018; Gilbert et al., 2018)~~(Cable et al., 2018; Gilbert et al., 2018).

The sub-permafrost groundwater often has hydraulic heads above hydrostatic, which results in artesian conditions. This is evident from the occurrence of several pingo springs and from artesian outflow from deep boreholes (> 100 m below ground level (b.g.l.)) at the confluence of Bolterdalen and Adventdalen (Malte Jochmann, pers. comm.; SNSK, Unpublished Reports SN1981_008 and SN1983_004). ~~Nearby~~Based on artesian outflow during a drilling experiment nearby, Braathen et al. (2012) deduce a hydraulic pressure of 18 to 23 bars at a depth of ~ 175 m b.g.l. in well

Formatted: English (United Kingdom)
Formatted: English (United Kingdom)
Formatted: English (United Kingdom)
Formatted: Indent: First line: 1,27 cm
Formatted: English (United Kingdom)
Formatted: English (United Kingdom)
Formatted: English (United Kingdom)
Formatted: English (United Kingdom)
Field Code Changed
Formatted: English (United Kingdom)
Formatted: English (United Kingdom)
Formatted: English (United Kingdom)
Formatted: English (United Kingdom)
Field Code Changed
Formatted: English (United Kingdom)
Formatted: English (United Kingdom)
Formatted: English (United Kingdom)
Formatted: English (United Kingdom)
Formatted: English (United Kingdom)
Formatted: English (United Kingdom)
Formatted: English (United Kingdom)
Field Code Changed
Formatted: English (United Kingdom)
Formatted: English (United Kingdom)
Formatted: English (United Kingdom)
Formatted: English (United Kingdom)
Formatted: English (United Kingdom)
Formatted: English (United Kingdom)
Formatted: English (United Kingdom)
Formatted: English (United Kingdom)
Formatted: English (United Kingdom)
Formatted: English (United Kingdom)
Formatted: English (United Kingdom)

DH4 (Festningen Member, Fig. 2), which corresponds to a hydraulic head of 9 to 60 m above hydrostatic when the potential pressure effects of the dissolved gasses are excluded. Significant under-pressure ~ 50 bar below hydrostatic is ~~recognized~~recognised in deeper stratigraphical layers (~ 800 m b.g.l.) and is believed to relate to glacial unloading, extensive fracturing and matrix expansion ~~(Birchall et al., in review.; Braathen et al., 2012; Wangen et al., 2016)~~(Birchall et al., 2020; Braathen et al., 2012; Wangen et al., 2016). The low pressure indicates hydrogeological separation from upper groundwaters immediately beneath the permafrost, in line with Sr-isotope analyses from the drill cores ~~(Huq et al., 2017; Ohm et al., 2019)~~(Huq et al., 2017; Ohm et al., 2019).

3.2 Late Weichselian and Holocene climate history

Air temperatures on Svalbard have been continuously recorded at Longyearbyen Airport since 1911 (Nordli et al., 2014). Until the 1990s, the 30-yr running mean of ~~mean annual air temperatures (MAAT)~~MAATs was -6.0 °C, while it has increased to -4.2 °C in the period 1988 to 2017 (Hanssen-Bauer et al., 2018). ~~The~~For the entire temperature record, the mean summer air temperature (MSAT) has consistently been 10 °C warmer than the MAAT (on the 30-yr scale, Førland et al., 1997).

~~Holocene temperatures on and around Svalbard are relatively well constrained by fossil-based temperature reconstructions.~~Further back in time, Holocene mean summer sea temperatures (MSST) in and around Svalbard are relatively well constrained by fossil-based temperature reconstructions (Fig. 3a, van der Bilt et al., 2018; Hald et al., 2007; Mangerud and Svendsen, 2017). Mangerud and Svendsen (2017) point out that the MSST is essentially identical to the MSAT.

Table 1 Absolute ages from Adventdalen constraining delta propagation. Depending on the dated material and the host sediment, the dating indicates minimum, approximate or maximum valley floor ages. See Fig. 2 for site locations. HML = Holocene marine limit. Compiled from [I]Åhman (1973), [II]Svensson (1970), [III]Gilbert et al. (2018), [IV]Yoshikawa and Nakamura (1996) and [V]Lønne and Nemec (2004).

Site/*Event	Distance to modern delta front [m]	Dating method	Dating material	Age of valley floor [yr BP]
LP	~340	C-14	Peat	> 240 (±50)[I]
LYRP	~3650	C-14	Driftwood	< 2650 (±55)[II]
S3	~4300	Quartz OSL	Quartz	~ 3000 (±200)[III]
FHP	~6400	C-14	Shell	< 6980 (±70)[IV]
S2	~7500	C-14	Plant matter	< 9178 (±153)[III]
HML	~16000	C-14	Shell	< 10025 (±160)[V]

~~infer a mean summer sea temperature (MSST) curve from the distribution and ^{14}C-dating of thermophilous bivalves and point out that the MSST is essentially identical to the MSAT.~~

Formatted: English (United Kingdom)
Formatted: English (United Kingdom)
Formatted: English (United States)
Formatted: English (United Kingdom)
Formatted: English (United Kingdom)
Field Code Changed
Formatted: English (United Kingdom)
Formatted: English (United Kingdom)
Formatted: English (United Kingdom)
Field Code Changed
Formatted: English (United Kingdom)
Formatted: English (United Kingdom)
Formatted: English (United Kingdom)
Field Code Changed
Formatted: English (United Kingdom)
Formatted: English (United Kingdom)
Formatted: Danish
Formatted: English (United States)
Formatted: English (United Kingdom)
Formatted: English (United Kingdom)
Formatted: English (United Kingdom)
Formatted: English (United Kingdom)
Formatted: English (United Kingdom)
Formatted: English (United Kingdom)
Field Code Changed
Formatted: English (United Kingdom)
Formatted: English (United Kingdom)
Formatted: Font: 10 pt, English (United Kingdom)
Formatted: English (United Kingdom)
Formatted Table
Formatted: English (United Kingdom)
Formatted: English (United Kingdom)
Formatted: English (United Kingdom)
Formatted: English (United Kingdom)
Formatted: English (United Kingdom)

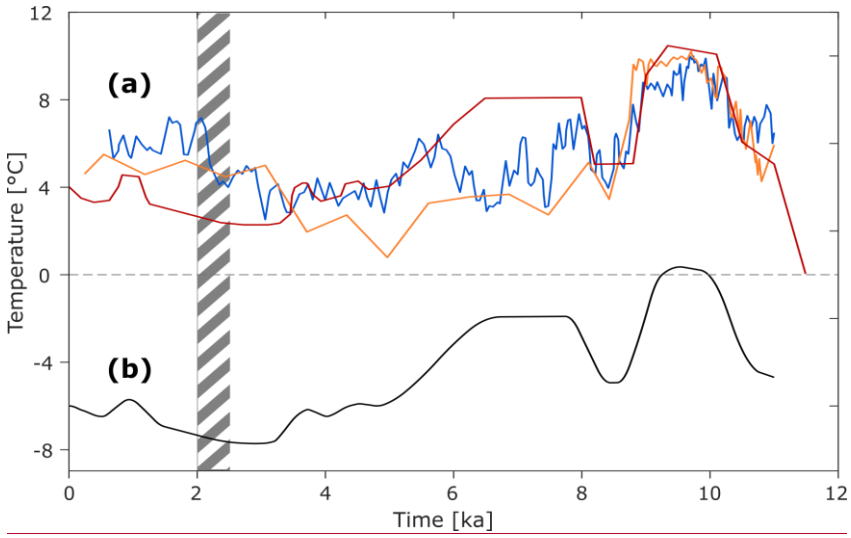

~~As illustrated on Fig. 3a, their MSST curve is largely in agreement with MSST temperature reconstructions from west and southwest of Svalbard (van der Bilt et al., 2018; Hald et al., 2007). Assuming that the present difference between MAAT and MSAT was alike for the entire Holocene, we use a MAAT reconstruction inferred by subtracting 10 °C from the MSST curve by Mangerud and Svendsen (2017) for the modelling of ground temperatures in this work (Fig. 3b). We choose to rely on Mangerud and Svendsen (2017) because; a) their curve is more local to our field area than the alternatives and; b) the suggested timing of the Holocene thermal minimum at ~ 3 to 2 ka is in agreement with the maximum of perennial or semi-permanent land fast sea ice at ~ 2.5 to 2 ka inferred from the minimal occurrence of dated driftwood (Dyke et al., 1997; Farnsworth, 2019; Funder et al., 2011). Furthermore, their curve is better supported by geomorphological evidence of glacier dynamics (Farnsworth, 2019).~~

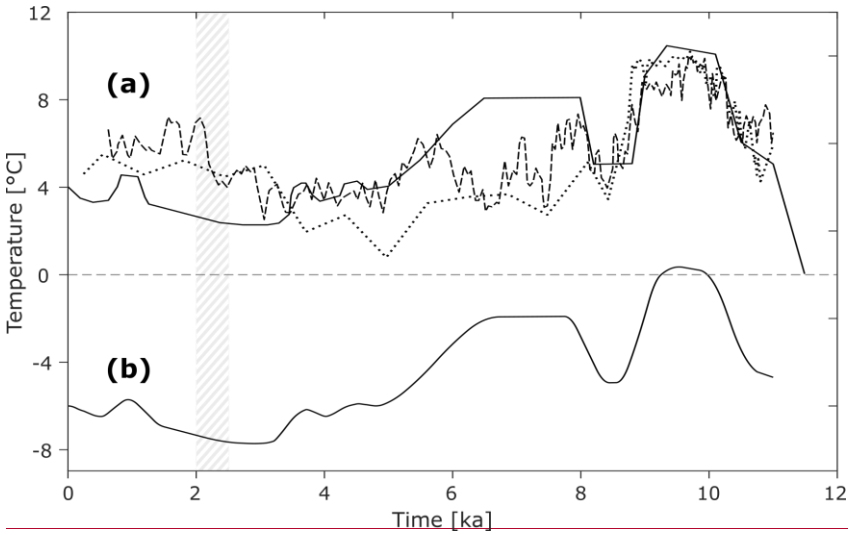

Figure 3 Holocene temperature reconstructions~~.~~ in and around Svalbard. Dashed ~~light~~ grey area indicate time of minimal driftwood arrival ~~(Farnsworth, 2019). **(a)** MSST curves (= MSAT, see text). Solid~~(Farnsworth et al., 2020). The unit of the time axis is ka = 10^3 years before present. **(a)** MSST curves (= MSAT, see text). Red line from Mangerud and Svendsen (2017). ~~Dotted~~Orange line from Hald et al. (2007). ~~Dashed~~Blue line from van der Bilt et al. (2018). **(b)** MAAT used in this work. Based on Mangerud and Svendsen (2017) and Førland et al. (1997~~).~~) (see Sect. 4.3.3).

At the last glacial maximum (LGM) occurring at ~ 20 ka, glaciers covered all fjords in Spitsbergen (Ingólfsson and Landvik, 2013). By ~ 11.5 ka the central parts of Isfjorden were glacier-free and its inner tributaries followed at ~ 11.2 ka (Forwick and Vorren, 2011; Gilbert et al., 2018). If any glacier ice remained in Adventdalen after then, it was certainly gone by ~ 10 ka when non-glacial sediments were deposited in the valley head (Lønne and Nemec, 2004). The eustatic sea-level rise caused by northern hemispheric deglaciation during Late Quaternary and Early Holocene was surpassed on Svalbard by the rate of its postglacial rebound. The Holocene marine limit (HML) ranges from ~ 20 m above sea level (a.s.l.) in the northwestern part of Spitsbergen to ~ 90 m a.s.l. in the central part (Forman, 1990). In Adventdalen, raised marine sediments suggest a HML of ~ 62 m a.s.l. and ~ 70 m a.s.l. in the inner and outer part of the valley, respectively (Lønne and Nemec, 2004). Although not well constrained, the relative sea level is estimated to have fallen pseudo-exponentially until reaching close to present levels ~ 5 ka (Lønne and Nemec, 2004). Despite the uncertainty of sea-level fall, the fjord retreat and the associated exposure of new valley floor are relatively well constrained by absolute dating presented in previous work (Table 1). ~~Depending on the dated material and the host sediment, the dating indicates minimum, approximate or maximum ages of subaerial exposure (i.e. exposure to MAATs).~~

~~***Table 1*** ***Absolute ages from Adventdalen constraining delta propagation***~~

~~Site/*Event~~	~~Distance to modern delta front (*m*)~~	~~Dating method~~	~~Dating material~~	~~Age of valley floor (yr BP)~~
~~LP~~	~~~340~~	~~C-14~~	~~Peat~~	~~≥ 240 (±50)[i]~~
~~LYRP~~	~~~3650~~	~~C-14~~	~~Driftwood~~	~~≤ 2650 (±55)[ii]~~
~~S3~~	~~~4300~~	~~Quartz OSL~~	~~Quartz~~	~~~ 3000 (±200)[iii]~~

Formatted: English (United Kingdom)
Formatted: English (United Kingdom)
Formatted: English (United Kingdom)
Formatted: English (United States)
Formatted: Danish
Formatted: Danish
Formatted: English (United Kingdom)
Field Code Changed
Formatted: English (United Kingdom)
Formatted: English (United Kingdom)
Formatted: English (United Kingdom)
Formatted: English (United Kingdom)
Formatted: Indent: First line: 1,27 cm
Field Code Changed
Formatted: English (United Kingdom)
Formatted: English (United Kingdom)
Field Code Changed
Formatted: English (United Kingdom)
Formatted: English (United Kingdom)
Field Code Changed
Formatted: English (United Kingdom)
Formatted: English (United Kingdom)
Field Code Changed
Formatted: English (United Kingdom)
Formatted: English (United Kingdom)
Field Code Changed
Formatted: English (United Kingdom)
Formatted: English (United Kingdom)
Field Code Changed
Formatted: English (United Kingdom)
Formatted: English (United Kingdom)
Formatted: English (United Kingdom)
Formatted: English (United Kingdom)
Formatted Table
Formatted: English (United Kingdom)
Formatted: English (United Kingdom)

FHP	~6400	C-14	Shell	< 6980 (±70)[IV]
S2	~7500	C-14	Plant matter	< 9178 (±153)[III]
HML	~16000	C-14	Shell	< 10025 (±160)[V]

See Fig. 2 for site locations. HML = Holocene marine limit. Compiled from [I]Åhman (1973), [II]Svensson (1970), [III]Gilbert et al. (2018), [IV]Yoshikawa and Nakamura (1996) and [V]Lønne and Nemec (2004).

3.3 Permafrost, pingos and the apparent lack of groundwater recharge

In the valley floor of Adventdalen, the permafrost thickness ranges from ~ 0 m at the coast to ~ 200 m inland. In the adjacent mountains it increases to > 450 m (Christiansen et al., 2005; Humlum et al., 2003; Liestøl, 1977)(Christiansen et al., 2005; Humlum et al., 2003; Liestøl, 1977). Specific depth observations support this regional characterization (Fig.One observation of the freezing front depth at Lagoon Pingo (Harada and Yoshikawa, 1996) and permafrost depth observations at well DH4 (Braathen et al., 2012), Endalen, Sarkofagen (both Liestøl, 1977), and Breinosa (Christiansen et al., 2005) support this regional characterisation (Fig. 2a). Mountain permafrost is presumably of Weichselian age, while permafrost in valleys postdates the Late Holocene (Humlum, 2005). The continuous permafrost and a lack of warm-based glaciers in the adjacent highlands most likely hinder subglacial recharge to the sub-permafrost aquifer due to the impervious frozen ground (Burt and Williams, 1976; McCauley et al., 2002; Walvoord and Kurylyk, 2016; Woo, 2012)(Burt and Williams, 1976; Haldorsen et al., 2010; McCauley et al., 2002; Walvoord and Kurylyk, 2016; Woo, 2012).

Sub-zero temperatures are a prerequisite for permafrost formation and its thickness essentially reflects equilibration to the geothermal heat flow (French, 2017). In the Adventdalen area, measurements of the geothermal gradient range from 0.02 °C m^{-1} in the highlands to 0.03 °C m^{-1} in the valley bottoms (Betlem et al., 2019; Liestøl, 1977).

Open-system pingos are a common feature in Svalbard and Adventdalen (Humlum et al., 2003)(Humlum et al., 2003), where five of them are distributed parallel to the valley axis (Fig. 2a). The three outermost; Lagoon, Longyear and Førstehytte Pingos, are all located on the northeastern side of the valley. All three have formed in Quaternary marine muds (Yoshikawa and Harada, 1995) and close to the sedimentary bedrock boundary (Fig. 2b). In the valley head, two additional pingos are located close to the boundary of HML; Innerhytte and River Pingos. They have formed in shales above a major fault and are situated in the valley floor in the path of the river Adventelva (Yoshikawa and Harada, 1995). With the exception of the seemingly inactive Longyear Pingo, groundwater has discharged perennially from springs located at the pingos, at least since the earliest recordings in the 1920s (Orvin, 1944). However, visible spring outflow (or winter icing) at Førstehytte Pingo was not observed from summer 2018 until October 2019. Presumably, during that time, groundwater flow through the permafrost continued, but instead of discharging to the surface, groundwater froze within the pingo and added to its growth. From Lagoon Pingo, Yoshikawa and Harada (1995) reported a spring discharge of 0.013 to 0.016 L s^{-1}, Hodson et al. (2019) estimated ca. 0.3 L s^{-1} during the 2017 summer, and we measured 0.26 L s^{-1} in August 2019. At Innerhytte Pingo, Yoshikawa and Harada (1995) measured a discharge rate of 0.11 L s^{-1}, which is somewhat smaller than Liestøl's (1977) estimate in 1976 of ~ 1 L s^{-1}. Based on our own "by the eye" observations, the discharge rate at Førstehytte Pingo was closer toin orders of 0.1 L s^{-1} when visited in fall of 2015, 2016 and 2017, and less than 0.01 L s^{-1} when rediscovered in October 2019.

4 Method - Numerical modelling

Several numerical model codes are capable of simulating coupled heat and groundwater transport in permafrost environments (Grenier et al., 2018). However, the benchmark models do not consider the overpressure produced by ice expansion. To include this process, we decoupled the modelling of heat flow from sub-permafrost groundwater flow and made use of a source term to mimic the pressure effects of permafrost aggradation. (Fig. 4). Ground temperatures and permafrost dynamics were simulated in the vertical dimension using a custom made finite-difference 1D transient heat transfer model (hereafter just 1DHT) coded in MATLAB ~~R2018b~~R2019b (MathWorks®, 2019). The 1DHT model script is ~~publically~~publicly available at DOI:10.5281/zenodo.3578839. Groundwater flow was modelled 3D steady-state with MODFLOW in the groundwater modelling software GMS 10.4 (AQUAVEO™, 2019). The connection between the two models was the permafrost aggradation rates simulated by the 1DHT, which determined the only water source for the groundwater model. ~~A schematic overview of the modelling approach is provided in the Supplement.~~ The decoupled approach does not simulate advective nor lateral heat transport. The potential limitations will be assessed in the Discussion (Sect. 6.2.1).

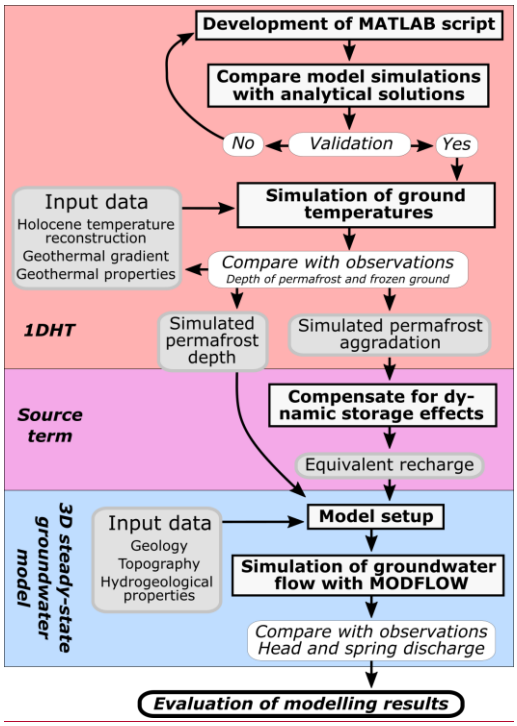

Figure 4 Schematic overview of the inner workings of the decoupled heat and groundwater model. Model setup, calculations and algorithms are indicated with sharp corners and bold text. Validation and comparison of simulations and observations are indicated with round corners and italics. Input and output data are indicated with rounded corners, grey background and normal text.

4.1 Heat flow

Heat flow was modelled one-dimensionally in the vertical dimension, which is a common approach for permafrost models (Riseborough et al., 2008). Following from Fourier's law and conservation of energy, the 1D conductive heat flow equation states that:

$$\frac{\delta T}{\delta t} = \frac{k_e}{\rho_e c_e} \cdot \frac{\delta^2 T}{\delta z} \frac{\delta^2 T}{\delta z^2} \quad (1)$$

where T is temperature [K], t is time [s], z is distance [m], and k_e, ρ_e, and c_e are the effective values of the thermal conductivity [W (m K)$^{-1}$], density [kg m^{-3}], and specific heat capacity [J (kg K)$^{-1}$], respectively. The term $\frac{k_e}{\rho_e c_e}$ equates to α_e the effective thermal diffusivity [m^2 s^{-1}]. As heat transfer was modelled one-dimensionally, simulating advective heat transfer was not possible. The ratio of advection to conduction heat transfer rates may be quantified by a Peclet number (Bergman et al., 2011):

$$P_{e_L} = \frac{v\, L}{\alpha_e} \quad (2)$$

where v is the pore water velocity and L is the characteristic length.

In the case of a saturated medium, heat conduction will flow be conducted through a matrix of sediments solids (i.e. sediment or rocks rock) and H_2O as liquid water, ice or a mixture. The effective thermal parameters were assumed independent of temperature, but the fractions of water and ice changed between the solidus and liquidus temperatures, T_S and T_L, respectively. The fraction of liquid water within the pore space, f_w, was determined using a smoothed step function (same approach as Mottaghy and Rath, 2006):

$$f_w = \begin{cases} \exp\left(-\left(\frac{T-T_L}{w}\right)^2\right) & if \quad T < T_L \\ 1 & if \quad T > T_L \end{cases} \quad (3)$$

where w [K] determines the shape of the freezing curve. For this work $w \approx 0.96$, implying that T_S = -2 °C and T_L = 0 °C. Bonacina and Comini (1973) and Mottaghy and Rath (2006) note that the exact shape of the freezing curve is of little importance for the calculated temperatures, but that a smoother function generally improves the performance of a numerical model due to a more efficient convergence of the numerical approximation. The total fractions of soil or rock (F_s), water (F_w), and ice (F_{ice}) are described respectively as; $F_s = 1 - n$, $F_w = f_w \cdot n$, and $F_{ice} = n - F_w$ with n being the total porosity. The effective thermal conductivity was calculated as root-square-mean, as done by Mottaghy and Rath (2006) and Govaerts et al. (2016). When temperature change occur occurs between T_S and T_L, freezing or thawing results in the release or absorption of latent heat, L = 333.6 kJ kg^{-1} (Mottaghy and Rath, 2006). The latent heat of fusion was included in the expression of the equivalent volumetric heat capacity [J (m^3 K^{-1}], C_{eq} (same approach as Govaerts et al., 2016):

$$C_{eq} = c_e \cdot \rho_e = F_s \cdot \rho_s \cdot c_s + F_w \cdot \rho_w \cdot \left(c_w + \frac{\delta f_w}{\delta T} \cdot L\right) + \cdots$$
$$\cdots F_{ice} F_{ice} \cdot \rho_{ice} \cdot \left(c_{ice} + \frac{\delta f_w}{\delta T} \cdot L\right) \quad (4)$$

where subscripts s, w, and ice indicate parameters of soil or rock, water, and ice, respectively.

To validate the model code we compared simulations with two analytical solutions; Neumann's solution as presented by Carslaw and Jaeger (1959) and Mottaghy and Rath (2006); and an analytical solution of a step change in temperature neglecting latent heat effects as presented by Carslaw and Jaeger (1959) and Eppelbaum et al. (2014). The model code was able to reproduce the analytical results with root-mean-square errors of respectively 1.1·10^{-2} and 1.3·10^{-}

[5] and these numbers were regarded to represent reasonable accuracy. The model code validation is described in detail in the supplementary info.

4.2 Groundwater flow

Following from Darcy's law and the conservation of mass, the 3D groundwater flow equation fundamental for groundwater modelling can be described as (Fitts, 2002):

$$K_x \frac{\delta^2 h}{\delta x^2} + K_y \frac{\delta^2 h}{\delta y^2} + K_z \frac{\delta^2 h}{\delta z^2} + Q_N = S_s \frac{\delta h}{\delta t} \quad (5)$$

where x, y and z are distances [m] in the three dimensions, K's are hydraulic conductivities [m s^{-1}] in those dimensions, h is the hydraulic head [m], Q_N is a term representing any potential sink or source [m^3 s^{-1}] (i.e. recharge, seepage, etc.), S_s is the specific storage, and t is time [s]. In this work, groundwater flow was modelled as a steady-state implying that the right-hand side of Eq. (5) equals 0. However, in the discussion of the model simulation results, hydrodynamic storage effects resulting from the glacial loading and unloading are considered.

Groundwater flow was simulated with MODFLOW, which solves the 3D groundwater flow equation with the finite-difference method (McDonald and Harbaugh, 1988). We approximated the pressure build-up from the simulated rate of permafrost aggradation, R_{PF}, by considering that it must correspond to some equivalent recharge rate (or source term, Q_N in Eq. 5), REq. Assuming no expansion or compression of the matrix, REq is specifically proportional to R_{PF}, the total porosity, n, and the expansion of water upon freezing, X_w:

$$REq = R_{PF} \cdot n \cdot X_w \quad [\text{m s}^{-1}] \quad (6)$$

$$Q_{REq} = REq \cdot A \quad [\text{m}^3\ \text{s}^{-1}]$$

where Q_{REq} is equivalent to the source term Q_N in Eq. ~~(5).~~(5), and A is an area [m^2].

4.3 Setup and boundary conditions

4.3.1 Geological model

In order to define proper geothermal and hydrogeological properties, a geological model of the subsurface in Adventdalen was built. ~~The~~Towards northwest, the model covers the tidal flat (Fig. 2a), but no other sea-covered areas were included. Elsewhere, the horizontal model boundary was a simplified outline of the ~~valley bottom and the~~ HML. The lower boundary ~~was~~is at 300 m b.g.l. (Fig. ~~4~~5a). We used data from boreholes, seismic lines (see locations and references on Fig. 2a), and a geological map with DEM provided by the ~~Norwegian Polar Institute (2019).~~Norwegian Polar Institute (2019). The general workflow was to map relevant geological boundaries in 3D with the petroleum industry software Petrel v2016 (Schlumberger©, 2019), then ~~used~~use them to build geological layers with the TIN and SOLIDS editor functions ~~in the groundwater modelling software GMS v10~~GMS 10.4 (AQUAVEO™, 2019). For the 1DHT model, the geology was simplified into one-dimensional columns for a total of 12 ~~subzones defined based age of the valley floor (Table 1).~~zones of the model area. The zones were defined as follows: The age of the valley floor (Table 1) was used to infer isochrones of valley floor exposure with intervals of 1000 yrs (Fig. 5a). The isochrones defined boundaries between zones and their names (i.e. the zone located between the 5 ka and 6 ka isochrones was named zone 5-6, Fig. 5b). The area between isochrones 9 ka and 10 ka was divided into two zones to incorporate geological variation.

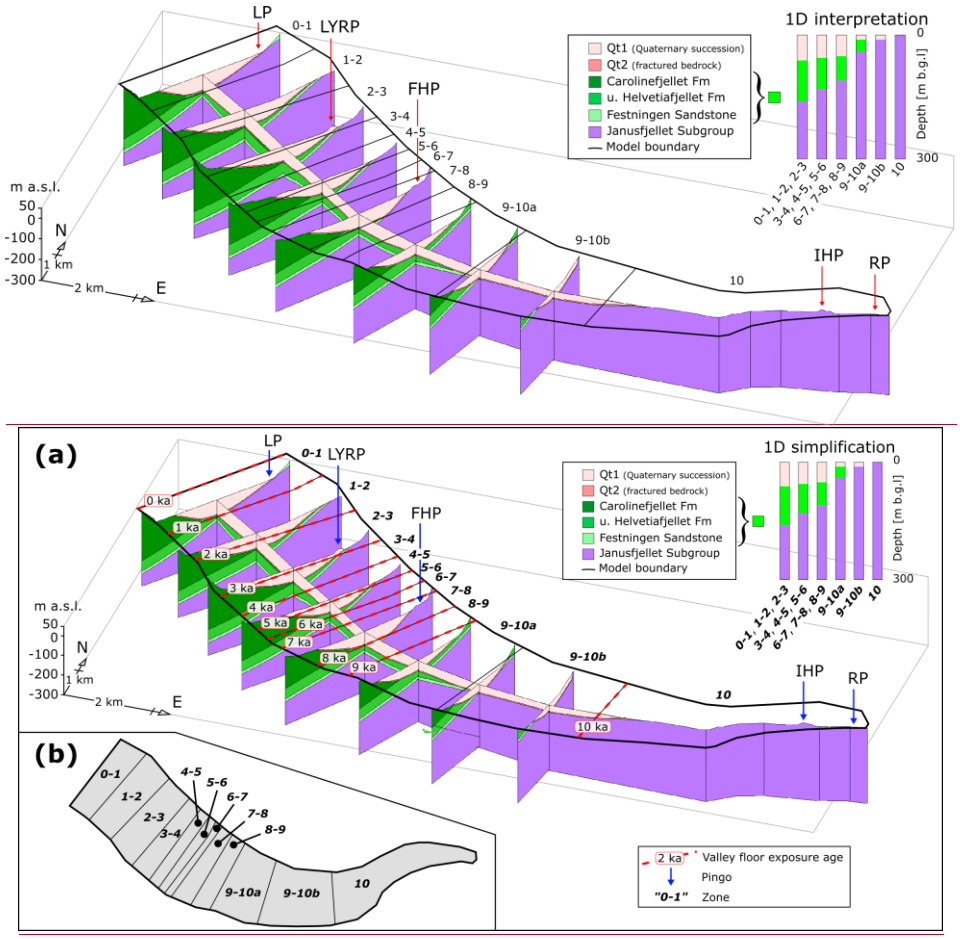

Figure 4 5 (a) 3D geological model of the subsurface below the valley floor in Adventdalen and vertical 1D simplifications (inset in upper right corner) below subzoneszones of the model area. The former determines the hydrogeological properties in the groundwater model (Table 3), whereas the latter determines the geothermal properties in the 1DHT model (Table 2). The subzones were defined based on the reconstruction of fjord retreat and their names indicate the exposure ages (i.e. The domain of the 1DHT model extends to 1000 m b.g.l. (not shown). Deeper than 300 m b.g.l., geothermal properties were defined as for Janusfjellet Subgroup. The sea retreat reconstruction was inferred from absolute datings (Table 1) and is illustrated by valley floor exposure isochrones (red dashed lines). Pingos are indicated with blue arrows. **(b)** Vertical view of the model area showing the zonation. The aforementioned isochrones defined the zone names so that the valley floor exposure age of a zone is apparent from its name (i.e. zone 0-1 became sub-aerially exposed between 1 and 0 ka, zone 1-2 between 2 and 1 ka, etc.).

Formatted: English (United Kingdom)

Formatted: English (United Kingdom)

Formatted: English (United Kingdom)

Formatted: English (United Kingdom)

Formatted: English (United Kingdom)

Formatted: English (United Kingdom)

4.3.2 Geothermal and hydrogeological properties

Due to the sparse data available from the field area, geothermal and hydrogeological properties of the lithologies in the model domain (Tables 2 and 3) were largely based on ~~typical values found in the literature. An exception was the measurements of porosity and vertical permeability, κ_v, in the sandstone units carried out by the Longyearbyen CO_2 Laboratory Project (Olaussen et al., n.d., and references therein). Porosity was found to be the most important parameter for permafrost growth, and realistic minimum, mean, and maximum values were therefore defined for the 1DHT model (Table 2).~~the available literature. The considerable contrast between the thermal properties of water and ice implied that porosity was the most important parameter for permafrost growth, and realistic minimum, intermediate, and maximum values were therefore defined for the 1DHT model (Table 2). The permafrost base is presently located within the upper two thirds of the Janusfjellet Subgroup (Figs. 2b and 5a). Estimated burial depths and thicknesses of overlying units (Grundvåg et al., 2019; Marshall et al., 2015) indicate that this strata has been buried to maximum depths between 2150 to 2600 m b.g.l. corresponding to effective vertical stresses between 34 to 41 MPa (assuming a rock density of 2.6 kg m^{-3} and hydrostatic equilibrium). Different studies on the compressibility of lithological and age equivalent rocks in the North Sea thus suggest porosities between 0.08 to 0.3 (Burland, 1990; Okiongbo, 2011; Skempton, 1969; Yang and Aplin, 2004) and we therefore used this range in our modelling experiments. An exception to the purely literature-based values is the sandstone units of which the matrix porosity and vertical permeability, κ_v, were measured as part of the Longyearbyen CO_2 Laboratory Project (Olaussen et al., 2020, and references therein). The small-scale horizontal permeability, κ_h, for sandstones is typically a factor two higher than κ_v (Domenico and Schwartz, 1998). The horizontal hydraulic conductivity, K_h, was therefore calculated using the measurements of κ_v by Braathen et al. (2012) as

$$K_h = C_{Kh/Kv} \cdot \frac{\kappa_v \cdot \rho_w \cdot g}{\mu} \quad (7)$$

where $C_{Kh/Kv}$ is the conversion factor (i.e. 2 for this work), κ_v is permeability [m^2], ρ_w is the density of water [kg m^{-3}], g is the gravitational acceleration [m s^{-2}], and μ is the dynamic viscosity of water [kg (m s)$^{-1}$]. The range of the hydraulic conductivity values of the Carolinefjellet and Helvetiafjellet formations (Festningen Sandstone not included) was defined by the 25 %, 50 % and 75 % percentiles of a Weibull probability fit of the measured values (Supplement). Ranges of hydraulic conductivity for the fluvio-deltaic succession were based on literature values from (Fitts, 2002). For the remaining bedrock units we also regarded the influence of fractures (Singhal and Gupta, 2010). All within these ranges, three sets of hydraulic conductivity defined the different model scenarios Sc1–~~3~~3x (Table 3). For steady-state simulations, the porosity does not affect the net groundwater fluxes (i.e. discharge and Darcy fluxes, Eq. 5). To evaluate the pore water velocities, however, the effective porosity is of importance. We used the same values of effective porosity for all groundwater model simulations (Table 3).

Table 2 Geothermal material properties used in the heat transfer model. Density and thermal properties compiled from [I]Williams and Smith (1989), [II]Robertson (1988), and [III]Manger (1963). Porosities from [IV]Fitts (2002), [V]Braathen et al. (2012), and based on works by [VI]Burland (1990), Grundvåg et al. (2019), Marshall et al. (2015), Okiongbo (2011), and Yang and Aplin (2004) (see text).

~~*Table 2 Geothermal properties*~~

Material	Thermal conductivity [J (yr m K)$^{-1}$]	Specific heat capacity [J (kg K)$^{-1}$]	Density [kg m^{-3}]	Thermal diffusivity [m^2 s^{-1}]	Total porosity [m^3 m^{-3}]		
					Min	~~Mean~~Intermediate	Max
Water	~~1~~[I]1.77·10^7	~~4180~~[I]4180	~~1000~~[I]1000	~~–~~1.34·10^{-7}	-	-	-

Ice	7 [I]7.06·10^{7}	2100 [I]2100	917 [I]917	– 1.16·10^{-6}	-	-	-
Silty sand (Qt)	1 [II]1.58·10^{7}	850 [I]850	2400 [III]2400	0.3 [I]2.46·10^{-7}	0.4 [IIV]0.3	0.5 [IIV]0.4	[IV]0.5
Sandstone	7 [II]7.88·10^{7}	900 [II]900	2600 [III]2600	0.06 [II]1.01·10^{-6}	0.1 [IIV]0.06	0.15 [IIV]0.1	[V]0.15
Shale	4 [II]4.73·10^{7}	800 [II]800	2600 [III]2600	0.1 [III]7.21·10^{-7}	0.2 [IIIVI]0.08	0.3 [IIIVI]0.19	[VI]0.3

Density and thermal properties compiled from Bergman et al. (2011) ,

Table 3 Properties of the hydrogeological units used in the groundwater model. Values based on [I]Williams and Smith (1989), Farouki (1981), and Robertson (1988). Porosities from [I]Fitts (2002), [II]Braathen et al. (2012), and [III]Manger (1963).

Table 3		***Hydraulic conductivity*** [m day^{-1}]			***Effective porosity***
Hydrogeological unit	**Lithology**	**Sc1**	**Sc2**	**Sc3**	**All**
Qt1	Clay, silt and sand	10^{-4}	10^{-3}	10^{-2}	0.4
Qt2	Heavily fractured bedrock	10^{-2}	0.1	1	0.4
[I]Carolinefjellet Fm	Sandstone	10^{-4}	10^{-3}	10^{-2}	0.1
[I]u. Helvetiafjellet Fm	Sandstone	10^{-4}	10^{-3}	10^{-2}	0.1
Festingen Sandstone	Fractured sandstone	10^{-2}	5·10^{-2}	0.1	0.1
Janusfjellet Subgroub	Shale	10^{-4}	5·10^{-4}	10^{-3}	0.1
Detachment zone	Fractured shale	10^{-3}	5·10^{-3}	10^{-2}	0.1

[I]Evaluated from Braathen et al. (2012). The remainder based on Fitts (2002), and [II]Singhal and Gupta (2010). or evaluated from [III]Braathen et al. (2012) (see Supplement).

		Hydraulic conductivity [m day^{-1}]			***Effective porosity***
Hydrogeological unit	**Lithology**	**Sc1*x***	**Sc2*x***	**Sc3*x***	**All**
[I]Qt1	Clay, silt and sand	10^{-4}	10^{-3}	10^{-2}	0.4
[I]Qt2	Heavily fractured bedrock	10^{-2}	0.1	1	0.4
[III]Carolinefjellet Fm	Sandstone	2·10^{-4}	6·10^{-4}	10^{-3}	0.1
[III]u. Helvetiafjellet Fm	Sandstone	2·10^{-4}	6·10^{-4}	10^{-3}	0.1
[I, II]Festingen Sandstone	Fractured sandstone	5·10^{-2}	7.5·10^{-2}	0.1	0.1
[I, II]Janusfjellet Subgroub	Shale	5·10^{-4}	7.5·10^{-4}	10^{-3}	0.1
[I, II]Detachment zone	Fractured shale	5·10^{-3}	7.5·10^{-3}	10^{-2}	0.1

4.3.3 1D transient heat transfer model (1DHT)

The model domain contained 12 one-dimensional gridscolumns, each 3001000 m long and consisting of 150500 cells with a height of 2 m. Each individual gridOne column was associated to each of the model area zones (Fig. 4) and the geothermal properties were defined accordingly. The names of the zones referaccording to the age associated geological 1D simplifications (see insert on Fig. 5b). Deeper than 300 m b.g.l., the properties were that of subaerial exposure (Table 1), which defined the Janusfjellet Subgroup. The simulation run time (e.g.was defined by the valley floor age inferred for that zone (Fig. 5), so that, for zone 0-1 the simulation period was 0.5 to 0 ka, for zone 1-2 it was 1.5 to 0 ka, etc. For zone 10, the simulation period was 10 to 0 ka).. The initial ground temperature distribution followed the geothermal gradient reported by Liestøl (1977) (0.025 °C m^{-1}) from a surface temperature of 0 °C. At any subsequent time, the lower boundary condition was defined from the same geothermal gradient resulting in a basal temperature change of less than 0.65°C. The upper boundary condition was defined by the Holocene MAAT curve presented in Fig. 3b. Assuming that the present 10 °C difference between MAAT and MSAT (Førland et al., 1997) was alike for the entire Holocene, we constructed this curve (Fig. 3b) by subtracting 10 °C from the MSST curve by Mangerud and Svendsen (2017) (Fig. 3a). As illustrated on Fig. 3a, their MSST curve is largely in agreement with MSST temperature reconstructions from west and southwest of Svalbard (0.025 °C m^{-1}) from a surface temperature of 0 °C. At any subsequent time, the lower boundary condition was defined from the same geothermal gradient. The Holocene temperature curve (Fig. 3) defined the upper boundary condition.

(van der Bilt et al., 2018; Hald et al., 2007). We chose to rely on Mangerud and Svendsen (2017) because; a) their curve is more local to our field area than the alternatives and; b) the suggested timing of the Holocene thermal minimum at ~ 3 to 2 ka is in agreement with the maximum of perennial or semi-permanent land fast sea ice at ~ 2.5 to 2 ka inferred from the minimal occurrence of dated driftwood (Dyke et al., 1997; Farnsworth et al., 2020; Funder et al., 2011). Furthermore, their curve is better supported by geomorphological evidence of glacier dynamics (Farnsworth et al., 2020).

4.3.4 Groundwater model

~~Each~~For the groundwater model, each grid cell measured 100 by 100 by 5 m (x y z) and their hydrogeological properties were defined from the geology (Fig. 45a, Table 3). The model domain was defined from the geological model therefore covering an elongated ground surface area of 59 km^2 that is < 4 km broad and ~ 18 km long (Fig. 45b). Frozen ground was considered impervious and cells shallower than the simulated freezing front depth were thus ~~inactivated~~de-activated. The lower boundary was at 300 m b.g.l. The fjord was simulated with a general head of 0 m a.s.l. assigned to the relevant cells and the conductance was determined according to hydraulic conductivity (Table 3). The MODFLOW drain package was used to simulate pingo springs. Because the cells located at the springs were inactivated, the drains were assigned to the uppermost active cells located closest to springs, but within the conductive Festningen Sandstone. if present in the underlying stratigraphy (i.e. Lagoon and Førstehytte Pingos, Fig. 5a). Drain levels were set according to spring elevations (i.e. 1, 20, 65, and 77 m a.s.l. for Lagoon, Førstehytte, Innerhytte, and River Pingos, respectively). The simulated springs were able drain more water than the cells they were situated in could transmit. That is, the conductance was set more than high enough not to restrict any discharge. Except for the fjord and the springs, all outer model boundaries were no-flow conditioned.

The only source of water in the groundwater model was defined from the basal permafrost aggradation rate simulated by the 1DHT model and assigned as recharge to the uppermost active cells in the model domain. To compensate for the lack of dynamic storage effects in the steady-state model, we applied a moving time-average to the simulated basal permafrost growth (or decay) before calculating the recharge equivalent (Eq. 6). The time window of the moving average was based on the possible range of the adjustment time, t_a, which is the time needed for fluids to redistribute to a pressure perturbation (e.g. Neuzil, 2012; Šuklje, 1969):

$$t_a = l^2 S_s K^{-1} \quad (8)$$

where l is half of the shortest dimension of the system (the characteristic length), S_s is the specific storage, and K is the hydraulic conductivity. We found t_a to be shortest in the vertical dimension, but assumed that hydraulic pressures could only dissipate in the horizontal dimension after the formation of continuous permafrost no earlier than 6 ka (Humlum, 2005; this research). Specifically, we estimated the horizontal t_a to be between 20 and 19000 yrs. To quantify this, we used a characteristic length of 1 km. For S_s we used a matrix compressibility of $7{\cdot}10^{-10}$ to $7{\cdot}10^{-8}$ Pa^{-1} (based on common estimates for fractured rocks, e.g. Domenico and Mifflin, 1965; Domenico and Schwartz, 1998; Fitts, 2002) yielding a S_s of $7{\cdot}10^{-6}$ to $7{\cdot}10^{-4}$ m^{-1} (in line with literature values, c.f. Singhal and Gupta, 2010). ~~5.1 1DHT model results~~

~~The raw simulation results from the 1DHT model were~~For K, we used the values estimated for the dominating geological unit (Janusfjellet Subgroup, Table 3). The time window used to compensate for dynamic storage effects were defined from the above, but no longer than the age of permafrost (i.e. 6000 yrs or less).

Formatted: English (United Kingdom)
Formatted: English (United Kingdom)
Formatted: English (United Kingdom)
Formatted: English (United Kingdom)
Formatted: English (United Kingdom)
Formatted: English (United Kingdom)
Formatted: English (United Kingdom)
Formatted: English (United Kingdom)
Formatted: English (United Kingdom)
Formatted: English (United Kingdom)
Formatted: English (United Kingdom)
Formatted: English (United Kingdom)
Formatted: English (United Kingdom)
Formatted: English (United Kingdom)
Formatted: English (United Kingdom)
Formatted: English (United Kingdom)
Formatted: English (United Kingdom)
Field Code Changed
Formatted: English (United Kingdom)
Formatted: English (United Kingdom)
Formatted: English (United Kingdom)
Formatted: English (United Kingdom)
Formatted: English (United Kingdom)

To represent the uncertainty of how permafrost aggradation affects sub-permafrost groundwater flow, we simulated nine different scenarios that were defined by having three sets of values for the two fundamental parameters in any combination; hydraulic conductivity (Scenarios Sc1–3*x*, Table 3) and equivalent recharge (Scenarios Sc*X*a–b, values calculated as described above and by Eq. 6). The nine scenarios are all labelled Sc*Xx* where *X* and *x* indicates the minimum, intermediate or maximum value sets of hydraulic conductivity and equivalent recharge, respectively. We further simulated a tenth scenario that takes additional pressure sources into account.

5 Results

5.1 1DHT model results

The direct output from running the 1DHT model code was matrices containing the temperatures throughout the model domain for each time step in the simulation period. ~~The evolution of~~For each time step, the permafrost and freezing front depths were ~~evaluated~~calculated by interpolating the depth at which the associated temperatures ~~for each time step~~occurred. The greatest phase change rate in the 1DHT model occurs at a temperature of -0.7 °C (following from Eq. ~~3) and the (always) downwards progression rate of this isotherm was therefore used for the calculation of the equivalent recharge (by net pore space loss, Eq. 6).~~3) and it was therefore the progression rate of this isotherm that was used for the calculation of the equivalent recharge (by net pore space loss, Eq. 6). Hereafter, 'permafrost aggradation' therefore means the downwards progression rate of this isotherm (-0.7 °C), although this is not entirely congruent with the thermal definition of permafrost (ground perennially below 0 °C, French, 2017). Since phase change occurs over a temperature range, the porosity used to calculate the equivalent recharge was taken as a weighted mean of the porosities in the corresponding cell range, where the weight was proportional to the phase change rate.

5.1.1 Permafrost and freezing front depth

In Fig. ~~5~~6, the simulated Holocene ground temperature development in Adventdalen is exemplified by the growth of frozen ground and permafrost in zones 2-3, 7-8 and 9-10b when using the intermediate porosity values (Table 2). For the oldest part of the model area (most inland), an early occurrence of frozen ground was simulated during the Early Holocene cooling of 9 to 8 ka (Figs. 3 and 5). However, due to the subsequent warming at 8 to 6.5 ka, frozen ground was thawed and not ~~reestablished~~re-established until ~ 6.5 ka. Since this time, deep ground temperatures were simulated to be cooling until present. The pattern was identical for simulations with lower and higher porosities (not shown) although the depths were different (as illustrated on ~~Fig. 6~~Figs. 7).

Formatted: English (United Kingdom)
Formatted: English (United Kingdom)
Formatted: English (United Kingdom)
Formatted: English (United Kingdom)
Formatted: English (United Kingdom)
Formatted: English (United Kingdom)
Formatted: Heading 3
Formatted: English (United Kingdom)
Formatted: English (United Kingdom)
Formatted: English (United Kingdom)

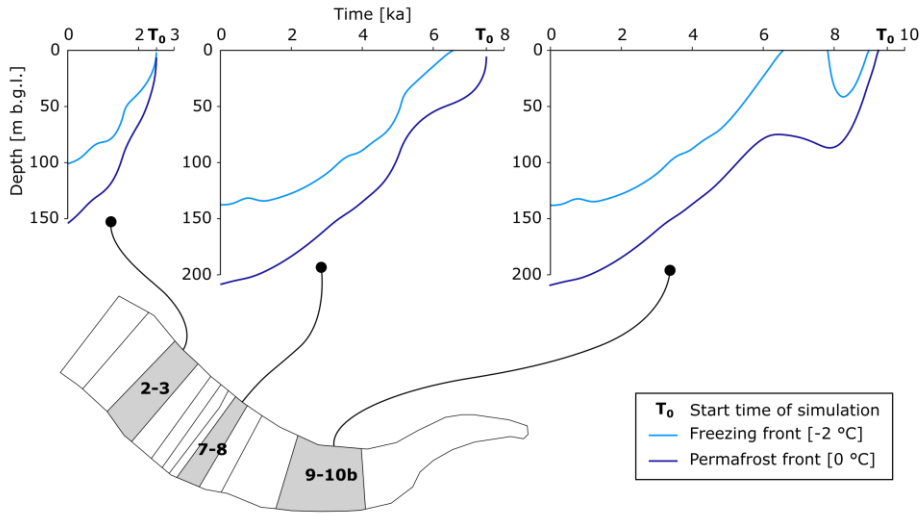

480

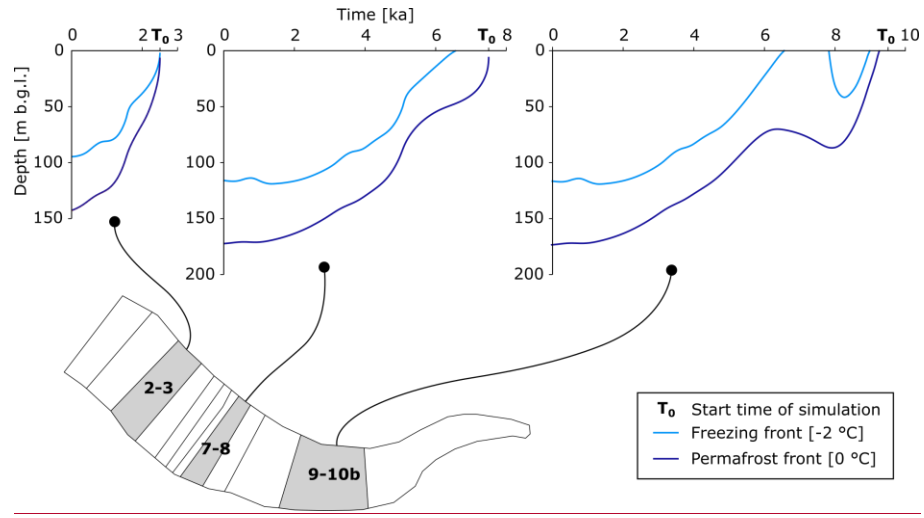

Figure ~~5~~6 Development of simulated freezing front and permafrost front depths from zones 2-3, 7-8 and 9-10b ~~(~~of the model area (see Fig. ~~4~~5). These simulation results derive when using the intermediate porosity values (Table 2). Note that completely frozen ground does not establish permanently until ~ 6.5 ka.

485 Depending on the scenario, the 1DHT model simulated present day permafrost and freezing front depths of respectively ~~192~~165 to ~~232~~184 and ~~125~~110 to ~~155~~124 m b.g.l. at distances further than 6 km from the delta front (Fig. ~~6~~7). Closer to the delta front both isotherms are located at shallower depths and decrease to 58 to ~~64~~65 m b.g.l. and 31 to 34 m b.g.l. The porosity plays an important role for the temperature development due to latent heat of the water (ice) filling the pore

Formatted: English (United Kingdom)
Formatted: English (United Kingdom)
Formatted: English (United Kingdom)
Formatted: English (United Kingdom)
Formatted: English (United Kingdom)
Formatted: English (United Kingdom)
Formatted: English (United Kingdom)
Formatted: English (United Kingdom)
Formatted: English (United Kingdom)
Formatted: English (United Kingdom)

space and because water and ice account for the minimum and maximum~~, respectively,~~ thermal diffusivities in the model domain~~.~~, respectively. In panel (a) ~~and (c)~~ of Fig. ~~6~~7, an uncertainty field is drawn (shading) as derived from the applied porosity range (Table 2). The upper and lower edge of the shaded area corresponds to the maximum and minimum porosity. The line corresponds to the intermediate porosity (Table 2). In panel (b), the simulated present permafrost aggradation rate is plotted by point symbols. The shaded area was drawn by applying the moving time-average correction defined using the estimated adjustment times (see Sect. 4.3.4, Eq. 8) and indicates the values used to calculate the equivalent recharge rates in panel (c). Here, the line indicates intermediate values of recharge added to the groundwater model, while the edges of the shaded area represent the lower and upper estimates. The scarcity of ground temperature observations does not allow for model calibration, but observations both at Lagoon Pingo (freezing front) and well DH4 (permafrost) agree relatively well with simulations.

Formatted: English (United Kingdom)

Formatted: English (United Kingdom)

Formatted: English (United Kingdom)

Formatted: English (United Kingdom)

Formatted: English (United Kingdom)

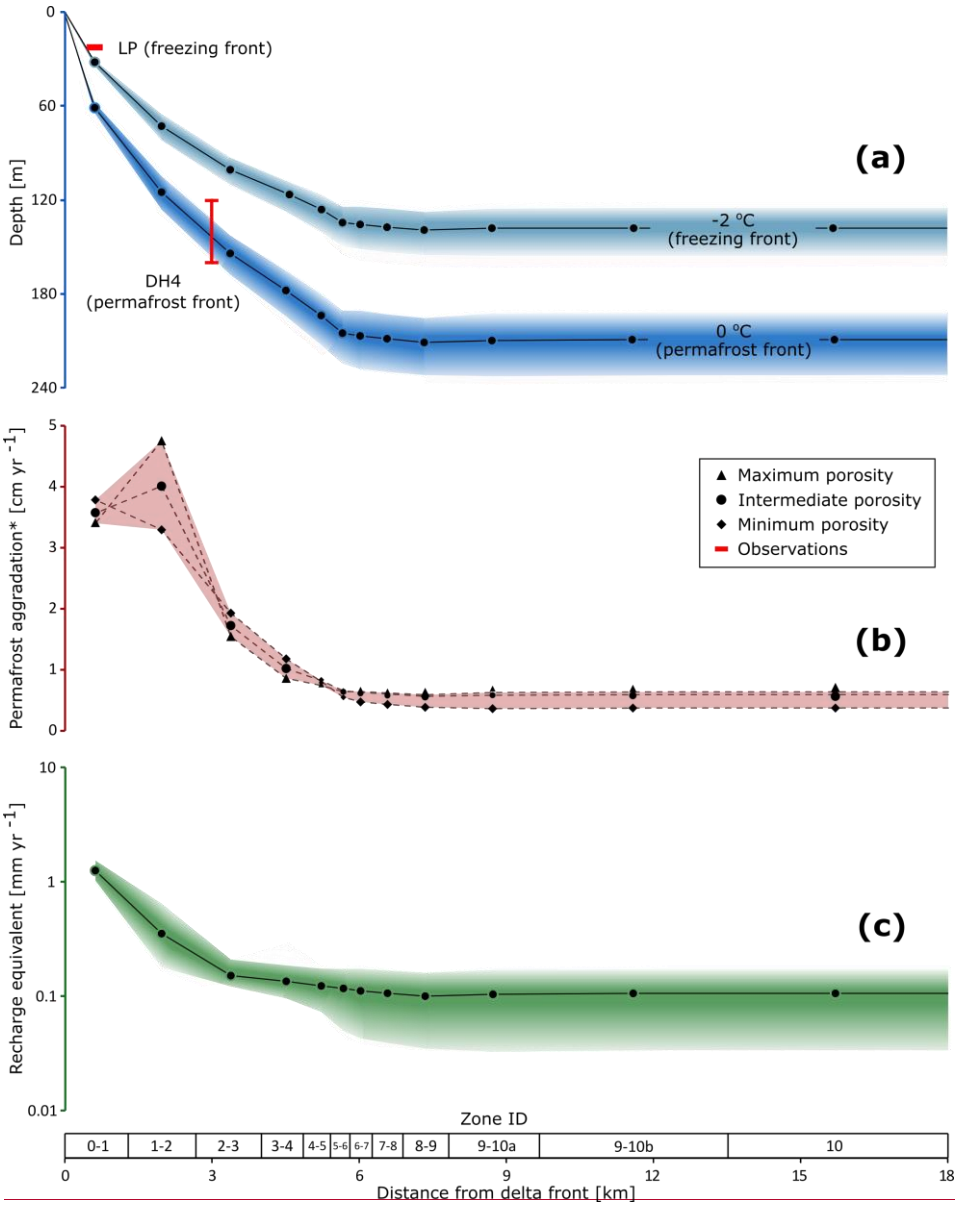
LP (freezing front)
(a)
Depth [m]
0
60
120
180
240
-2 °C
(freezing front)
DH4
(permafrost front)
0 °C
(permafrost front)
Permafrost aggradation* [cm yr -1]
5
4
3
2
1
0
Maximum porosity
Intermediate porosity
Minimum porosity
Observations
(b)
Recharge equivalent [mm yr -1]
10
1
0.1
0.01
(c)
Zone ID
0-1
1-2
2-3
3-4
4-5
5-6
6-7
7-8
8-9
9-10a
9-10b
10
0
3
6
9
12
15
18
Distance from delta front [km]

500

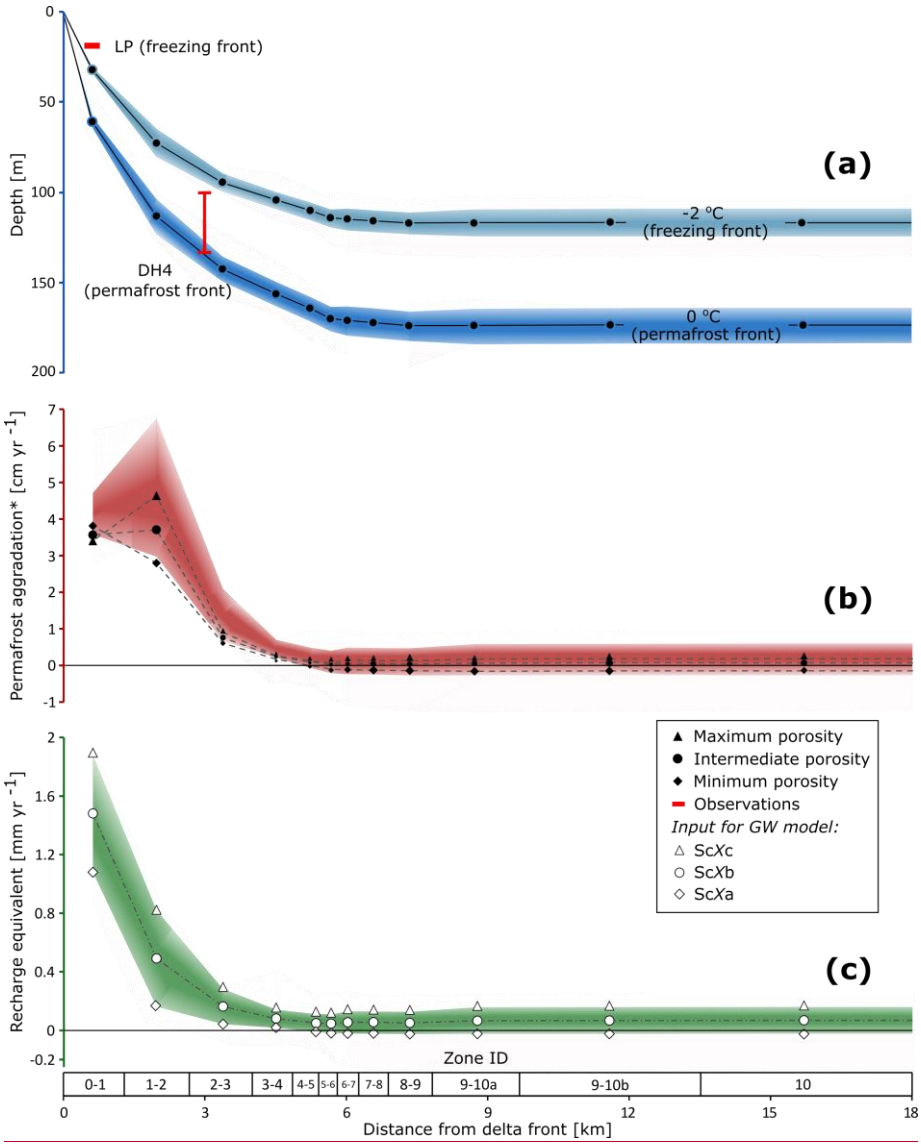

Figure 67 (previous page) Present-day permafrost conditions as simulated by the 1DHT model. ~~For both~~ **(a)** Freezing front and ~~(c), an uncertainty field is illustrated with shading.~~permafrost depths. The upper and lower edge of the shaded ~~areas~~area corresponds to the maximum and minimum limits of the porosity range, while the curve and the points corresponds to the intermediate (Table 2). ~~(a) Freezing front and permafrost depths. (b) Rate of permafrost aggradation.~~**(b)** Rate of permafrost aggradation. The point symbols represent the present permafrost aggradation, while the shaded area is drawn by applying a time-moving average as described in Sect.

Formatted: English (United Kingdom)
Formatted: English (United Kingdom)
Formatted: English (United Kingdom)
Formatted: English (United Kingdom)
Formatted: English (United Kingdom)
Formatted: English (United Kingdom)

4.3.4. and represents the values used to calculate the equivalent recharge rates. *It is the -0.7 °C isotherm, which has been used to calculate this as the greatest phase change rate takes place at that temperature. **(c)** Equivalent recharge rate (net rate of loss in pore space). The points on the curve and the outer edges of the shaded area represent the ~~values~~recharge rates, which were assigned to the corresponding zones in the groundwater model.

5.1.2 Permafrost aggradation and recharge equivalent

Simulated rates of present permafrost aggradation ranged from ~~5 –~~ 0.02 – 5 cm yr^{-1} and generally decreased up-valley with older exposure ages and for scenarios with lower porosity (Fig. ~~6b).~~7b). The correction for dynamic storage effects generally increased the "effective" permafrost aggradation rate that was used to calculate the recharge equivalent. The reason for this was that basal permafrost growth was generally faster in the past (Fig. 6). At first surprising, the model simulations generally did not suggest that the highest aggradation rate occurred where permafrost is youngest (zone 0-1), but instead at zone 1-2 ~~(the exception was the simulation with the lowest porosities in Table 2).~~ This was due to the different properties of the sediments and bedrock undergoing freezing ~~(Fig. 4).~~ In zone 0-1, closest to the shore, phase change took place at < 60 m b.g.l. corresponding to the most porous and least thermally diffusive unit (~~the fluvio-deltaic succession).~~Qt1, insert on Fig. 5 and Table 2). Thus, a relatively high amount of latent heat had to be released for the freezing front to aggrade. By contrast, the opposite was the case in zone 1-2, where the freezing front just entered the sandstone unit that possessed the lowest porosity~~.~~ (Carolinefjellet Fm, insert on Fig. 5 and Table 2). For the same reason, Fig. ~~6c~~7c shows that the pattern of the equivalent recharge decreases from 1 ~~–~~ 1.5 – 1.9 mm yr^{-1} closest to delta front (zone 0-1), to ~~-~~0.0402 – 0.~~15~~16 mm yr^{-1} in zone 10 furthest up-valley~~. Fig. 6 also shows the permafrost and freezing front depths, with the uncertainty range derived from the application of the range in porosity values~~.

5.2 Simulated ~~aquifer~~groundwater flow paths and flow velocity distributions

The above simulated recharge equivalent rates were assigned to cells within the corresponding zones of the model area (Fig. ~~4~~5b). The resulting outputs of the groundwater model for all scenarios are shown in Fig. ~~7~~8. The equivalent recharge rates, REq_i, calculated from the 1DHT model simulations resulted in a total inflow of water, Q_{REq}, to the groundwater system of ~~25.4~~20, 40.65 and ~~56.7~~63.4 m^3 day^{-1}~~, respectively,~~ for the ~~maximum~~minimum, intermediate and ~~minimum porosity~~maximum effective permafrost aggradation rate scenarios~~. These values correspond to average~~, respectively. For the minimum recharge equivalent scenarios (Fig. 8a, the slightly negative recharge equivalent rates (i.e. permafrost thaw) simulated at distances further than 6 km from the delta front result in a total hydraulic pressure loss that corresponds to a discharge rate of ~~0.16, 0.25 and 0.35 mm~~2.4 m^3 day^{-1} ~~if distributed over the entire model area.~~

~~Simulated hydraulic heads ranged from sea level to maxima of either 406 m a.s.l. (maximum Q_{REq} and minimum K scenario, Fig. 7-1c) or 28 m a.s.l. (minimum Q_{REq} and maximum K scenario, Fig. 7-3a). For all of the minimum K scenarios (Figs. 7-1a–c), the simulated hydraulic head in well DH4 was significantly higher than observed. The simulated head fell slightly below the lowest end of the range of the observed head in the scenario with minimum Q_{REq} and maximum K (Fig. 7-3a). For the remaining five scenarios, the groundwater model simulated heads within the uncertainty range of the observation (Figs. 7-2a–c and 7-3b–c). Entirely or almost entirely artesian conditions were simulated for all but three scenarios (small Q_{REq} and high K, Figs. 7-2a and 7-3a–b), where the up-valley part of the system has hydraulic pressures below hydrostatic.~~

For the minimum Qreq and intermediate to maximum K scenarios, simulated heads were lower two scenarios (simulated heads Simulated hydraulic heads ranged from sea level to maxima between 119 m a.s.l. (maximum Q_{REq} and minimum K scenario, Fig. 8-1c) and 10 m a.s.l. (minimum Q_{REq} and maximum K scenario, Fig. 8-3a). The only two exceptions except for the minimum Q_{REq} and intermediate to maximum K scenarios (Figs. 8-2a and 8-3a) for which hydraulic heads went down to -6 and -10 m a.s.l., respectively, in the up-valley part of the system. The simulated hydraulic head in well DH4 was generally within the range deduced from well outflow (Braathen et al., 2012), but significantly above for the maximum Q_{REq} and minimum K scenario (Fig. 8-1c). For two other scenarios, the simulated head fell slightly outside the deduced range (above and below, respectively for the intermediate Q_{REq} and minimum K scenario and the minimum Q_{REq} and maximum K scenario, Figs. 8-1b and 8-3a). For the remaining six scenarios, the groundwater model simulated heads within the uncertainty range of the observation. As illustrated by the colour fill on Fig. 8, entirely or almost entirely artesian conditions were simulated for all but four scenarios (all small Q_{REq} scenarios and the intermediate Q_{REq} and maximum K scenario, Figs. 8-1a, 8-2a and 8-3a–b), where the up-valley part of the system has hydraulic pressures below ground level.

With the porosities listed in Table 3, groundwater flow paths and pore water velocities were evaluated from all simulations using particle tracking (Pollock, 2016). ~~This enabled us~~In order to visualise groundwater movement towards the outlet points, we used the particle tracking to draw 3 kyr catchment zones ~~for each outlet point~~ (the term 'catchment' is somewhat misleading in this context as no actual recharge takes place). The 3 kyr duration was chosen because it is on that order of time that the modelled permafrost and groundwater conditions likely existed. For most scenarios, water particle path lines (blue lines, Fig. ~~7) depict~~8) depicted a multidirectional flow pattern with local catchment zones for each outlet point. A more uniform down-valley-directed flow pattern was simulated for the ~~scenarios with small~~intermediate Q_{REq} and ~~high~~maximum K scenario (Figs. ~~7~~8-3b). For the minimum Q_{REq} scenarios (Sc*X*a, Figs. 8-1a, 8-2a and ~~7~~8-3a ~~b). These~~), the negative equivalent recharge rates in the up-valley part of the system (Fig. 7c) resulted in a bidirectional flow pattern with groundwater flowing away from a groundwater divide located ~ 2 km from the delta front. The uniform and bidirectional flow patterns coincide with the partly non-artesian conditions and the lack of discharge ~~at some of~~ the up-valley pingo springs. As also illustrated by the size of the 3 kyr catchment zones, the simulated mean pore water velocities ranged from 0.~~03~~05 to 0.~~01~~14 m yr^{-1} (Figs. ~~7~~8-1a and ~~7~~8-3c, respectively) and suggest a relatively stagnant groundwater system. This is in accordance with mean residence times that ranged from ~~70~~60 to ~~300~~950 kyr (respectively, maximum K and Q_{REq} and minimum K and Q_{REq} scenarios, Figs. ~~7~~8-3c and ~~7~~8-3a) and by far exceed the duration of the Holocene.

The ~~artesian/non-artesian conditions clearly determine whether~~colour fill and the pie charts on Fig. 8 together show that outflow at a pingo site only takes place ~~at~~ if the hydraulic pressure is artesian. Outflow from all pingo ~~spring~~ sites~~, as was indeed the case~~ were simulated for four scenarios including all ~~but~~ three ~~simulations (small~~ with maximum Q_{REq} ~~and high K,~~ and the one with intermediate Q_{REq} and minimum K (Figs. ~~7-2a~~8-1b–c, 8-2c and ~~7-3a-b~~8-3c). The simulated spring discharge rates (pie charts, Fig. ~~7~~8) increased with increasing Q_{REq} and decreasing K, and had a maximum value of 0.~~2~~31 L s^{-1} at FHP for the scenario with maximum Q_{REq} and minimum K (Fig. ~~7~~8-1c). The simulated proportion of the total outflow not discharging ~~to~~at the ~~fjord~~springs varied from ~~42~~30 % to ~~90~~89 % (the extremes respectively illustrated by Figs. ~~7~~8-1c and ~~7-3a).~~8-3a). For intermediate and maximum Q_{REq} scenarios (Sc*X*b–c, Fig. 8) and all of this discharged to the fjord, while a minor proportion of the outflow is caused by permafrost thaw for the

Formatted: English (United Kingdom)
Formatted: Indent: First line: 1,27 cm
Formatted ...
Formatted ...
Formatted ...
Formatted ...
Formatted ...
Formatted ...
Formatted ...
Formatted: English (United Kingdom)
Formatted ...
Formatted ...
Formatted ...

minimum Q_{REq} scenarios. Larger proportions were simulated in the case of ~~high K~~ maximum K and a small total inflow Q_{REq}, with the former being the most important parameter.

Figure ~~7~~8 (next page) Groundwater model simulations from all 9 scenarios. The individual diagrams are sorted so that the hydraulic conductivity increase along the right-hand axis **(~~1–3~~**scenarios **Sc1–3x)** and the equivalent recharge produced by permafrost aggradation increase along the left-hand axis **(~~a~~**scenarios **ScXa~~–c~~)**. On each diagram, the following simulation results are illustrated: Heads from the uppermost grid layer are shown in m a.s.l. by isopotential contours (note that the colour scales are different) and in m a.g.l. by the colour fill~~.~~ (see scale at the bottom of the figure). The latter indicates if artesian conditions are simulated (reddish) or not (blueish~~)~~ ~~(note that **1a–c** each has their own colour scales, whereas the remaining have identical ones~~). The outflow distribution and discharge rates are illustrated by pie charts with the location of the discharge points (pingos and fjord) indicated on **(1c)**. *For minimun Q_{REq} scenarios (**1a**, **2a** and **3a**) part of the outflow is caused by basal permafrost thaw (Figs. 7b–c). Flow patterns are illustrated by thin blue lines, which each depict pathways of particles released in the uppermost grid layer. The mean pore water velocities, shown in the upper left-hand corners, were calculated from the aforementioned particles and using the same porosities for all scenarios (Table 3). The areas outlined with thick dashed lines show where each outlet point were simulated to receive water from during 3 kyr. In the lower right-hand corner, the simulated head in well DH4 is illustrated on a range plot with the ~~observed head defining the range.~~range defined as deduced by Braathen et al. (2012). The colour of the bar indicates if the simulated head falls within (green) or outside the deduced range with less (yellow) or more (red) than 10 % of the total range. The location of DH4 and the pingo springs is marked on **(1c)**.

Formatted: English (United Kingdom)
Formatted: English (United Kingdom)
Formatted: English (United Kingdom)
Formatted: Font: 9 pt, Bold, English (United Kingdom)
Formatted: Indent: First line: 0 cm
Formatted: English (United Kingdom)
Formatted: English (United Kingdom)
Formatted: English (United Kingdom)
Formatted: English (United Kingdom)
Formatted: English (United Kingdom)
Formatted: English (United Kingdom)
Formatted: English (United Kingdom)
Formatted: English (United Kingdom)

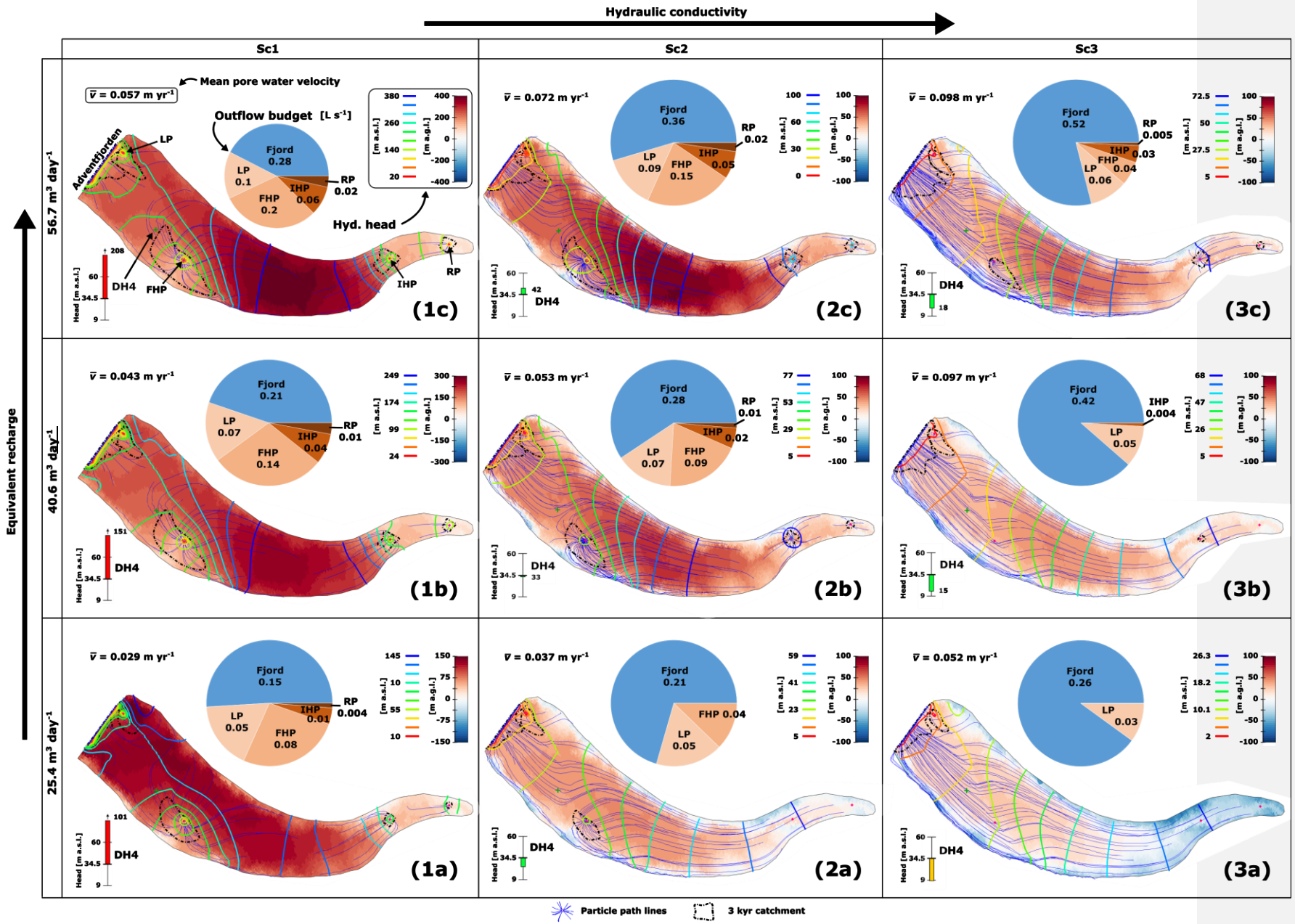
Hydraulic conductivity
Equivalent recharge
Sc1
Sc2
Sc3
56.7 m³ day⁻¹
40.6 m³ day⁻¹
25.4 m³ day⁻¹
Mean pore water velocity
Outflow budget [L s⁻¹]
Hyd. head
Adventfjorden
LP
FHP
IHP
RP
DH4
Fjord
Head [m a.s.l.]
[m a.s.l.]
[m a.g.l.]
(1c)
(2c)
(3c)
(1b)
(2b)
(3b)
(1a)
(2a)
(3a)
Particle path lines
3 kyr catchment

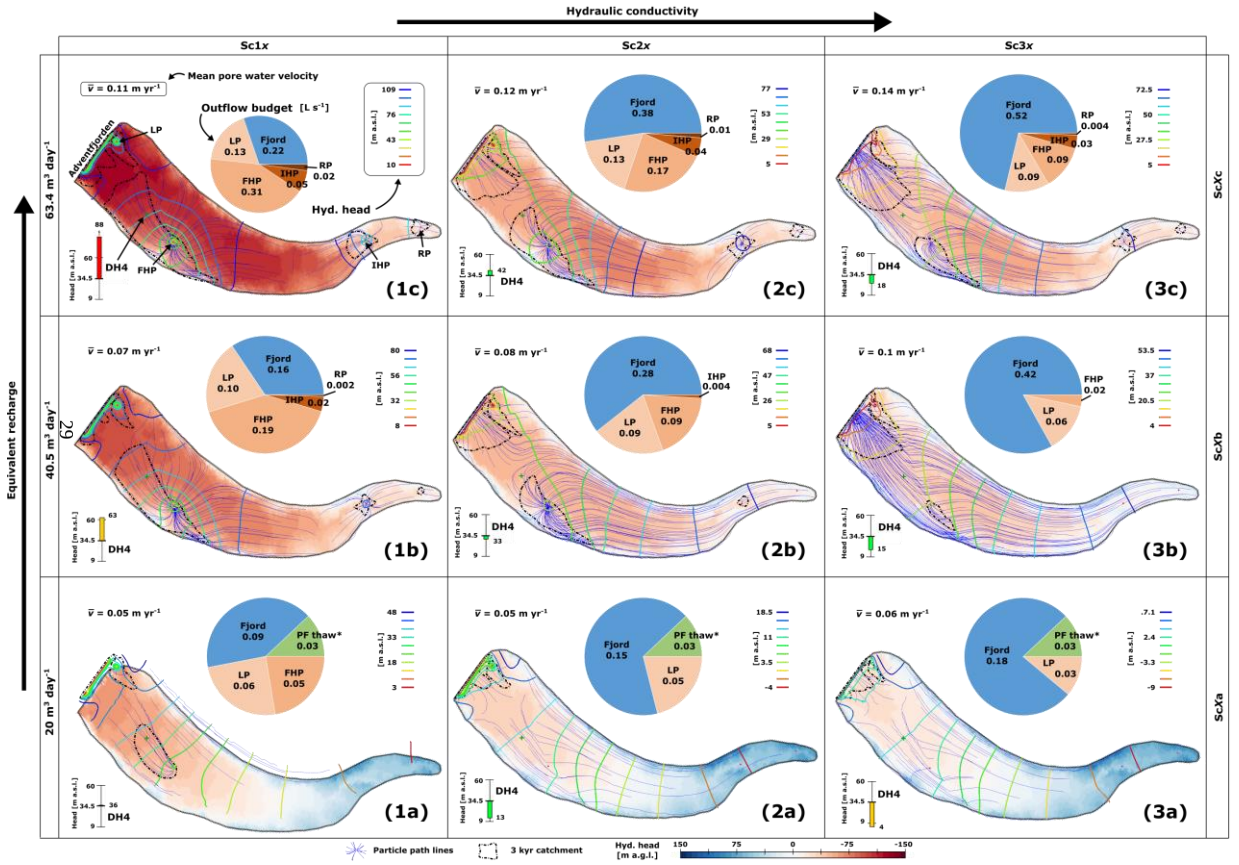
Hydraulic conductivity
Sc1x
Sc2x
Sc3x
Equivalent recharge
63.4 m³ day⁻¹
40.5 m³ day⁻¹
20 m³ day⁻¹
ScXc
ScXb
ScXa
Mean pore water velocity
Outflow budget [L s⁻¹]
Hyd. head
Adventfjorden
LP
FHP
DH4
IHP
RP
Fjord
PF thaw*
(1c)
(2c)
(3c)
(1b)
(2b)
(3b)
(1a)
(2a)
(3a)
Particle path lines
3 kyr catchment
Hyd. head [m a.g.l.]

6 Discussion

6.1 Alternative processes producing sub-permafrost overpressures

In this work, we contemplate the implication of deep (sub-permafrost) groundwater systems being restricted from recharge by impervious continuous permafrost. It seems enigmatic that anomalous overpressures and springs still persist in such landscapes, where the lack of warm-based ice at the bottom of glaciers or ice-sheets, or other features capable of maintaining through-taliks as pathways for groundwater flow, seem to rule out recharge from precipitation. Directly supporting the main research hypothesis, the outcomes of our investigation suggest that basal permafrost aggradation due to equilibration of ground temperatures may produce sufficient artesian pressures to sustain such a system. However, other mechanisms producing anomalous pressures relative to hydrostatic conditions cannot be excluded and are therefore considered below.

Anomalous pressures may occur in groundwater systems that are either hydrodynamically equilibrated or disequilibrated (Neuzil, 1995). In this context equilibrated means being in steady-state condition with the geological and hydrological setting, while disequilibrated systems are not. For the former, anomalous pressures are typically produced by topography-driven head gradients, but as the permafrost conditions in Adventdalen seem to rule out this process, we focus on the disequilibrium-type of anomalous pressures. These result from geological or glacial processes and can be further classified into systems where anomalous pressures equilibrate to past or ongoing perturbations. Anomalous pressure produced by permafrost aggradation is an example of the latter and we will discuss this in Sect. 6.3 using the model simulation results. ~~In the following, first~~First we consider the alternative processes.

6.1.1 Equilibration to past perturbations – glacial loading

A possible interpretation of anomalous overpressure is that a previous perturbation was long-lived enough to redistribute groundwater (and other fluids) and recent enough for groundwater not to have adjusted to the present conditions (Bahr et al., 1994). The notion of adjustment time (Sect. 4.3.4, Eq. 8) becomes convenient when assessing whether an ice-load removed > 10^4 yr ago could be responsible for present anomalous pressures. For shallow, low-permeable and well-consolidated bedrock systems like the one investigated in this work, we found the vertical t_a to be between 80 and 7500. To calculate this, we used the lowest *K*-estimate of the dominant hydrogeological unit (Janusfjellet Subgroup, Table 3) and a characteristic length of 200 (approximating half of the thickness of the aforementioned unit). The specific storage was defined like when calculating the horizontal adjustment time (Sect. 4.3.4). Conclusively, we argue that overpressures in systems like the investigated case cannot be explained by equilibration from past glacial loading.

6.1.2 Equilibration to ongoing perturbations – density contrasts and gases

~~A possible interpretation of anomalous overpressure is that a previous perturbation occurred long enough ago to redistribute groundwater (and other fluids) and recently enough for groundwater not to have adjusted to the present conditions (Bahr et al., 1994). The notion of adjustment time becomes convenient when assessing whether an ice-load removed > 10^4 yr ago could be~~

Formatted: English (United Kingdom)
Formatted: English (United Kingdom)
Formatted: Indent: First line: 1,27 cm
Field Code Changed
Formatted: English (United Kingdom)
Formatted: English (United Kingdom)
Formatted: English (United Kingdom)
Formatted: English (United Kingdom)
Formatted: English (United Kingdom)

~~responsible for present anomalous pressures. It has been established that the time needed for fluids to redistribute to a pressure perturbation can be expressed by $t_a = l^2 S_s K^{-1}$ (e.g. Neuzil, 2012; Šuklje, 1969), where t_a is the adjustment time, l is half of the shortest dimension of the system, S_s is the specific storage, and K is the hydraulic conductivity. For shallow, low-permeable and well-consolidated bedrock systems like the one investigated in this work, we found t_a to be shorter than the duration of the Holocene. Specifically, we estimated t_a to be between 80 and 7500 years. To quantify this, we used a characteristic length of 200 m. For S_s, we used a matrix compressibility of $7{\cdot}10^{-10}$ to $7{\cdot}10^{-8}$ Pa^{-1} (based on common estimates for fractured rocks, e.g. Domenico and Mifflin, 1965; Domenico and Schwartz, 1998; Fitts, 2002) yielding a S_s of $7{\cdot}10^{-6}$ to $7{\cdot}10^{-4}$ m^{-1} (in line with literature values, c.f. Singhal and Gupta, 2010). For K, we used the lowest estimate of any of the hydrogeological units in question (Table 3) divided by 5 to convert to vertical K. Conclusively, we argue that overpressures in systems like the investigated case cannot be explained by equilibration from past glacial loading.~~

6.1.2 Equilibration to ongoing perturbations – density contrasts and gases

Past geological or climatic events may be indirectly responsible for ongoing pressure perturbations in systems that adjust to active hydrodynamic processes (Neuzil, 1995). Here, we consider the potential pressure contribution derived from groundwater density contrasts and the occurrence and possible production of gases and gas hydrates.

For a coastal setting like our field site, it is relevant to consider how a potential disequilibrium of the freshwater-saltwater interface could drive groundwater flow. During glaciation, the equilibrium depth of this interface must have been considerably deeper than today if subglacial melting could replenish the groundwater system. Following glacial unloading, the fresh groundwater body is in disequilibrium with the decreased surficial pressure and the density contrast directs hydraulic gradients upwards. Specifically, the freshwater head approximates to 0.025 times the depth of the seawater-freshwater interface, assuming hydrostatic conditions and densities of 1025 and 1000 kg m^{-3} respectively (following the Ghyben-Herzberg relation, Verruijt, 1968). In other terms, to explain artesian pressures resulting in outflow from springs situated at elevations of up to 77 m a.s.l., the seawater-freshwater interface has to be situated at depths down to 3 km b.g.l. unless extensive brine is present. The actual seawater-freshwater interface is most certainly located above this depth, and the observed low-pressures at ~ 800 m b.g.l. (Braathen et al., 2012) definitively exclude density contrasts as a main cause for the overpressures in the shallower system. We conclude that density contrasts may theoretically contribute to the artesian pressures, but only insignificantly.

The presence of gases, either free in solution or bound in gas hydrate complexes (i.e. clathrates), may affect hydraulic pressures (Neuzil, 2003). Pingo spring waters and sub-permafrost groundwater in Adventdalen indeed contain both CH_4 and CO_2 ~~(Hodson et al., In Review).~~ (Hodson et al., in review). The methane is dominated by a biogenic fingerprint (Hodson et al., 2019) and contemporary methanogenesis is probable (Huq et al., 2017). In order to explain pressure build-up, the essential question is whether any ongoing process produces or releases gas to the groundwater, thereby increasing pressure. Such processes may be exemplified by methanogenesis or clathrate dissolution ~~that causes~~, which cause the partial gas pressure to

exceed the hydrostatic pressure, so that free gas forms and replaces groundwater in the pore space. We speculate that, over time, groundwater flow driven by this process is limited, as it represents neither a groundwater source nor a net loss in pore space. In Adventdalen, the pressure and temperature conditions at the base of permafrost are at the threshold for gas hydrate stability, and controlled mainly by the gas composition (Betlem et al., 2019). Whether partly responsible for groundwater flow or not, this proximity to the boundary of hydrate stability means gas clathrates may currently represent a pressure buffer. This is because should clathrates be present, any decrease in pressure to conditions below thermodynamic stability initiates clathrate dissolution, thereby releasing gases and increasing the pressure. It is as yet unclear which form the methane predominantly takes below the permafrost in Adventdalen. However, the near-stability conditions, the documented sub-permafrost gas accumulation and the recent history of climate warming do make the buffering effects of clathrate dissolution more likely.

6.2 Model limitations, extent and uncertainties

For sub-permafrost groundwater systems, an extraordinary amount of relevant data and research exists for Adventdalen (van der Ploeg et al., 2012) and this arguably makes Adventdalen an optimal case for investigation. There were, nevertheless, too few observations for calibrating the numerical models in a statistical way, and so in the following, we consider the model limitations carefully before drawing conclusions from the simulation results.

6.2.1 Limitations related to model approach

Using an approach where transient one-dimensional heat flow modelling was decoupled from steady-state three-dimensional groundwater modelling required an array of assumptions that deserve attention. Modelling heat transfer one-dimensionally in the vertical dimension implies that no lateral conduction was considered. The inherent assumption was thus that the isotherms are horizontally parallel. This assumption holds inland, but for a coastal setting the slope of an isotherm is expected to increase seawards and in some cases cause a thermal "bulge" under the sea floor (c.f. Gregersen and Eidsmoen, 1988; Taniguchi, 2000). The 1DHT model simulations indicated that even the largest isotherm slope gradients in Adventdalen are quite small (Fig. ~~6a~~7a). Between the two most seawards points, the gradients for the -2 °C and 0 °C isotherms are -25 and -35 m km^{-1} ($\Delta z\ \Delta x^{-1}$), respectively, in landwards direction. Effectively, if heat transfer in this work had been modelled in 2D, the simulated permafrost aggradation rate would have been ~~simulated~~ slightly slower close to the coast due to lateral heat transfer. Nevertheless, considering how small the isotherm slope gradients are, the lateral heat flow component was considered negligible and we found the one-dimensional modelling approach appropriate.

The inability to model advective heat transfer represents an uncertainty proportional to the importance of this process over the time scale in question. From the hydrogeological properties and the spring water chemistry discussed later on, we ~~realized~~realised that the groundwater system must be relatively stagnant. We therefore assumed that the only uncertainty related to the omission of advective heat transfer arose from neglecting the energy leaving the system with the groundwater. By definition, the greatest discrepancy between simulations and actual conditions must occur locally at the outflow points to which the advective heat transfer rate is greatest. On the regional scale, however, we infer that advective heat transfer played

Formatted: English (United Kingdom)
Formatted: English (United Kingdom)
Field Code Changed
Field Code Changed
Formatted: English (United Kingdom)
Formatted: English (United Kingdom)
Formatted: Indent: First line: 1,27 cm
Field Code Changed
Formatted: English (United Kingdom)
Formatted: English (United Kingdom)
Formatted: English (United Kingdom)
Formatted: English (United Kingdom)
Formatted: English (United Kingdom)
Formatted: English (United Kingdom)
Formatted: English (United Kingdom)
Formatted: English (United Kingdom)

an insignificant role. Disregarding shallow formation of visible ground ice, the total pore water expulsion by freezing approximates to 9 % of the volume of ice in the pore space. The average pore water velocity of this water when it got expelled from the system can be approximated by half of the frozen ground depth (assuming this represents the mean travelled distanced) divided by the porosity and the time it took for frozen ground to establish. For the investigated system this yields a Peclet number of $P_{e_L} < 0.02$, implying that advective heat transfer played an insignificant role on the regional scale (taking 100 m as an average frozen ground thickness and characteristic length, and the thermal diffusivity of frozen ground).

The steady-state approach of groundwater modelling implied that dynamic storage effects could not be simulated (S_s Eq. 5). ~~In Sect. 6.1.1, we estimated that the groundwater system in Adventdalen has an adjustment time of 80 to 7500 yr. This suggests that hydraulic pressures can build up on this time scale. In effect, because of the general decrease of permafrost aggradation rates following the initial formation of frozen ground at ~ 6.5 ka (Fig. 5), the steady-state assumption therefore likely results in an underestimation of the present-day pressures produced by basal permafrost aggradation.~~To account for the present pressure contributions from previous permafrost dynamics, we instead applied the time-moving average to the development of the permafrost base before calculating the recharge equivalent (Fig. 4). Another drawback from the steady-state approach, which was not accounted for in the model setup, is the possible overestimation of the pressure contribution that arrives from not considering the effects of the Holocene sea level fall. This represents an uncertainty of the simulation results, but because sea levels already reached levels close to the present day by 5 ka, we regard it as insignificant.

6.2.2 Model extent uncertainty

~~Given the lack of known geological boundaries or groundwater divides, the lateral extent of the model domain was defined using a simplified outline of the HML, but this may be somewhat arbitrary.~~ The boundary conditions of the groundwater model define a bathtub-like system with the pingo springs and the fjord as the only discharge points, and with the expansion of water upon freezing within the model regime as the only source of hydraulic pressure. In reality, the hydrological system in Adventdalen may not entirely conform to this description as groundwater flow across the model boundaries cannot be rejected. Additional recharge could, for example, occur through microcracks below the valley floor induced during glaciation (Leith et al., 2014). Likewise, hydraulic pressures may, to a greater extent than simulated, dissipate directly to the fjord through unknown pathways. In this respect, our model serves to isolate the pressure effect of freezing expansion in Adventdalen and systems like it. This should be taken into account before drawing site-specific conclusions from the modelling results.

Due to Early Holocene warming (Fig. 3), the 1DHT simulation results showed that continuous frozen ground in Adventdalen is likely younger than 6.5 ka even where the valley floor is older (Fig. ~~5~~6). This is supported by geomorphological and geochronological evidence (Humlum, 2005). As such, there seems to be no reason why permafrost dynamics in the valley bottom outside the HML should be markedly different from that in the up-valley part of the model area. Based on the above, it is possible that basal permafrost aggradation goes on beyond the model area (HML) and model simulations may have underestimated the freezing-induced pressures affecting spring discharge.

Formatted: English (United Kingdom)
Formatted: English (United Kingdom)
Formatted: English (United Kingdom)
Formatted: English (United Kingdom)
Formatted: English (United Kingdom)
Formatted: English (United Kingdom)
Formatted: Indent: First line: 1,27 cm
Formatted: English (United Kingdom)
Formatted: English (United Kingdom)
Formatted: English (United Kingdom)
Formatted: English (United Kingdom)

The dominantly low-~~permeable~~permeability groundwater system challenged a physically determined lower boundary for the model domain. From the significant low-pressures observed in deeper stratigraphic layers (~ 800 m b.g.l~~.~~,. at DH4, Braathen et al., 2012), we inferred isolation of the investigated groundwater system from that below and simply assigned the base to a depth of 300 m b.g.l. By simulating scenarios with a lower base of 250 and 400 m b.g.l., we found that simulation results did not change significantly (< 1 % deviation of simulated heads and discharge rates).

6.3 Do model simulations represent the processes in the groundwater system in Adventdalen?

The amount of hydrogeological data from Adventdalen was insufficient for automatic calibration of model parameters~~.~~ and the model simulations should therefore at best be taken as possible scenarios for the conditions in Adventdalen. However, some scenarios yielded simulations that must be considered at odds with the available observations. For the ~~low~~minimum K ~~scenarios~~and maximum Q_{REq} scenario (Figs. ~~7-1a–c~~8-1c), the simulated hydraulic heads were almost certainly too high. The only head observation supports this view and we therefore suggest that the real hydraulic conductivities in reality must be ~~greater than those~~higher if the recharge rate (real and/or equivalent) is as employed here~~.~~ (or higher). Further, discharge from ~~all of~~ the ~~observed~~up-valley pingo springs was not simulated for scenarios with ~~high K's and low equivalent recharge.~~minimum Q_{REq} and maximum K (Sc*X*a and Sc3b, Figs. 8-1a, 8-2a, 8-3a–b). This could indicate that the real ~~K~~ Q_{REq} values are in effect ~~lower~~higher than those employed for these scenarios. However, since ~~dynamic storage effects and~~ alternative processes contributing to hydraulic ~~pressure~~pressures were not incorporated in the model, ~~these high K scenarios are almost certainly wrong. Therefore~~such conclusion is speculative. If permafrost aggradation is the main driver of pingo spring outflow in Adventdalen, the most plausible representation of the system is likely to be found within the scenarios shown in Figs. ~~7~~8-1b, ~~8~~-2b–c and ~~7~~8-3c).

For the flow pattern, a more certain conclusion could be drawn. The flow was simulated to be multidirectional, with local sub-catchments appearing whenever the groundwater model was able to simulate artesian spring discharges from the pingos. This indicates that regional groundwater flow across the model area is very limited.

On Fig. ~~8~~9, simulated spring outflows from all model simulations are plotted together with the few available observations. Validation of any particular model scenario was not possible due to the variability and paucity of observations. Nevertheless, assuming that only a small fraction of the discharge (if any) freezes within the pingo and becomes part of its core, the comparable observed and simulated discharges suggest that permafrost aggradation alone ~~can~~may explain the presence of the pingos and their springs in ~~a~~ low-permeability ~~system like Adventdalen~~systems comparable to the one modelled. To investigate the effect of additional pressure sources, we ran the groundwater model with maximum K values (Table 3) and different, uniformly distributed recharge rates, all resulting in a greater total inflow of groundwater than from permafrost aggradation alone (Fig. ~~7). Figure 9~~8). We used the maximum K-values to allow for the highest amount of recharge to enter the system. Figure 10 illustrates such a scenario with a recharge rate of 1 mm yr^{-1}. We found that, if the pressure production exceeds that equivalent to a recharge rate of 1 mm yr^{-1}, hydraulic heads rise unrealistically (i.e. > 200 m a.g.l.). Within the model limitations (Sect. 6.2), Fig. ~~9~~10 may thus be regarded as an approximation of the upper limit of possible total

Formatted: English (United Kingdom)
Formatted: English (United Kingdom)
Formatted: English (United Kingdom)
Formatted: English (United Kingdom)
Field Code Changed
Formatted: Indent: Left: 0 cm, First line: 0 cm
Formatted: English (United Kingdom)
Formatted: English (United Kingdom)
Formatted: English (United Kingdom)
Formatted: English (United Kingdom)
Formatted: English (United Kingdom)
Formatted: English (United Kingdom)
Formatted: English (United Kingdom)
Formatted: English (United Kingdom)
Formatted: English (United Kingdom)
Formatted: English (United Kingdom)
Formatted: English (United Kingdom)
Formatted: English (United Kingdom)
Formatted: English (United Kingdom)
Formatted: English (United Kingdom)
Formatted: English (United Kingdom)
Formatted: English (United Kingdom)
Formatted: Indent: First line: 1,27 cm
Formatted: English (United Kingdom)
Formatted: English (United Kingdom)
Formatted: English (United Kingdom)
Formatted: English (United Kingdom)
Formatted: English (United Kingdom)
Formatted: English (United Kingdom)

inflow (or pore space loss) rates (161.4 m^3 day^{-1}). The corresponding spring water discharge rates range from 0.~~11~~12 to 0.~~46~~56 L s^{-1} (Fig. ~~8~~9) and the mean residence time is 24 kyr.

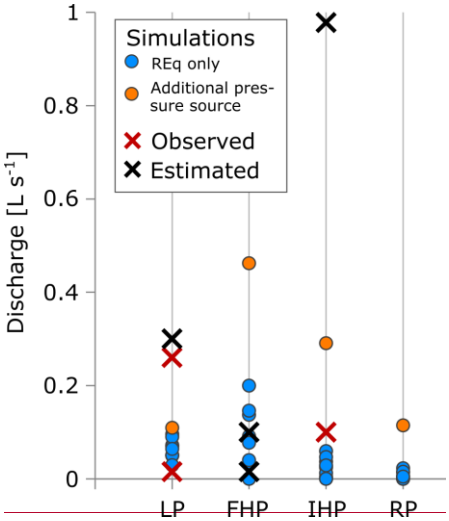

765

Formatted: English (United Kingdom)

Formatted: English (United Kingdom)

Formatted: English (United Kingdom)

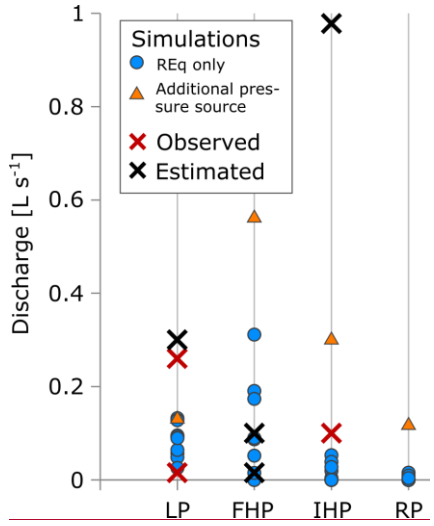

Figure 89. Simulated, observed (measured) and estimated ("by the eye") spring discharge rates. Blue dots are discharge rates simulated for groundwater model scenarios where the source term is defined by the rate of basal permafrost aggradation (Figs. 67 and 78). The orange dots are discharge rates simulated for a groundwater scenario with an additional unknown pressure source (Fig. 910).

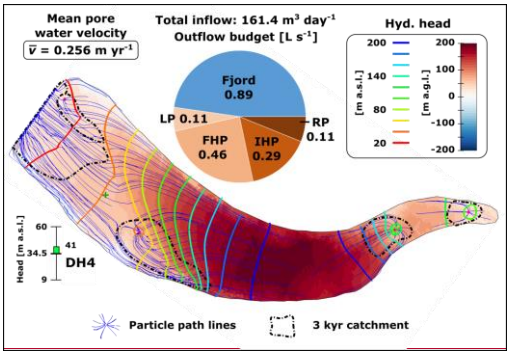

Formatted: English (United Kingdom)
Formatted: English (United Kingdom)
Formatted: English (United Kingdom)
Formatted: English (United Kingdom)
Formatted: English (United Kingdom)

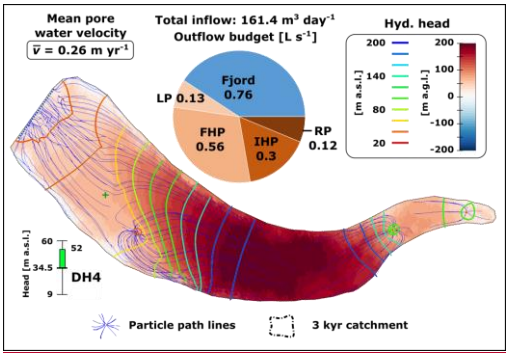

Figure 910 Groundwater model simulation representing additional pressure sources. Recharge is distributed uniformly with a rate of 1 mm yr^{-1}.

Formatted: English (United Kingdom)

Formatted: English (United Kingdom)

6.4 Comparison with hydrological processes inferred from pingo spring water chemistry

~~The lack of data for model calibration and other shortcomings related to our model approach posed challenges for conclusive interpretations based on the modelling results alone. However, hydrochemical data from 25 pingo spring water samples from 2014 to 2017 presented by Hodson et al. (In Review) and publically available from DOI:10.5285/3d82fd3f-884b-47b6-b11c-6c96d66b950d give additional insights into the groundwater system. Water~~The lack of hydrological data for model calibration make comparison with other information on the groundwater system ever so important. In this context, hydrochemical data from 25 pingo spring water samples from 2014 to 2017 (Hodson et al., in review: see DOI:10.5285/3d82fd3f-884b-47b6-b11c-6c96d66b950d) give additional insights into the groundwater system. Accordingly, water samples from LP, FHP, IHP and RP reveal that all these pingo springs share the same sodium-bicarbonate ($NaHCO_3$) water type (illustrated in the Supplement), which is commonly associated with freshening of a saline groundwater system (e.g. Giménez-Forcada, 2010). The only exceptions are four samples taken near River Pingo in 2017 of a magnesium-sulfate water type. ~~These four samples were excluded from the following discussion because they might not be associated with a pingo according to Hodson et al. (In Review)~~These four samples were excluded from the following discussion because they might not be associated with a pingo according to Hodson et al. (in review).

Formatted: English (United Kingdom)

Formatted: English (United Kingdom)

Formatted: English (United Kingdom)

Formatted: English (United Kingdom)

Formatted: English (United Kingdom)

Formatted: English (United Kingdom)

Formatted: Indent: First line: 1,27 cm

Formatted: English (United Kingdom)

Formatted: English (United Kingdom)

Formatted: English (United Kingdom)

Formatted: English (United Kingdom)

Formatted: English (United Kingdom)

Formatted: English (United Kingdom)

Formatted: English (United Kingdom)

Formatted: English (United Kingdom)

Formatted: English (United Kingdom)

Formatted: English (United Kingdom)

Formatted: English (United Kingdom)

Among the 21 $NaHCO_3$-dominated samples a few distinct trends were observed in the hydrochemistry. Specifically, the concentration of Cl^- and heavy stable water isotopes both increase in the up-valley direction. To illustrate this, the concentration of Cl^- is plotted against $\delta^{18}O_{H_2O}$ in Fig. ~~10~~11. The former has a relatively constant concentration at each site compared to the latter. We inferred that the variation of the Cl^- concentrations between the different springs reflects an up-valley variation in the sub-permafrost groundwater system, and not processes acting locally along the flow paths towards the individual pingos. If the latter had been the case, we would expect to see greater intra-site variation.

In order to explain the increasing Cl^- concentration and $\delta^{18}O_{H_2O}$ we considered solute rejection and isotope fractionation associated with freezing as well as mixing between seawater and freshwater. For the former, we found that the positive relationship between the two parameters was incongruent with this being a major control in the investigated system: when ice forms, water molecules containing the heavier isotope ^{18}O (and D) are preferentially included in the ice, while the residual water becomes isotopically lighter. For freezing in a well-mixed and closed reservoir, the isotopic ratio in the residual water, δ_w, may be expressed by a Rayleigh-type fractionation according to the following equation (Lacelle, 2011):

$$\delta_w = \delta_0 + \ln(\alpha_{i-w}) \cdot 1000 \cdot \ln(f) \qquad (8)$$

where δ_0 is the initial isotopic ratio in the water, α_{i-w} is the fractionation coefficient between ice and water, and f is the fraction of residual water. α_{i-w} = 1.003 (Lehmann and Siegenthaler, 1991) at equilibrium and approaches 1 for faster freezing rates (non-equilibrium). The decrease of $\delta^{18}O_{H_2O}$ in the residual water resulting from freezing is exemplified ~~on~~in Fig. ~~10~~11 by taking a typical LP water sample (i.e. with the lowest salinity) and assuming that Cl^- is completely excluded from the ice. The shading indicates the possible range of $\delta^{18}O_{H_2O}$ that can be derived from this process. Although two samples from FHP fall within the shaded area, it was hard to explain the composition of these with freezing from a LP-type water, as the remaining samples did not comply with this interpretation (Fig. ~~10~~11).

Another model line on Fig. ~~10~~11 is drawn by assuming that the LP samples result from mixing of seawater and a freshwater end-member with zero Cl^- concentration. Generally, the remaining samples agree with this model line and hence we argue that mixing is the more feasible explanation. This was also in line with the interpretation that the $NaHCO_3$-dominated hydrochemistry reflects freshening.

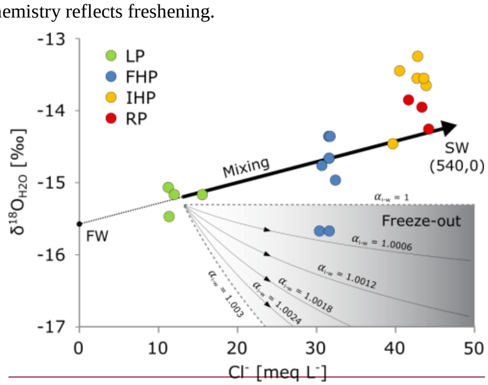

Formatted: English (United Kingdom)
Formatted: English (United Kingdom)
Formatted: English (United Kingdom)
Formatted: English (United Kingdom)
Formatted: English (United Kingdom)
Formatted: English (United Kingdom)
Formatted: English (United Kingdom)
Formatted: English (United Kingdom)
Formatted: English (United Kingdom)
Formatted: English (United Kingdom)
Formatted: English (United Kingdom)
Formatted: English (United Kingdom)
Formatted: English (United Kingdom)
Formatted: English (United Kingdom)
Formatted: English (United Kingdom)
Formatted: English (United Kingdom)
Formatted: English (United Kingdom)
Formatted: English (United Kingdom)
Formatted: English (United Kingdom)
Formatted: English (United Kingdom)
Formatted: English (United Kingdom)
Formatted: English (United Kingdom)
Formatted: English (United Kingdom)
Formatted: English (United Kingdom)
Formatted: English (United Kingdom)
Formatted: English (United Kingdom)
Formatted: English (United Kingdom)
Formatted: English (United Kingdom)
Formatted: English (United Kingdom)
Formatted: English (United Kingdom)
Formatted: English (United Kingdom)
Formatted: Indent: First line: 1,27 cm
Formatted: English (United Kingdom)
Formatted: English (United Kingdom)
Formatted: English (United Kingdom)

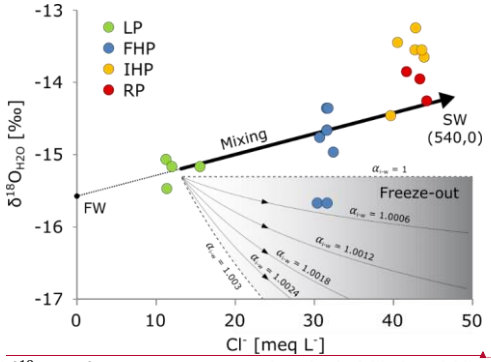

Figure ~~10~~11 Cl^- concentration and $\delta^{18}O_{H_2O}$ of pingo spring water samples. The thick black model line is drawn by assuming that the LP samples result from mixing of seawater and a freshwater endmember with a zero Cl^- concentration. The range of possible $\delta^{18}O_{H_2O}$ values following freeze-out (Eq. 8) from water with an initial composition alike LP is illustrated with the shaded area. Here, Cl^- is assumed to be completely excluded from the ice. The lower and upper edges of the shading represent equilibrium fractionation and no fractionation, respectively, while the intermediate model lines illustrate fractionation at 20 %, 40 %, 60 % and 80 % (top–down) of equilibrium conditions.

For the above mixing scenario, field surveys suggested a somewhat unusual trend with greater fractions of freshwater towards the sea, where $\delta^{18}O_{H_2O}$ and Cl^- concentrations approach those of the inferred freshwater end-member in Fig. ~~10~~11. In the case of present-day recharge from the adjacent mountains (as demonstrated at a pingo 35 km South West of Adventdalen by Demidov et al., 2019), we would not expect to observe such a systematic trend along the valley axis, as this would be unlikely in a system dependent upon ~~localized~~localised areas for infiltration. We therefore suggest that the unexpected landwards increase in Cl^- is difficult to explain without the sequence of events illustrated in Fig. ~~11~~12. During glaciation, the groundwater system was recharged by subglacial melting (Fig. ~~11a~~12a). Despite being covered by the sea during the Early Holocene, seawater could not infiltrate substantially into the groundwater system to replace the fresh groundwater (Fig. ~~11b~~12b). On Fig. ~~11c~~12c, the body of freshwater forms a wedge that thins inland below the freezing front due to the density difference with seawater. Moving away from the sea, the springs expel more saline groundwater because the wedge thins in this direction and the permafrost thickness increases (Fig. ~~11c~~12c). Therefore both the sources of water and the hydraulic conditions of the groundwater system seem intricately linked to landscape evolution throughout the Holocene.

Formatted: English (United Kingdom)
Formatted: English (United Kingdom)
Formatted: English (United Kingdom)
Formatted: English (United Kingdom)
Formatted: English (United Kingdom)
Formatted: English (United Kingdom)
Formatted: English (United Kingdom)
Formatted: Indent: First line: 0 cm
Formatted: English (United Kingdom)
Formatted: English (United Kingdom)
Formatted: English (United Kingdom)
Formatted: English (United Kingdom)
Formatted: English (United Kingdom)
Formatted: English (United Kingdom)
Formatted: English (United Kingdom)
Formatted: English (United Kingdom)
Formatted: English (United Kingdom)
Formatted: English (United Kingdom)

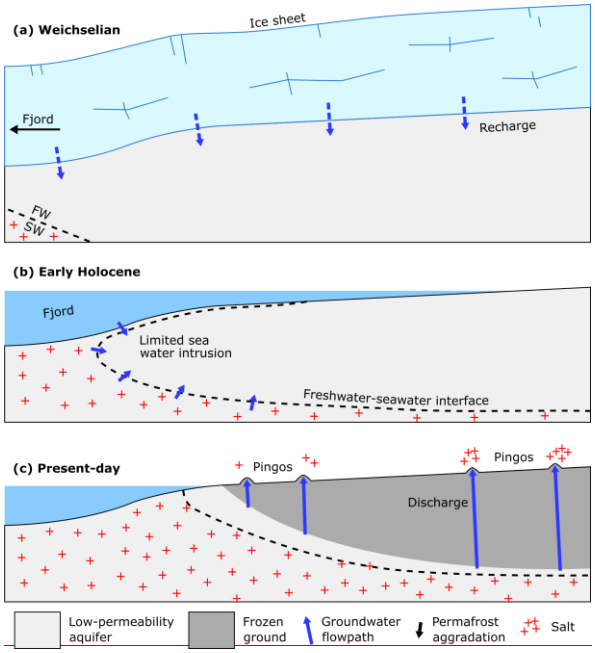
(a) Weichselian
Ice sheet
Fjord
Recharge
FW
SW
(b) Early Holocene
Fjord
Limited sea
water intrusion
Freshwater-seawater interface
(c) Present-day
Pingos
Pingos
Discharge
Low-permeability
aquifer
Frozen
ground
Groundwater
flowpath
Permafrost
aggradation
Salt

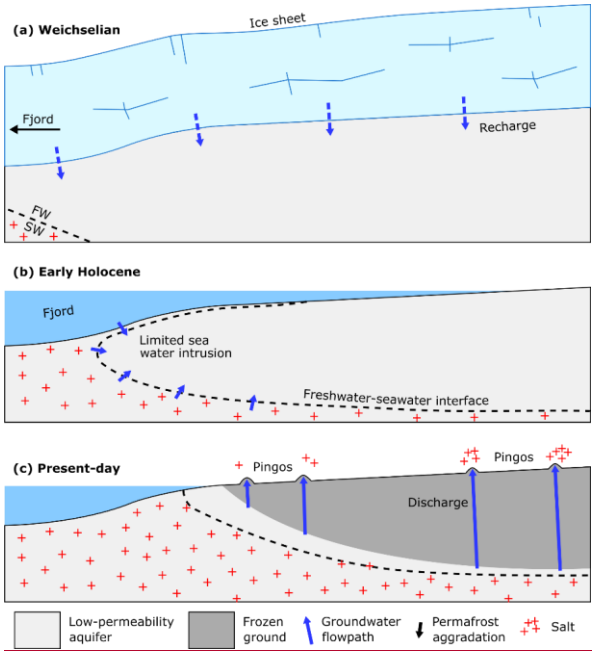

Figure ~~11~~12 Possible interpretation of hydrochemical trends observed in pingo spring waters. **(a)** Subglacial melting from the Weichselian ice sheet recharged the groundwater system with freshwater. **(b)** Although covered by the sea during Early Holocene, low-permeability rocks limited infiltration of sea water and the fresh groundwater body persisted. **(c)** Due to the shallower permafrost depth towards the sea, spring water sampled in this direction holds a lower concentration of sea water (salt).

Formatted: English (United Kingdom)

Formatted: English (United Kingdom)

7 Conclusions

Results from the decoupled heat and groundwater model show that millennial-scale basal permafrost aggradation may alone produce hydraulic pressures sufficient for the formation of pingos and their spring water outflows. when the right conditions are met. In addition to the climate cooling necessary for permafrost aggradation, a relatively low-permeability groundwater system with limited dissipation of hydraulic pressures are also required for pingo formation. Pingos formed in this way do not conform to the traditional differentiation between open-system and closed-system types, but constitute a borderline case: by definition, they classify as open-system pingos, because the groundwater body from which spring water is expelled is not enclosed in permafrost. Generically though, they relate more to closed-system pingos, because the causal mechanism of hydraulic pressures is essentially similar, although operating over much longer time-scales. We ~~emphasize~~emphasise that this

Formatted: English (United Kingdom)

Formatted: English (United Kingdom)

conceptual model for pingo formation represents an end-member of pingo-forming processes, which is not exclusive, but may act in combination with others, such as those reported nearby by Demidov et al. (2019).

The simulation results from the 1DHT model suggested that basal permafrost aggradation in Adventdalen presently induces head gradients corresponding to the effect of a recharge rate of ~ 0.1 mm yr^{-1} furthest up-valley, and increasing to ~ 1 mm yr^{-1} towards the sea. By applying these rates to the groundwater model, we simulated spring outflow rates of the order of 10^{-1} L s^{-1}. Due to the ~~omission of dynamic storage effects (i.e. a steady-state assumption), and to the~~ probable occurrence of basal permafrost aggradation outside the model area, these ~~are likely to~~may be underestimations. Nevertheless, the simulated and observed spring outflow rates at Adventdalen pingos were of the same order of magnitude, suggesting that they likely form at least partly in accordance with our conceptual model ~~that is driven by basal permafrost aggradation.~~ This further suggests that overpressures induced by water expansion during freezing in other sub-permafrost groundwater systems can result from permafrost aggradation.

The simulated aquifer flow paths and flow velocity distributions suggested that sub-permafrost groundwater flow in Adventdalen is ~~characterized~~characterised by slow mean pore water velocities (<0.25 m yr^{-1}) and long residence times (> $2.5 \cdot 10^4$ yr) that exceed the duration of the Holocene. The groundwater system most likely has a multidirectional flow pattern with individual catchments around each pingo.

The presence of a positive relationship between Cl^- and $\delta^{18}O_{H_2O}$ in the pingo spring water samples suggests that mixing between seawater and freshwater is the major control of hydrogeochemistry in the sub-permafrost groundwater system prior to aggradation. As a result, a somewhat ~~unusual~~unexpected but clear trend of increasing salinity in an up-valley direction was found. Therefore, given the relatively stagnant groundwater system, Weichselian subglacial meltwater could endure the Early Holocene inundation and result in the present-day situation where a freshwater body forms a wedge that thins in the inland direction below the permafrost. This possible interpretation readily explains the inland increase of the spring salinity because the inland springs expel groundwater from greater and hence more saline depths.

Alternative and non-recharge-related processes that may also affect sub-permafrost pressures were considered. The role of gases may be particularly important in this context because it is likely that methane hydrates have influenced the groundwater system under investigation. However, methane hydrate dissolution may in fact act as a pressure buffer and prolong artesian pressures after permafrost ceases aggrading (or starts thawing). This represents an uncertainty in forecasting how groundwater and methane fluxes will react to climate change. Unresolved questions regarding the occurrence and formation of gases in sub-permafrost groundwater systems therefore constitute an ongoing challenge for Arctic science.

8 Code availability

The 1DHT model code is publicly available at DOI:10.5281/zenodo.3578839.

Formatted: Indent: First line: 1,27 cm
Formatted: English (United Kingdom)
Formatted: English (United Kingdom)
Formatted: English (United Kingdom)
Formatted: English (United Kingdom)
Formatted: English (United Kingdom)
Formatted: English (United Kingdom)
Formatted: Indent: First line: 1,27 cm
Formatted: English (United Kingdom)
Formatted: English (United Kingdom)
Formatted: English (United Kingdom)

Author contributions

MTH developed the 1DHT model code and designed the modelling experiments with contributions from VB. AJH, SJ and MTH ~~analyzed~~analysed the hydrochemical data. MTH prepared the manuscript with contributions from all the co-authors.

Competing financial interest

The authors declare no competing financial interests.

Acknowledgements

This paper largely emanated from work initiated with MTH's MSc thesis (Hornum, 2018) and the authors acknowledge Prof. Peter Engesgaard for supervising the thesis work. The authors also acknowledge The Research Council of Norway grant 294764.

References

Åhman, R.: Studier av pingoer i Adventdalen och Reindalen på Spetsbergen, Lunds Univ. Naturgeografiska Institution. Rapp. och Not., 15, 27–44, 1973.

Andersen, D. T., Pollard, W. H., McKay, C. P. and Heldmann, J.: Cold springs in permafrost on Earth and Mars, J. Geophys. Res. E Planets, 107(3), doi:10.1029/2000je001436, 2002.

AQUAVEO™: Groundwater Modeling System 10.4.4, [online] Available from: https://www.aquaveo.com/software/gms-groundwater-modeling-system-introduction, 2019.

Bælum, K., Johansen, T. A., Johnsen, H., Rød, K., Ruud, B. O. and Braathen, A.: Subsurface structures of the longyearbyen CO2 lab study area in central spitsbergen (arctic Norway), as mapped by reflection seismic data, Nor. Geol. Tidsskr., 92(4), 377–389, 2012.

Bahr, J. M., Moline, G. R. and Nadon, G. C.: Anomalous Pressures in the Deep Michigan Basin, in AAPG Memoir 61: Basin Compartmensts and Seals, pp. 153–165., 1994.

Ballantyne, C. K.: Periglacial geomorphology, 1st ed., Wiley-Blackwell., 2018.

Benn, D. I. and Evans, D. J. A.: Glaciers & Glaciation, 2nd ed., Hodder Education., 2010.

Bense, V. F., Kooi, H., Ferguson, G. and Read, T.: Permafrost degradation as a control on hydrogeological regime shifts in a warming climate, J. Geophys. Res. Earth Surf., 117(3), 1–18, doi:10.1029/2011JF002143, 2012.

Formatted: English (United Kingdom)

Formatted: English (United Kingdom)

Formatted: English (United Kingdom)

Formatted: English (United Kingdom)

Formatted: Danish

Bergman, T. L., Lavine, A. S., Incropera, F. P. and Dewitt, D. P.: Fundamentals of Heat and Mass Transfer, 7th ed., John Wiley & Sons., 2011.

Betlem, P., Senger, K. and Hodson, A.: 3D thermobaric modelling of the gas hydrate stability zone onshore central Spitsbergen, Arctic Norway, Mar. Pet. Geol., 100(August 2018), 246–262, doi:10.1016/j.marpetgeo.2018.10.050, 2019.

van der Bilt, W. G. M., D'Andrea, W. J., Bakke, J., Balascio, N. L., Werner, J. P., Gjerde, M. and Bradley, R. S.: Alkenone-based reconstructions reveal four-phase Holocene temperature evolution for High Arctic Svalbard, Quat. Sci. Rev., 183, 204–213, doi:10.1016/j.quascirev.2016.10.006, 2018.

Birchall, T., Senger, K., Hornum, M. T., Olaussen, S. and Braathen, A.: Underpressure of the Northern Barents Shelf: distribution, causes and implications on the petroleum. ~~In Review~~Pre-proof, Am. Assoc. Pet. Geol. Bull., ~~n.d~~doi:10.1306/02272019146, 2020.

Bonacina, C. and Comini, G.: On the solution of the nonlinear heat conduction equations by numerical methods, Int. J. Heat Mass Transf., 16(3), 581–589, doi:10.1016/0017-9310(73)90225-1, 1973.

Braathen, A., Bælum, K., Christiansen, H. H., Dahl, T., Eiken, O., Elvebakk, H., Hansen, F., Hanssen, T. H., Jochmann, M., Johansen, T. A., Johnsen, H., Larsen, L., Lie, T., Mertes, J., Mørk, A., Mørk, M. B., Nemec, W., Olaussen, S., Oye, V., Rød, K., Titlestad, G. O., Tveranger, J. and Vagle, K.: The Longyearbyen CO2 Lab of Svalbard, Norway - Initial Assessment of the Geological Conditions for CO2 Sequestration, Nor. Geol. Tidsskr., 92(4), 353–376, 2012.

Burland, J. B.: On the compressibility and shear strength of natural clays., 1990.

Burr, D. M., Tanaka, K. L. and Yoshikawa, K.: Pingos on Earth and Mars, Planet. Space Sci., 57(5–6), 541–555, doi:10.1016/j.pss.2008.11.003, 2009.

Burt, T. P. and Williams, P. J.: Hydraulic conductivity in frozen soils, Earth Surf. Process., 1(4), 349–360, doi:10.1002/esp.3290010404, 1976.

Cable, S., Elberling, B. and Kroon, A.: Holocene permafrost history and cryostratigraphy in the High-Arctic Adventdalen Valley, central Svalbard, Boreas, 47(2), 423–442, doi:10.1111/bor.12286, 2018.

Carslaw, H. S. and Jaeger, J. C.: Conduction of heat in solids, 2nd ed., Clarendon Press., 1959.

Christiansen, H. H., French, H. M. and Humlum, O.: Permafrost in the Gruve-7 mine, Adventdalen, Svalbard, Nor. Geogr. Tidsskr., 59(2), 109–115, doi:10.1080/00291950510020592, 2005.

Demidov, N., Wetterich, S., Verkulich, S., Ekaykin, A., Meyer, H., Anisimov, M., Schirrmeister, L., Demidov, V. and Hodson, A. J.: Geochemical signatures of pingo ice and its origin in Grøndalen, west Spitsbergen, Cryosph., 13(11), 3155–3169, doi:10.5194/tc-13-3155-2019, 2019.

Domenico, P. A. and Mifflin, M. D.: Water from low-permeability sediments and land subsidence, Water Resour. Res., 1(4), 563–576, doi:10.1029/WR001i004p00563, 1965.

Domenico, P. A. and Schwartz, F. W.: Physical and chemical hydrogeology, Wiley & Sons., 1998.

Dyke, A. S., England, J., Reimnitz, E. and Jette, H.: Changes in driftwood delivery to the Canadian Arctic Archipelago, Arctic ~~Anthropol.,~~ 50(1), 1–16, 1997.

Elverhøi, A., Svendsen, J. I., Solheim, A., Andersen, E. S., Milliman, J., Mangerud, J. and Hooke, R. L.: Late Quaternary Sediment Yield from the High Arctic Svalbard Area, J. Geol., 103(1), 1–17, doi:10.1086/629718, 1995.

Eppelbaum, L., Kutasov, I. and Pilchin, A.: Applied Geothermics, Lect. Notes Earth Syst. Sci., 757, doi:10.1007/978-3-642-34023-9, 2014.

Farnsworth, W.~~: Holocene glacier history of Svalbard: Retracing the style of (de-)glaciation, UiT The Arctic University of Norway., 2019~~. R., Ingólfsson, Ó., Alexanderson, H., Allaart, L., Forwick, M., Noormets, R., Retelle, M. and Schomacker, A.: Holocene glacial history of Svalbard: Status, perspectives and challenges, Earth-Science Rev., doi:10.1016/j.earscirev.2020.103249, 2020.

~~Farouki, O. T.: Thermal Properties of Soils - CRREL Monograph, US Army Cold Reg. Res. Eng. Lab., 1981.~~

Fitts, C. R.: Groundwater Science, 1st ed., Academic Press., 2002.

Førland, E. J., Hanssen-Bauer, I. and Nordli, Ø.: Climate statistics and longterm series of temperature and precipitation at Svalbard and Jan Mayen, Norwegian Meteorological Institute, DNMI Nor. Meteorol. Inst. Rep., 21, 1997.

Forman, S. L.: Post-glacial relative sea-level history of northwestern Spitsbergen, Svalbard, Geol. Soc. Am. Bull., 102(11), 1580–1590, doi:10.1130/0016-7606(1990)102<1580:PGRSLH>2.3.CO;2, 1990.

Forwick, M. and Vorren, T. O.: Stratigraphy and deglaciation of the Isfjorden area, Spitsbergen, Nor. Geol. Tidsskr., 90(4), 163–179, 2011.

French, H. M.: The Periglacial Environment, 4th ed., John Wiley & Sons Ltd., 2017.

Funder, S., Goosse, H., Jepsen, H., Kaas, E., Kjær, K. H., Korsgaard, N. J., Larsen, N. K., Linderson, H., Lyså, A., Möller, P., Olsen, J. and Willerslev, E.: A 10,000-year record of Arctic Ocean Sea-ice variability - View from the beach, Science (80-.)., 333(6043), 747–750, doi:10.1126/science.1202760, 2011.

Gilbert, G. L., O'Neill, H. B., Nemec, W., Thiel, C., Christiansen, H. H. and Buylaert, J. P.: Late Quaternary sedimentation and permafrost development in a Svalbard fjord-valley, Norwegian high Arctic, Sedimentology, 65(7), 2531–2558, doi:10.1111/sed.12476, 2018.

Giménez-Forcada, E.: Dynamic of sea water interface using hydrochemical facies evolution diagram, Ground Water, 48(2),

212–216, doi:10.1111/j.1745-6584.2009.00649.x, 2010.

Govaerts, J., Beerten, K. and Ten Veen, J.: Weichselian permafrost depth in the Netherlands: A comprehensive uncertainty and sensitivity analysis, Cryosphere, 10(6), 2907–2922, doi:10.5194/tc-10-2907-2016, 2016.

Grasby, S. E., Beauchamp, B. and Bense, V.: Sulfuric acid speleogenesis associated with a glacially driven groundwater system-paleo-spring "pipes" at Borup Fiord Pass, Nunavut, Astrobiology, 12(1), 19–28, doi:10.1089/ast.2011.0700, 2012.

Grasby, S. E., Proemse, B. C. and Beauchamp, B.: Deep groundwater circulation through the High Arctic cryosphere forms Mars-like gullies, Geology, 42(8), 651–654, doi:10.1130/G35599.1, 2014.

Gregersen, O. and Eidsmoen, T.: Permafrost conditions in the shore area at Svalbard, in Permafrost, proceedings of the Fifth International Conference on Permafrost, August 2-5, 1988, Trondheim, Norway, vol. 2, edited by K. Senneset, pp. 933–936, Tapir Publishers., 1988.

Grenier, C., Anbergen, H., Bense, V., Chanzy, Q., Coon, E., Collier, N., Costard, F., Ferry, M., Frampton, A., Frederick, J., Gonçalvès, J., Holmén, J., Jost, A., Kokh, S., Kurylyk, B., McKenzie, J., Molson, J., Mouche, E., Orgogozo, L., Pannetier, R., Rivière, A., Roux, N., Rühaak, W., Scheidegger, J., Selroos, J. O., Therrien, R., Vidstrand, P. and Voss, C.: Groundwater flow and heat transport for systems undergoing freeze-thaw: Intercomparison of numerical simulators for 2D test cases, Adv. Water Resour., 114(February), 196–218, doi:10.1016/j.advwatres.2018.02.001, 2018.

Grosse, G., Goetz, S., McGuire, A. D., Romanovsky, V. E. and Schuur, E. A. G.: Changing permafrost in a warming world and feedbacks to the Earth system, Environ. Res. Lett., 11, 040201, doi:10.1088/1748-9326/11/4/040201, 2016.

Grundvåg, S.-A., Jelby, M. E., Sliwinska, K. K., Nøhr-Hansen, H., Aadland, T., Sandvik, S. E., Tennvassås, I., Engen, T. and Olaussen, S.: Sedimentology and palynology of the Lower Cretaceous succession of central Spitsbergen: integration of subsurface and outcrop data, Nor. J. Geol., 99(2), doi:10.17850/njg006, 2019.

Hald, M., Andersson, C., Ebbesen, H., Jansen, E., Klitgaard-Kristensen, D., Risebrobakken, B., Salomonsen, G. R., Sarnthein, M., Sejrup, H. P. and Telford, R. J.: Variations in temperature and extent of Atlantic Water in the northern North Atlantic during the Holocene, Quat. Sci. Rev., 26, 3423–3440, doi:10.1016/j.quascirev.2007.10.005, 2007.

Haldorsen, S., Heim, M. and Lauritzen, S. E.: Subpermafrost Groundwater, Western Svalbard, Nord. Hydrol., 27(1–2), 57–68, doi:~~https://doi.org/~~10.2166/nh.1996.0019, 1996.

Haldorsen, S., Heim, M., Dale, B., Landvik, J. Y., van der Ploeg, M., Leijnse, A., Salvigsen, O., Hagen, J. O. and Banks, D.: Sensitivity to long-term climate change of subpermafrost groundwater systems in Svalbard, Quat. Res., 73(2), 393–402, doi:10.1016/j.yqres.2009.11.002, 2010.

Hanssen-Bauer, I., Førland, E. J., Hisdal, H., Mayer, S., Sandø, A. B., Sorteberg, A., Adakudlu, M., Andresen, J., Bakke, J., Beldring, S., Benestad, R., Bilt, W., Bogen, J., Borstad, C., Breili, K., Breivik, Ø., Børsheim, K. Y., Christiansen, H. H.,

Dobler, A., Engeset, R., Frauenfelder, R., Gerland, S., Gjelten, H. M., Gundersen, J., Isaksen, K., Jaedicke, C., Kierulf, H., Kohler, J., Li, H., Lutz, J., Melvold, K., Mezghani, A., Nilsen, F., Nilsen, I. B., Nilsen, J. E. Ø., Pavlova, O., Ravndal, O., Risebrobakken, B., Saloranta, T., Sandven, S., Schuler, T. V, Simpson, M. J. R., Skogen, M., Smedsrud, L. H., Sund, M., Vikhamar-Schuler, D., Westermann, S. and Wong, W. K.: Climate in Svalbard 2100. [online] Available from: http://www.miljodirektoratet.no/M1242 (Accessed 12 September 2019), 2018.

Harada, K. and Yoshikawa, K.: Permafrost age and thickness near Adventfjorden, Spitsbergen, Polar Geogr., 20(4), 267–281, doi:10.1080/10889379609377607, 1996.

Hodson, A., Nowak, A., Senger, K., Redeker, K. R., Christiansen, H. H., Jessen, S., Hornum, M. T., Betlem, P., Thornton, S., Turchyn, A. V., Olaussen, S. and Marca, A.: Open system pingos as hotspots for sub-permafrost methane emission in Svalbard, in review, Cryosph. Discuss., doi:~~https://doi.org/~~10.5194/tc-2020-11~~, in review~~, 2020.

Hodson, A. J., Nowak, A., Redeker, K. R., Holmlund, E. S., Christiansen, H. H. and Turchyn, A. V.: Seasonal dynamics of methane and carbon dioxide evasion from an open system pingo: Lagoon pingo, svalbard, Front. Earth Sci., 7, 30, doi:10.3389/feart.2019.00030, 2019.

Hornum, M. T.: Postglacial Rebound, Permafrost Growth, and its Impact on Groundwater Flow and Pingo Formation, University of Copenhagen. [online] Available from: https://www.researchgate.net/profile/Mikkel_Hornum2, 2018.

Humlum, O.: Holocene permafrost aggradation in Svalbard, Geol. Soc. Spec. Publ., 242, 119–130, doi:10.1144/GSL.SP.2005.242.01.11, 2005.

Humlum, O., Instanes, A. and Sollid, J. L.: Permafrost in Svalbard: A review of research history, climatic background and engineering challenges, Polar Res., 22(2), 191–215, doi:~~https://doi.org/~~10.3402/polar.v22i2.6455, 2003.

Huq, F., Smalley, P. C., Mørkved, P. T., Johansen, I., Yarushina, V. and Johansen, H.: The Longyearbyen CO2 Lab: Fluid communication in reservoir and caprock, Int. J. Greenh. Gas Control, doi:10.1016/j.ijggc.2017.05.005, 2017.

Ingólfsson, Ó. and Landvik, J. Y.: The Svalbard-Barents Sea ice-sheet-Historical, current and future perspectives, Quat. Sci. Rev., 64, 33–60, doi:10.1016/j.quascirev.2012.11.034, 2013.

Koevoets, M. J., Hammer, Ø., Olaussen, S., Senger, K. and Smelror, M.: Integrating subsurface and outcrop data of the Middle Jurassic to Lower Cretaceous Agardhfjellet Formation in central Spitsbergen, Nor. J. Geol., 98(4), doi:10.17850/njg98-4-01, 2018.

Kottek, M., Grieser, J., Beck, C., Rudolf, B. and Rubel, F.: World Map of the Köppen-Geiger climate classification updated, , 15(3), 259–263, doi:10.1127/0941-2948/2006/0130, 2006.

Lacelle, D.: On the δ18O, δD and D-excess relations in meteoric precipitation and during equilibrium freezing: Theoretical approach and field examples, Permafr. Periglac. Process., 22(1), 13–25, doi:10.1002/ppp.712, 2011.

Lehmann, M. and Siegenthaler, U.: Equilibrium oxygen- and hydrogen-isotope fractionation between ice and water, J. Glaciol., 37(125), 23–26, doi:10.3189/s0022143000042751, 1991.

Leith, K., Moore, J. R., Amann, F. and Loew, S.: Subglacial extensional fracture development and implications for Alpine Valley evolution, J. Geophys. Res. Earth Surf., 119(1), 62–81, doi:10.1002/2012JF002691, 2014.

Liestøl, O.: Pingos, springs, and permafrost in Spitsbergen, Nor. Polarinstitutt Årb. 1975, 7–29, 1977.

Liestøl, O.: Open-system pingos in Spitsbergen, Nor. Geogr. Tidsskr., doi:10.1080/00291959608552355, 1996.

Lønne, I. and Nemec, W.: High-arctic fan delta recording deglaciation and environment disequilibrium, Sedimentology, 51(3), 553–589, doi:10.1111/j.1365-3091.2004.00636.x, 2004.

Mackay, J. R.: Pingo growth and collapse, Tuktoyaktuk Peninsula area, western arctic coast, Canada: A long-term field study, Geogr. Phys. Quat., 52(3), 271–323, doi:10.7202/004847ar, 1998.

Manger, G. E.: Porosity and Bulk Density of Sedimentary Rocks, Geol. Surv. Bull., 1144-E, doi:10.1111/nan.12452, 1963.

Mangerud, J. and Svendsen, J. I.: The Holocene Thermal Maximum around Svalbard, Arctic North Atlantic; molluscs show early and exceptional warmth, The Holocene, 28(1), 65–83, doi:10.1177/0959683617715701, 2017.

Marshall, C., Uguna, J., Large, D. J., Meredith, W., Jochmann, M., Friis, B., Vane, C., Spiro, B. F., Snape, C. E. and Orheim, A.: Geochemistry and petrology of palaeocene coals from Spitzbergen - Part 2: Maturity variations and implications for local and regional burial models, Int. J. Coal Geol., 143, 1–10, doi:10.1016/j.coal.2015.03.013, 2015.

MathWorks®: MATLAB R2019b, [online] Available from: https://se.mathworks.com/products/matlab.html, 2019.

Mau, S., Römer, M., Torres, M. E., Bussmann, I., Pape, T., Damm, E., Geprägs, P., Wintersteller, P., Hsu, C. W., Loher, M. and Bohrmann, G.: Widespread methane seepage along the continental margin off Svalbard-from Bjørnøya to Kongsfjorden, Sci. Rep., 7, doi:10.1038/srep42997, 2017.

McCauley, C. A., White, D. M., Lilly, M. R. and Nyman, D. M.: A comparison of hydraulic conductivities, permeabilities and infiltration rates in frozen and unfrozen soils, Cold Reg. Sci. Technol., 34(2), 117–125, doi:10.1016/S0165-232X(01)00064-7, 2002.

McDonald, M. G. and Harbaugh, A. W.: A modular three-dimensional finite-difference ground-water flow model - Techniques of Water-Resources Investigations 06-A1., 1988.

Mottaghy, D. and Rath, V.: Latent heat effects in subsurface heat transport modelling and their impact on palaeotemperature reconstructions, Geophys. J. Int., 164(1), 236–245, doi:10.1111/j.1365-246X.2005.02843.x, 2006.

Myhre, C. L., Ferré, B., Platt, S. M., Silyakova, A., Hermansen, O., Allen, G., Pisso, I., Schmidbauer, N., Stohl, A., Pitt, J., Jansson, P., Greinert, J., Percival, C., Fjaeraa, A. M., O'Shea, S. J., Gallagher, M., Le Breton, M., Bower, K. N., Bauguitte, S.

J. B., Dalsøren, S., Vadakkepuliyambatta, S., Fisher, R. E., Nisbet, E. G., Lowry, D., Myhre, G., Pyle, J. A., Cain, M. and Mienert, J.: Extensive release of methane from Arctic seabed west of Svalbard during summer 2014 does not influence the atmosphere, Geophys. Res. Lett., 43(9), 4624–4631, doi:10.1002/2016GL068999, 2016.

Neuzil, C. E.: Abnormal pressures as hydrodynamic phenomena, Am. J. Sci., 295(6), 742–786, doi:10.2475/ajs.295.6.742, 1995.

Neuzil, C. E.: Hydromechanical coupling in geologic processes, Hydrogeol. J., 11(1), 41–83, doi:10.1007/s10040-002-0230-8, 2003.

Neuzil, C. E.: Hydromechanical effects of continental glaciation on groundwater systems, Geofluids, 12(1), 22–37, doi:10.1111/j.1468-8123.2011.00347.x, 2012.

Nordli, Ø., Przybylak, R., Ogilvie, A. E. J. and Isaksen, K.: Long-term temperature trends and variability on spitsbergen: The extended svalbard airport temperature series, 1898-2012, Polar Res., 33(1), 21349, doi:10.3402/polar.v33.21349, 2014.

Norwegian Polar Institute: Map data, [online] Available from: https://geodata.npolar.no/ (Accessed 13 ~~September 2019~~May 2020), 2019.

Ohm, S. E., Larsen, L., Olaussen, S., Senger, K., Birchall, T., Demchuk, T., Hodson, A., Johansen, I., Titlestad, G. O., Karlsen, D. A. and Braathen, A.: Discovery of shale gas in organic-rich Jurassic successions, Adventdalen, Central Spitsbergen, Norway, ,Nor. J. Geol., 99(2), 1–28, doi:10.17850/njg007, 2019.

Okiongbo, K. S.: Effective Stress-Porosity Relationship above and Within the Oil Window in the North Sea Basin, Res. J. Appl. Sci. Eng. Technol., 3(1), 32–38, 2011.

Olaussen, S., Senger, K., Braathen, A., Grundvåg, S.-A. and Mørk, A.: You learn as long as you drill; research synthesis from the Longyearbyen CO2 Laboratory, Svalbard, Norway, Nor. J. Geol., ~~n.d~~99(2), 157–187, doi:10.17850/njg008, 2020.

Orvin, A. K.: Litt om kilder på Svalbard, Nor. Geol. Tidsskr. Norges Svalbard- og Ishavsundersøgelser, 10(57), 15–38, 1944.

van der Ploeg, M. J., Haldorsen, S., Leijnse, A. and Heim, M.: Subpermafrost groundwater systems: Dealing with virtual reality while having virtually no data, J. Hydrol., 475, 42–52, doi:10.1016/j.jhydrol.2012.08.046, 2012.

Pollock, D. W.: User Guide for MODPATH Version 7-A Particle-Tracking Model for MODFLOW, U.S. Geol. Surv. Open File Rep., 1086, 41, doi:10.3133/ofr20161086, 2016.

Riseborough, D., Shiklomanov, N., Etzelmüller, B., Gruber, S. and Marchenko, S.: Recent advances in permafrost modelling, Permafr. Periglac. Process., 19(2), 137–156, doi:10.1002/ppp.615, 2008.

Robertson, E. C.: Thermal properties of rocks. Report 88-441, US Dep. Inter. Geol. Surv., 106, 1988.

Scheidegger, J. M. and Bense, V. F.: Impacts of glacially recharged groundwater flow systems on talik evolution, J. Geophys.

Res. Earth Surf., 119(4), 758–778, doi:10.1002/2013JF002894, 2014.

Scheidegger, J. M., Bense, V. F. and Grasby, S. E.: Transient nature of Arctic spring systems driven by subglacial meltwater, Geophys. Res. Lett., 39(12), 1–6, doi:10.1029/2012GL051445, 2012.

Schlumberger©: Petrel E&P, [online] Available from: https://www.software.slb.com/products/petrel, 2019.

Schuster, P. F., Schaefer, K. M., Aiken, G. R., Antweiler, R. C., Dewild, J. F., Gryziec, J. D., Gusmeroli, A., Hugelius, G., Jafarov, E., Krabbenhoft, D. P., Liu, L., Herman-Mercer, N., Mu, C., Roth, D. A., Schaefer, T., Striegl, R. G., Wickland, K. P. and Zhang, T.: Permafrost Stores a Globally Significant Amount of Mercury, Geophys. Res. Lett., 45(3), 1463–1471, doi:10.1002/2017GL075571, 2018.

Singhal, B. B. S. and Gupta, R. P.: Applied Hydrogeology of Fractured Rocks, 2nd ed., Springer Netherlands., 2010.

Skempton, A. W.: The consolidation of clays by gravitational compaction, Q. J. Geol. Soc. London, 125(1–4), 373–408, doi:10.1144/gsjgs.125.1.0373, 1969.

Šuklje, L.: Rheologic Aspects of Soil Mechanics, 1st ed., Wiley-Interscience., 1969.

Svensson, H.: Pingos i yttre delen av Adventdalen, Nor. Polarinstitutt Årb. 1969, 168–174, 1970.

Taniguchi, M.: Evaluations of the saltwater-groundwater interface from borehole temperature in a coastal region, Geophys. Res. Lett., 27(5), 713–716, doi:10.1029/1999GL002366, 2000.

Verruijt, A.: A note on the ghyben-herzberg formula, Int. Assoc. Sci. Hydrol. Bull., 13, 43–46, doi:10.1080/02626666809493624, 1968.

Walvoord, M. A. and Kurylyk, B. L.: Hydrologic impacts of thawing permafrost—a review, Vadose Zo. J., 15(6), doi:10.2136/vzj2016.01.0010, 2016.

Wangen, M., Souche, A. and Johansen, H.: A model for underpressure development in a glacial valley, an example from Adventdalen, Svalbard, Basin Res., 28(6), 752–769, doi:10.1111/bre.12130, 2016.

Williams, J. R.: Ground Water in the Permafrost Regions of Alaska, US Geol. Surv. Prof. Pap., 1970.

Williams, P. J. and Smith, M. W.: The ground thermal regime, in The Frozen Earth, pp. 83–121, Cambridge University Press., 1989.

Woo, M. K.: Permafrost Hydrology, Springer-Verlag Berlin Heidelberg., 2012.

Yang, Y. and Aplin, A. C.: Definition and practical application of mudstone porosity-effective stress relationships, Pet. Geosci., 10(2), 153–162, doi:https://doi.org/10.1144/1354-079302-567, 2004.

Yoshikawa, K. and Harada, K.: Observations on nearshore pingo growth, Adventdalen, Spitsbergen, Permafr. Periglac.

Process., 6(4), 361–372, doi:10.1002/ppp.3430060407, 1995.

Yoshikawa, K. and Nakamura, T.: Pingo growth ages in the delta area, Adventdalen, Spitsbergen, Polar Rec. (Gr. Brit)., doi:10.1017/S0032247400067565, 1996.

Formatted: Font: Times New Roman, Danish, Not Expanded by / Condensed by